EXPERIMENTAL TESTS OF POLYMER REPTATION

A thesis presented in partial fulfillment of the requirements for the degree of Doctor of Philosophy in Physics at Massey University

Michal Komlosh

1999

ABSTRACT

Pulsed Gradient Spin Echo Nuclear Magnetic Resonance (PGSE-NMR) and rheology measurements were used to test whether the dynamics of entangled polymer chains in semidilute solution follow the reptation theory. Nine molar masses from 1 to 20 million daltons at a fixed concentration of 4.96% w/v along with a range of concentrations from 4.96% to 23.58% w/v at fixed molar mass of 3 million daltons were studied using PGSE-NMR techniques. The response to mechanical deformation of five different concentrations from 4.96% to 23.58% w/v at fixed molar mass of 3.9 million daltons was also studied. The distance and time scales accessed by PGSE-NMR were 20 to 1000 nm and 10 to 3000 ms respectively. As a result the mean square segmental motion over three reptation regimes was obtained and the reptation finger print, $\langle (r(t) - r(0)) \rangle \sim t^{1/4}$, was observed. The resulting concentration and molecular weight scaling laws for the tube disengagement time, center of mass diffusion and the tube diameter, which were obtained in PGSE-NMR and rheology experiments, were found to be in good agreement with the reptation theory and its standard modifications, and a good quantitative fit to the mean square displacement was given by this theory.

Local anisotropic motion of polymer chains at the level of the Rouse time was observed using double-PGSE NMR methods. These suggested a possible cooperative motion of polymer chains in entangled environment which challenges the basic assumptions of the reptation theory.

Evidence of intra-chain spin diffusion was found. As a consequence relevant corrections incorporating the phenomenon into the PGSE-NMR data had to be made.

ACKNOWLEDGMENTS

First of all I would like to thank my supervisor, Professor Paul Callaghan, for providing continuing guidance and careful instructions throughout the project and for his great patience while this thesis has been written.

I would like to express my gratitude to the New Zealand Federation of University Women Wellington Branch for the award of an NZFUW scholarship and the Royal Society of New Zealand for the RHT Bates memorial scholarship.

I also would like to acknowledge the following people:

Mr. Robin Dykstra the electronics wizard who helped me with all the bits and pieces of my apparatus (for better and for worse).

The workshop guys, Barry, Steve, Noel, Keith and Peter who were always there to build and replace everything I have destroyed.

The members of the NMR group, Melanie, Sarah, Elmar, Maria, Sasha, Ryan, Vanessa, Toni and Suz, who tolerated my mess.

All my friends beyond the NMR group and Downtown Cinema 8 for being there for me.

Last but not least I would like to thank my friends and family in Israel for their support.

CONTENTS

1
INTRODUCTION

When a polymer solution exceeds a certain concentration, c^*, the different chains start to overlap each other and form entanglements which become denser with increasing concentration. The polymer motion in the entangled state is very different from that of the unentangled state due to those constraints. Entangled polymer dynamics is a subject where complexity arises not only from the fact that its theoretical description depends on a solution to a many body problem, but also from the difficulties associated with experimental observation.

Amongst the competing theories which seek to describe polymer motion in the presence of entanglements, the reptation model is one of the most intuitive and successful. The reptation theory[1] treats the dynamics of an entangled polymer coil in terms of a single chain inside a mean potential field, in which a polymer coil creeps inside a tube formed by the surrounding polymer matrix. The theory makes specific predictions about the linear and non-linear response of polymer melts and semidilute solutions to mechanical deformation. It also gives a specific quantitative description of the translational motion of the polymer segments over a wide range of length and time scales. In this description the mean square displacements of the polymer segments scale characteristically in time i.e. $\left\langle (r(t)-r(0))^2 \right\rangle \sim t^{1/2};t^{1/4};t^1$ where the scaling exponent depends on the length of motion with respect to the tube dimension[2]. The $t^{1/2}$ and the $t^{1/4}$ behavior arise from the anisotropic motion of a polymer segment when surrounded by an entangled polymer matrix while the t^1 behavior indicates isotropic center of mass diffusion. However, the $t^{1/2}$ and t^1 behavior is not specific to the reptation theory, and in fact, the simplest model for dynamics of a single polymer chain, the Rouse model[3], predicts similar scaling laws. The $t^{1/4}$ scaling behavior is specific only for the reptation theory and is considered as its "finger print". Other scaling laws has been derived from the reptative motion, among them the center of mass diffusion coefficient scaling as M^{-2} and the longest relaxation time τ_d scaling as M^{-3}. Although those scaling laws were confirmed for polymer melts a few questions about the dynamics of polymer system in a semidilute solution remained open. Recently, another theory, i.e. the mode-mode coupling[4], was developed which predicts similar scaling behavior for the segmental mean square displacement but is still lacking any quantitative description of the quantity $\left\langle (r(t)-r(0))^2 \right\rangle$.

In order to observe the $t^{1/4}$ regime one should be able to detect mean square displacements in the range of few hundreds of Angstroms. Neutron inelastic scattering[5] and, in particular neutron spin echo experiments[6,7] have gained access to the regime of rms displacement below 50 $\mathring{A}$ and while these suggest the possibility of $t^{1/4}$ regime, they are not convincing. Detection of the mean square displacements in the $t^{1/2}$ and t^{1} regimes is possible by using Pulsed-Gradient-Spin-Echo Nuclear Magnetic Resonance (PGSE-NMR) techniques. Pulsed Gradient Spin Echo NMR is a common method for measuring diffusion coefficients, in which one magnetically labels the nuclear spin and then detects its motion over a period of time. However, in order to observe mean square displacements of few hundred Angstroms one needs to be able to measure self diffusion coefficients on the order of 10^{-16} m^2 s^{-1}, which are slower than the current limit of the method.

The goals of this thesis were to detect the anisotropic motion of a polymer segment in a semidilute solution, to observe the reptation finger print and confirm the reptation scaling laws, and to compare our results for the key reptation parameters with those obtained by mechanical measurements. The choice of semidilute polymer solutions rather than polymer melts is based on a careful consideration of relevant length and time scales. The PGSE-NMR technique can cover length scales from 100 $\mathring{A}$ (given the improvements made as part of this thesis) up to a few 100 μm. Its characteristic time scale ranges from a few ms to a few s. We are required to fit the polymer dynamics under study to these "windows". In the case of melts of polymers where molar mass exceed 10^6 daltons, the method gives access to relevant length scales but the polymer time scales are too long. In order to speed up the polymer motion, but retain the spatial dimensional scale, we can use semidilute solutions in which the concentration may be "tuned" to place the polymer dynamics in our available time window. This choice requires that we consider any adaptation of the reptation theory needed to deal with the case of semidilute solutions.

In order to achieve the goals of this thesis we had to build and optimize a pulsed magnetic field gradient apparatus which could enable us to obtain mean square displacements of few hundred Angstroms. Detecting such small motion involved various hardware problems, and required a careful consideration of the phenomenon of nuclear magnetization transport.

The following chapter contain a presentation of the reptation theory, its deficiencies and modifications as well as a description of its principal rival the mode-mode-coupling model. The third chapter gives an introduction to Nuclear Magnetic

Resonance technique with an emphasis on the PGSE-NMR method while the fourth chapter describes the apparatus and gives some insight regarding the problems associated with such fine displacement detection. Chapter 5 presents the PGSE-NMR results while chapter 6 presents the rheology results and the comparison between the different experiments and the reptation theory. The findings regarding nuclear magnetism transport by spin-diffusion were a bonus from our reptation research, and appeared as a artifact in our self diffusion measurements for high molecular weight. This topic is introduced in chapter 7. Chapter 8 presents a direct measurement of anisotropic segmental motion using double-PGSE NMR methods. As a conclusion the last chapter give some ideas for new experiments and suggestions for future work.

2
THEORETICAL MODELS OF POLYMER DYNAMICS

The dynamics of polymer coils in an entangled matrix is a controversial subject. As a many body problem the solution requires debatable assumptions and approximations. Currently, two major theoretical approaches are used to deal with the problem. The first treats the dynamics using a mean field approximation and the second attempts to derive the dynamics from first principles. In this chapter we focus on the mean field theory known as the reptation model, but some overview of the rival theory in also presented. The reptation model is very intuitive and describes the dynamics of entangled polymers by considering how an isolated coil creeps inside a mean field tube. Even though the idea seems to be bold and simplified, the theory provides quantitative parameters and scaling laws which agree with the experiment to a first approximation. This chapter gives an extensive overview of the reptation theory, where it fails and where various modifications should be made. The chapter ends with a brief discussion of the mode-mode coupling model which is based on a first principles Langevin equation approach.

2.1 Rouse model

The reptation theory is based on the Rouse model. Hence, it will be appropriate to briefly describe this model in order to discuss the reptation phenomena in the following chapters. The Rouse model[3] was intended to describe the basic dynamics of random coil polymers in dilute solutions. In the Rouse approach the polymer is represented by a set of beads connected by springs along a chain. Thus one can look at the polymer chain as a set of coupled harmonic oscillators which are damped by the surrounding liquid. By referring to the problem in such a simplified way one can immediately visualize the two forces which act on each bead of the chain. First the harmonic potential, which expresses the entropic free energy associated with the polymer chain conformation, and second the fluctuating random force due to the Brownian collisions of surrounding solvent molecules. Note that this model ignores the hydrodynamic interactions and excluded volume effects.

The Langevin equation which represents this model is[2]:

$$\frac{\partial}{\partial t}\boldsymbol{R}_n(t) = \sum_m \boldsymbol{H}_{nm} \cdot \left(-\frac{\partial U}{\partial \boldsymbol{R}_m} + f_m(t) \right) \tag{2.1}$$

where $\{\boldsymbol{R}_n(t)\} \equiv (\boldsymbol{R}_1, \boldsymbol{R}_2, \ldots, \boldsymbol{R}_N)$ are the vectors locating the beads at time t (figure 2.1). $\boldsymbol{H}_{nm}$ is the mobility matrix, the inverse of the friction matrix. By neglecting long range hydrodynamic interactions one can write:

$$\boldsymbol{H}_{nm} = \frac{\boldsymbol{I}}{\zeta}\delta_{nm}. \tag{2.2}$$

Where ζ is the bead friction factor and $\mathbf{I}$ is the identity matrix. The first part of the Langevin equation contains the force due to an harmonic potential $\left(-\frac{\partial U}{\partial \boldsymbol{R}} \right)$. where:

$$U = \frac{k}{2}\sum_{n=2}^{N} (\boldsymbol{R}_n - \boldsymbol{R}_{n-1})^2 \tag{2.3}$$

and

$$k = \frac{3k_B T}{b^2} \tag{2.4}$$

b being the Kuhn statistical segment.

Each bead, apart from the two terminal beads, feels the harmonic potential coming from its two adjacent neighboring beads. Thus one can write the harmonic force which acts on the internal beads $n = (2,3,\ldots,N-1)$ as:

$$-k(2\boldsymbol{R}_n - \boldsymbol{R}_{n+1} - \boldsymbol{R}_{n-1}). \tag{2.5}$$

The harmonic forces which the terminal, $n = 1$ and N, beads feel are:

$$-k(\boldsymbol{R}_1 - \boldsymbol{R}_2) \quad \text{and} \quad -k(\boldsymbol{R}_N - \boldsymbol{R}_{N-1}) \tag{2.6}$$

$f_m(t)$ is the force which represents the continuous Brownian collisions of the solvent molecules. As is standard in Langevin equation treatments, one assumes that the

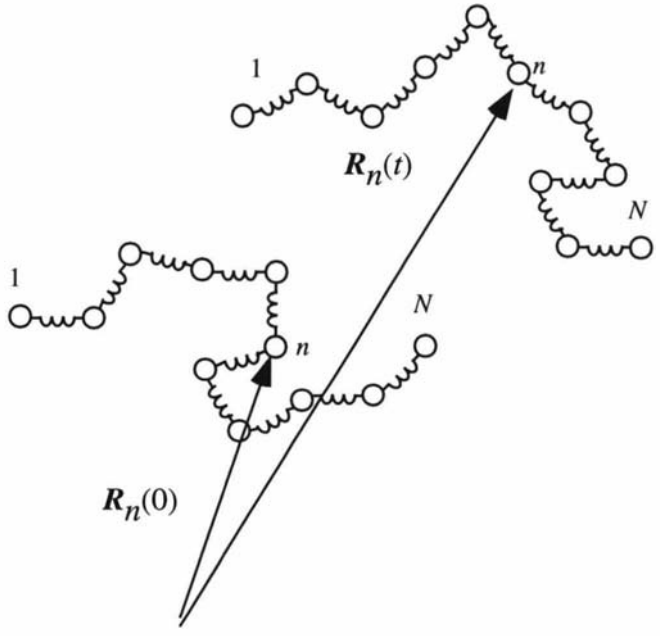

Figure 2.1:
The vector locating the *n*th bead at time 0 and time t in a Rouse chain.

distribution of the random force is Gaussian and its first and second moments are given by:

$$\langle \boldsymbol{f}_n(t) \rangle = 0$$

$$\left\langle f_{n\alpha}(t) f_{m\beta}(t') \right\rangle = 2\zeta k_B T \delta_{nm} \delta_{\alpha\beta} \delta(t-t') \cdot \tag{2.7}$$

When n is sufficiently large it can be regarded as a continuous variable, an approximation which reflects the large size of the polymer molecule. In this case Langevin equation can be written as:

$$\zeta \frac{\partial \boldsymbol{R}_n}{\partial t} = k \frac{\partial^2 \boldsymbol{R}_n}{\partial n^2} + \boldsymbol{f}_n . \tag{2.8}$$

The boundary conditions for this equation, which mimic the absence of the extra springs on the last bead in equation 2.5, are:

$$\boldsymbol{R}_0 = \boldsymbol{R}_1, \qquad \boldsymbol{R}_{N+1} = \boldsymbol{R}_N \tag{2.9}$$

hence, expressed as derivative with respect to the continuous variable n,

$$\left.\frac{\partial \boldsymbol{R}_n}{\partial n}\right|_{n=0} = 0 \qquad \left.\frac{\partial \boldsymbol{R}_n}{\partial n}\right|_{n=N} = 0. \tag{2.10}$$

The solution requires the use of normal modes, each representing an independent spatial frequency of the chain.

$$X_p \equiv \frac{1}{N} \int_0^N dn \cos\left(\frac{p\pi n}{N}\right) \boldsymbol{R}_n(t) \quad \text{with} \quad p = 0,1,2,\ldots \tag{2.11}$$

One can visualize each of the normal modes, p, as a step in resolution starting at the lowest ("resolution") mode which represent the mean position in space of beads on the polymer chain. Stepping up to higher and higher modes one can start to see the fine structure of the polymer which eventually, at the highest mode, reflects the mean change in the vector $\boldsymbol{R}_n(t)$ due to fluctuation in one segment of the polymer (figure 2.2).

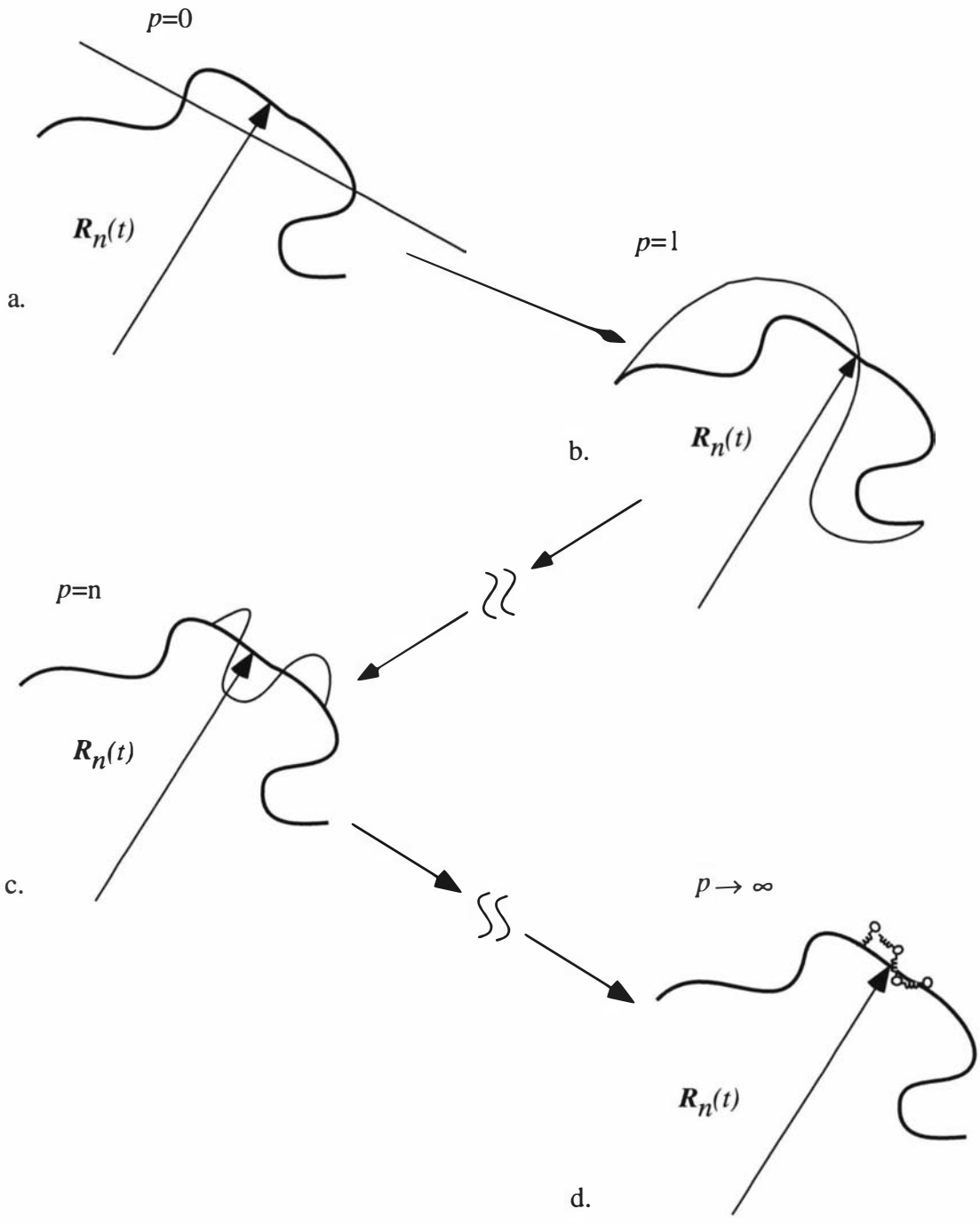

Figure 2.2:
A simple way to visualize the normal modes. The modes are essentially steps in resolution. a) p=0, is the motion of the polymer center of mass. b) p=1, c) p=n, and d) is a random motion of a single bead.

The normal modes, $X_p(t)$, simplify the Langevin equation 2.8, and lead to independent equations for each mode, p. Because equation 2.11 is a Fourier relationship the Brownian motion of coupled oscillators can be written in term of a Fourier series:

$$\boldsymbol{R}_n(t) = \boldsymbol{X}_0 + 2\sum_{p=1}^{\infty} \boldsymbol{X}_p(t)\cos\left(\frac{p\pi n}{N}\right). \tag{2.12}$$

Using the approximations of this model, the Rouse model dynamics of random polymer coil in a dilute solution can be derived. First one may express the center of mass,

$$\boldsymbol{R}_G \equiv \frac{1}{N}\int_0^N dn\boldsymbol{R}_n = \boldsymbol{X}_0. \tag{2.13}$$

Taking into account the assumption of a Gaussian distribution of the vector $\boldsymbol{R}_n(t)$ and the correlation function for $f_n(t)$ given in equation 2.7, it may be shown that:

$$\phi_G(t) = \left\langle \left(\boldsymbol{R}_G(t) - \boldsymbol{R}_G(0)\right)^2 \right\rangle = \sum_{\alpha=x,y,z} \left\langle \left(X_{0\alpha}(t) - X_{0\alpha}(0)\right)^2 \right\rangle = 6\frac{k_B T}{N\zeta} t. \tag{2.14}$$

The self diffusion constant of the center of mass is defined by:

$$D_G = \lim_{t\to\infty} \frac{1}{6t}\left\langle \left(\boldsymbol{R}_G(t) - \boldsymbol{R}_G(0)\right)^2 \right\rangle = \frac{k_B T}{N\zeta}. \tag{2.15}$$

The mean square displacement of an individual segment, n, is represented by:

$$\phi_n(t) = \left\langle \left(\boldsymbol{R}_n(t) - \boldsymbol{R}_n(0)\right)^2 \right\rangle \tag{2.16}$$

where the segmental average mean square displacement is:

$$\phi(t) = \frac{1}{N}\sum_{n=1}^{N} \left\langle \left(\boldsymbol{R}_n(t) - \boldsymbol{R}_n(0)\right)^2 \right\rangle. \tag{2.17}$$

The Rouse solution for the segmental mean square displacement in eq. 2.8 with the boundary conditions given in eq. 2.9 & 2.10 is:

$$\phi_n(t) = \left\langle \left(\boldsymbol{R}_n(t) - \boldsymbol{R}_n(0) \right)^2 \right\rangle$$
$$= 6D_G t + \frac{4Nb^2}{\pi^2} \sum_{p=1}^{\infty} \frac{1}{p^2} \cos^2\left(\frac{p\pi n}{N} \right) \left(1 - \exp(-tp^2 / \tau_R) \right) \qquad (2.18)$$

τ_R is the terminal relaxation time of the end to end vector $\tau_R = \zeta N^2 b^2 / 3\pi^2 k_B T$.

Note, two limiting cases can be identified for the segmental average mean square displacement, $\phi(t)$.
When $t \leq \tau_R$,

$$\phi(t) \propto t^{1/2} \qquad (2.19)$$

and when $t \geq \tau_R$,

$$\phi(t) \propto t. \qquad (2.20)$$

Eq. 2.19 shows that below the terminal relaxation time, the polymer segments diffuse with a fractal time exponent. This reflects the fact that at $t \leq \tau_R$, the polymer motion is dominated by its internal modes. The fact that above the terminal relaxation time, the mean square displacement of the polymer segment is linear in time, indicates that in this regime the displacements are dominated by the center of mass diffusion of the polymer.

It is important to note that neglect of hydrodynamic interactions and the excluded volume effect simplifies the treatment of polymer chain dynamics in dilute solution at the expense of accuracy. In fact, there is a poor agreement between the Rouse theory and the experimental results for dilute solutions. The Zimm model[2] takes into account these important interactions and successfully overcomes the discrepancies between theory and experimental work, but at the expense of simplicity. However, even though the Rouse model fails to describe accurately the case of a polymer coil in a dilute solution it becomes much more accurate when the hydrodynamic and excluded volume effects are screened. This is the case for semidilute and concentrated solutions.

2.2 The Reptation model

The reptation model for entangled polymer dynamics was first proposed by de Gennes in 1971[1]. The model utilizes the tube concept presented by Edwards in 1967[8,9]. Eventually Doi & Edwards translated the reptation ideas to a self-consistent set of quantitative equations and scaling laws[2]. In this chapter, I will describe the reptation theory in more detail so that one can understand the origin of the various scaling laws which are characteristic of the model.

In order to build the theory some assumptions have to be made:

1) The intrinsic properties of the polymer are considered to arise from a Rouse chain consisting N segments with statistical segment length b and friction coefficient ζ.

2) The obstacles, presented by other chains, are assumed to be thin lines which have no effect on static properties but have a major effect on dynamical properties by imposing topological constraints.

Consider a particular (e.g. labeled) polymer chain entangled with the neighboring chains (figure 2.3a). The primitive path is the shortest path connecting the two ends of the chain with the same topology as the chain itself relative to the obstacles. As shown in figure 2.3b, we can regard the primitive path as a thin line positioned at the center of the diameter of the tube which those obstacles create. The polymer motion may be resolved into components of displacement transverse to the primitive path, and components along the primitive path. At this point we shall concern ourselves mostly with the latter and for this purpose we need only consider the motion of a primitive chain.

The dynamics of the primitive chain are characterized by the following assumptions:

(i) The primitive chain has constant contour length L.

(ii) The primitive chain can move in Brownian motion back and forth only along the primitive path with a one dimensional curvilinear diffusion constant D_c.

(iii)The correlation of the tangent vectors to the primitive path, $\boldsymbol{u}(s,t)$ and $\boldsymbol{u}(s',t)$, decreases quickly with $|s-s'|$, reflecting the fact that the primitive path is a "random flight".

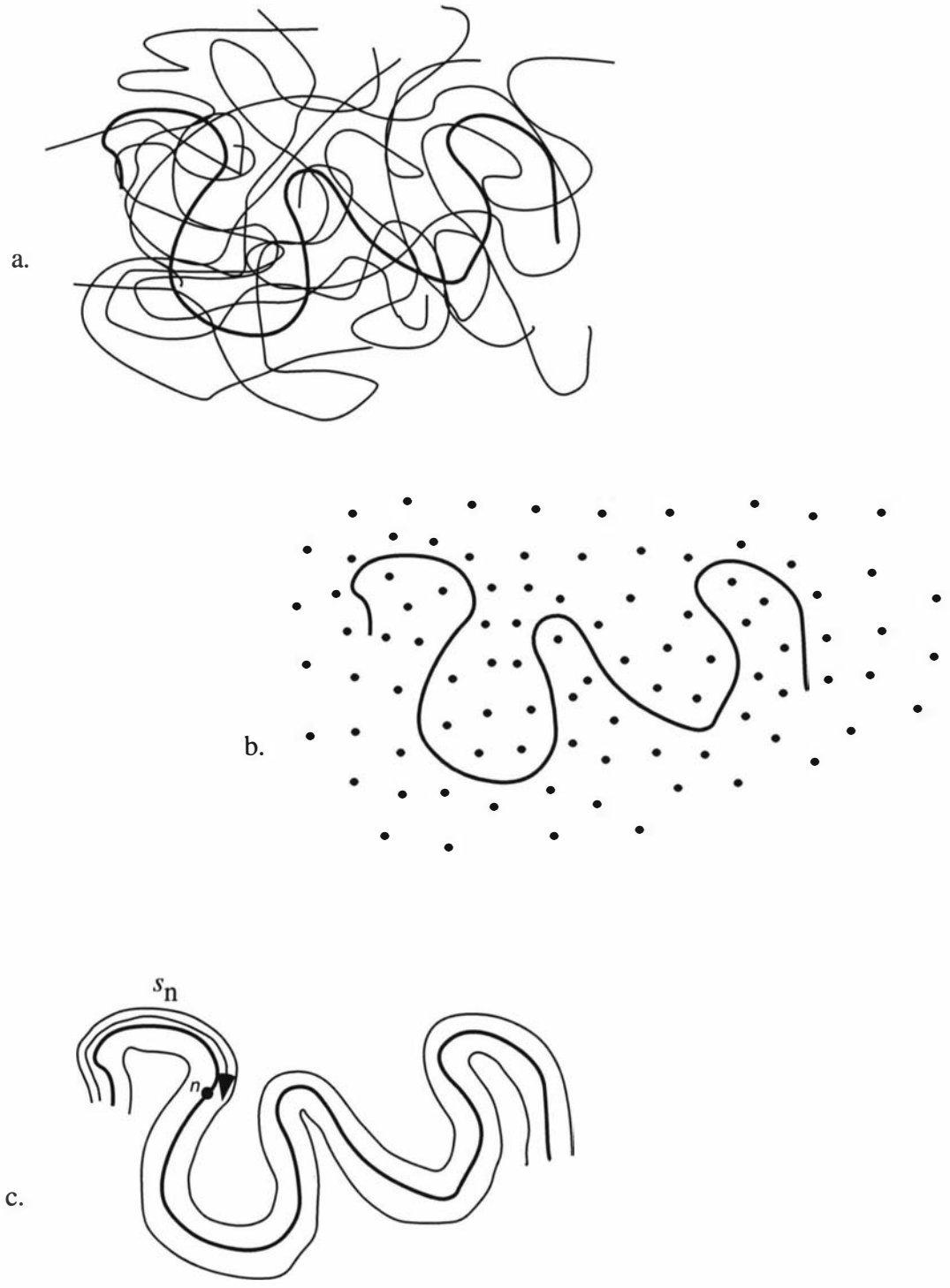

Figure 2.3:
The tube model. a) A random coil polymer chain in either a melt state or semidilute solution. The polymer coil is entangled with the surrounding polymer matrix. b) The polymer chain inside the tube which was created by the entanglement (the dots). c) The primitive path and the contour length, s_n, along it.

As shown in figure 2.3c, s, is the contour length measured from the chain end to a point on the primitive path. With the assumption of a Gaussian distribution of the end to end vector, the mean square displacement is written :

$$\left\langle (\boldsymbol{R}(s,t) - \boldsymbol{R}(s',t))^2 \right\rangle = a|s - s'| \quad \text{for } |s - s'| >> a \tag{2.21}$$

a is a fitted parameter which relates the curvilinear displacement, $|s - s'|$, to the straight vector, $(\boldsymbol{R}(s,t) - \boldsymbol{R}(s',t))$, that connects the two segments. This fitted parameter gives an impression of the diameter of the tube that confines the curvilinear path.

When seeking to derive the dynamical properties of a polymer in entangled environment it is helpful to visualize the polymer at different resolutions. When we view the motion at short time scales we can see the rapid motion of the polymer segments in their fluctuation around the primitive path. When we look at the motion with a coarser length scale, or equivalently, at long time scale, the fluctuations about the primitive path are averaged and we can only see the segment motion along the primitive path.

We first consider the long range motion of the polymer chain as shown in figure 2.4. The first figure, 2.4a, shows the initial tube as defined at the time of origin. Subsequently, the polymer segments start to diffuse along the tube, creating a new tube on the left, and destroying the right hand end of the tube (2.4b). The polymer continues to diffuse back and forth creating a new tube on the right while destroying the original tube on the left (2.4c,d) and eventually, the original tube is gone. Note that the last part to be destroyed is the center of the tube. The mean square displacement, $\left\langle \left\langle (\boldsymbol{R}(s,t) - \boldsymbol{R}(s,0))^2 \right\rangle \right\rangle \equiv \phi(s,s;t)$, of a segment located at a curvilinear position s, in the long range motion, can be evaluated by simply looking at one segment as it diffuses the distance $\Delta\xi$ on the primitive path, at the time interval Δt. A convenient way to calculate the mean square displacement is by first solving the diffusion equation using the general time correlation function $\phi(s,s';t) = \left\langle (\boldsymbol{R}(s,t) - \boldsymbol{R}(s',0))^2 \right\rangle$ and later converting the result to $\phi(s,s;t)$. This calculation must take under consideration the fact that if $s + \Delta\xi$ is not between 0 and L then the segment is on a newly created part of the tube, which can be expressed by writing the boundary conditions as follows:

$$\frac{\partial}{\partial s}\phi(s,s';t) = \frac{\partial}{\partial s}a(s - s')\Big|_{s=L} = a \qquad \text{at} \quad s = L \tag{2.22}$$

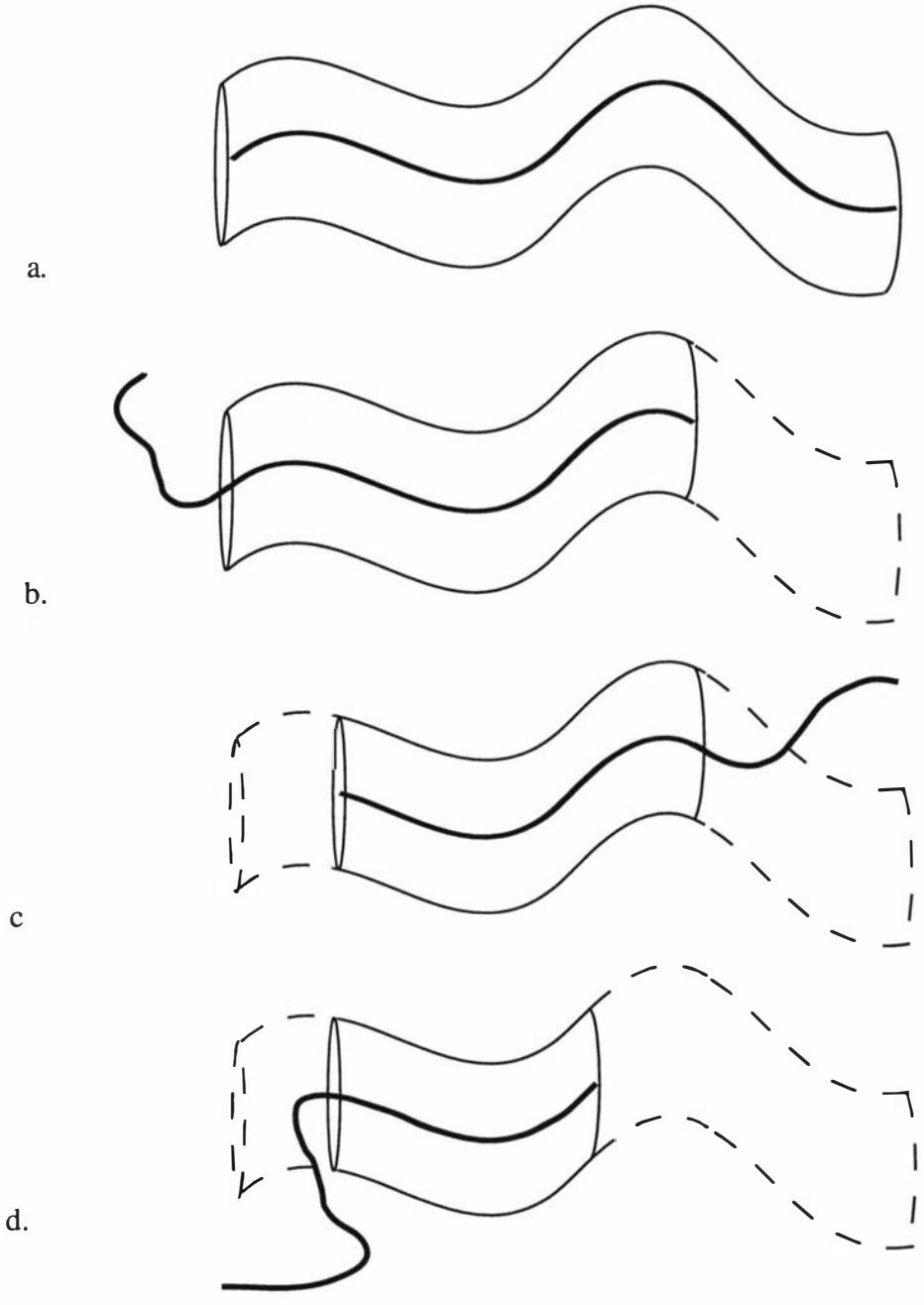

Figure 2.4:
Motion of a polymer chain according to the reptation theory. a)The initial tube as defined at t=0. b) The polymer segments diffuse along the tube. As a consequence a new tube was created on the left and the right side of the tube was destroyed. c,d) The polymer continues to diffuse back and forth creating a new tube on the right while destroying the original tube on the left until eventually, the original tube will be totally destroyed.

and

$$\frac{\partial}{\partial s}\phi(s,s';t) = -a \qquad \text{at} \quad s = 0. \tag{2.23}$$

The solution of the diffusion equation:

$$\frac{\partial}{\partial t}\phi(s,s';t) = D_c \frac{\partial^2}{\partial s^2}\phi(s,s';t) \tag{2.24}$$

with the boundary condition and the initial condition eq. 2.21 is[2]:

$$\phi(s,s';t) = |s-s'|a + 2\frac{a}{L}D_c t + \frac{4La}{\pi^2}\sum_{p=1}^{\infty}\frac{1}{p^2}\cos\left(\frac{p\pi s}{L}\right)\cos\left(\frac{p\pi s'}{L}\right)\left[1-\exp(-tp^2/\tau_d)\right]. \tag{2.25}$$

Thus when s=s':

$$\phi(s,s;t) = \frac{2}{Z}D_c t + \frac{4La}{\pi^2}\sum_{p=1}^{\infty}\frac{1}{p^2}\cos^2\left(\frac{p\pi s}{L}\right)\left[1-\exp(-tp^2/\tau_d)\right] \tag{2.26}$$

τ_d defines the tube lifetime and is called the tube disengagement time. It is given by[2]:

$$\tau_d = L^2 / D_c\pi^2. \tag{2.27}$$

Note that $\tau_d = 3Z\tau_R$ where $Z = L/a = Nb^2/a^2$ is the number of steps on the primitive path. The factor of $3Z$ increase of τ_d over the Rouse time, reflects in part the one dimensional nature of reptation diffusion in the curvilinear path (factor of 3) and the topological constraint of the tube (factor of Z).

As we can see, this equation is very similar to equation 2.18 in the previous section. In a sense this is not surprising since we used a Rouse chain to derive this model. Indeed the underlying Rouse motion means that one can identify D_c as the diffusion coefficient of the Rouse model:

$$D_c = k_B T / N\zeta \tag{2.28}$$

When $t \ll \tau_d$ the dominant term in the eq. 2.26 is the second part of the equation. Averaging over s, $\cos^2(p\pi s/L)$ can be replaced with 1/2 and, by converting the sum into an integral, one gets:

$$\phi(s,s:t) = 2a\left(\frac{D_c}{\pi}\right)^{1/2} t^{1/2}. \tag{2.29}$$

Consequently, the mean square displacement scales as $t^{1/2}$. When $t > \tau_d$ the first term of eq. 2.26 is dominant and hence the equation can be written as:

$$\phi(s,s:t) = 2\frac{D_c}{Z}t. \tag{2.30}$$

The diffusion constant, D_G, of the center of mass is given as:

$$D_G = \lim_{t\to\infty}\frac{\phi(s,s;t)}{6t} = \frac{D_c}{3Z} = \frac{k_B T a^2}{3N^2\zeta b^2}. \tag{2.31}$$

Thus the self-diffusion coefficient is proportional to N^{-2} and hence to M^{-2}, where M is the polymer molar mass. We can see that in the limit $t >> \tau_d$, the rms segmental displacement is much larger than the polymer dimension and hence dominated by center of mass diffusion, in agreement with the Stokes-Einstein equation for which the mean square displacement scales linearly with time.

As previously stated the shortest time scale of motion comprises the fluctuations around the primitive path. The segmental displacement equations which may be derived for this case are based on the dynamics of a free Rouse chain, for displacement up to, but not, beyond the tube diameter a. When the polymer segments diffuse a distance much smaller than the tube diameter they cannot feel the constraints and the free three dimensional Rouse chain equation applies:

$$\phi(t) = \left\langle \left(\boldsymbol{R}_n(t) - \boldsymbol{R}_n(0)\right)^2 \right\rangle = 6D_c t + \frac{4Nb^2}{\pi^2}\sum_{p=1}^{\infty}\frac{1}{p^2}\cos^2\left(\frac{p\pi n}{N}\right)\left[1 - \exp(-tp^2/\tau_R)\right] \tag{2.32}$$

τ_e is the time at which the segmental displacement reaches the dimension of the tube diameter, a, and is given by $\tau_e \cong a^4\zeta / k_B T b^2$.

Once the polymer mean square displacement reaches the dimension of the tube diameter the perpendicular motion to the primitive path of the Rouse segment is restricted, but the motion along the primitive path is free. The simplest way to describe this motion is to represent it as a one dimensional Rouse motion on the curvilinear primitive path. The normal modes will be as for 3D Rouse dynamics except for exchanging the vector $\boldsymbol{R}_n$, in the previous calculation, with s_n-(the curvilinear coordinate of the nth Rouse segment measured from a certain fixed point on the tube) and by reducing the dimensionally factor from 3 to 1.

$$Y_p = \frac{1}{N}\int_0^N dn \cos\left(\frac{p\pi n}{N}\right) s_n(t) \qquad \text{for} \qquad p=1,2,\ldots, \tag{2.33}$$

The mean square displacement along the tube is:

$$\left\langle \left(s_n(t) - s_n(0)\right)^2 \right\rangle = 2\frac{k_B T}{N\zeta} t + \frac{4Nb^2}{3\pi^2} \sum_{p=1}^{\infty} \frac{1}{p^2} \cos^2\left(\frac{p\pi n}{N}\right) \left[1 - \exp(-tp^2 / \tau_R)\right] \tag{2.34}$$

τ_R is the Rouse relaxation time. In order to translate this relation to the laboratory frame one may write:

$$\phi_n(t) = \frac{1}{N}\sum_{n=1}^{n} \left\langle \left(R_n(s,t) - R_n(s,0)\right)^2 \right\rangle = a\left\langle \left| s_n(t) - s_n(0) \right| \right\rangle \cong a\left\langle \left(s_n(t) - s_n(0)\right)^2 \right\rangle^{1/2}. \tag{2.35}$$

Note that equations 2.34 and 2.35 predicts $\phi(t) \sim t^{\frac{1}{4}}$ for $\tau_e \le t \le \tau_R$ and $\phi(t) \sim t^{\frac{1}{2}}$ for $t \ge \tau_R$. This latter behavior corresponds to the $t^{\frac{1}{2}}$ region $\left(t \ge \tau_R\right)$ of equation 2.26.

The mean square displacement for regimes II to IV (see figure 2.5) can be written as:

$$\phi(t) = 2\frac{D_c}{Z}t + \left(\frac{2}{\pi}\right)^{1/2} a\left\{\left(\frac{2Nb^2}{a\pi}\sum_{p=1}^{\infty}\frac{1}{p^2}\frac{1}{2}\times\left(1-\exp\left(-tp^2/\tau_d\right)\right)\right)^2 + \frac{4Nb^2}{3\pi^3}\sum_{p=1}^{\infty}\frac{1}{p^2}\frac{1}{2}\times\left(1-\exp\left(-tp^2/\tau_R\right)\right)\right\}^{1/2} \tag{2.36}$$

and the reptation dynamics can be summarized as follows (figure 2.5):

$$\phi(t) \cong \begin{cases} Nb^2(t/\tau_R)^{1/2} & t \le \tau_e \\ Nb^2(t/Z^2\tau_R)^{1/4} & \tau_e \le t \le \tau_R \\ Nb^2(t/\tau_d)^{1/2} & \tau_R \le t \le \tau_d \\ Nb^2(t/\tau_d) & \tau_d \le t \end{cases} \tag{2.37}$$

2.3 Rheology

Rheology is the science of deformation and flow of matter[10] and is concerned with the measurement of viscous and elastic responses to a mechanical deformation. Viscoelastic materials are materials which are have both viscous (energy loss) and elastic (energy storage) properties. Polymer melts and solutions are examples of such materials.

Although most of the data and the associated theory dealt with in this research concern the equilibrium (undeformed) state, many of the fundamental properties of random polymer coils, which are predicted both by the reptation theory and the Rouse model, can be observed by measuring the viscoelasticity. In this thesis some viscoelasticity data are presented in order to provide an independent check on parameters measured by NMR. Consequently we will dedicate a short chapter to describing aspects of rheology which are relevant to this work.

In order to deform a material it is necessary to apply stress, which is the tensorial pressure, σ. The deformation relative to a reference configuration of length, area or volume is called the strain, γ[10]. The constitutive equation relates the stress tensor to the rate of strain. For small deformation the response of most systems is linear and the linear constitutive equation is based on the principle that the effect of sequential changes in strain are additive:

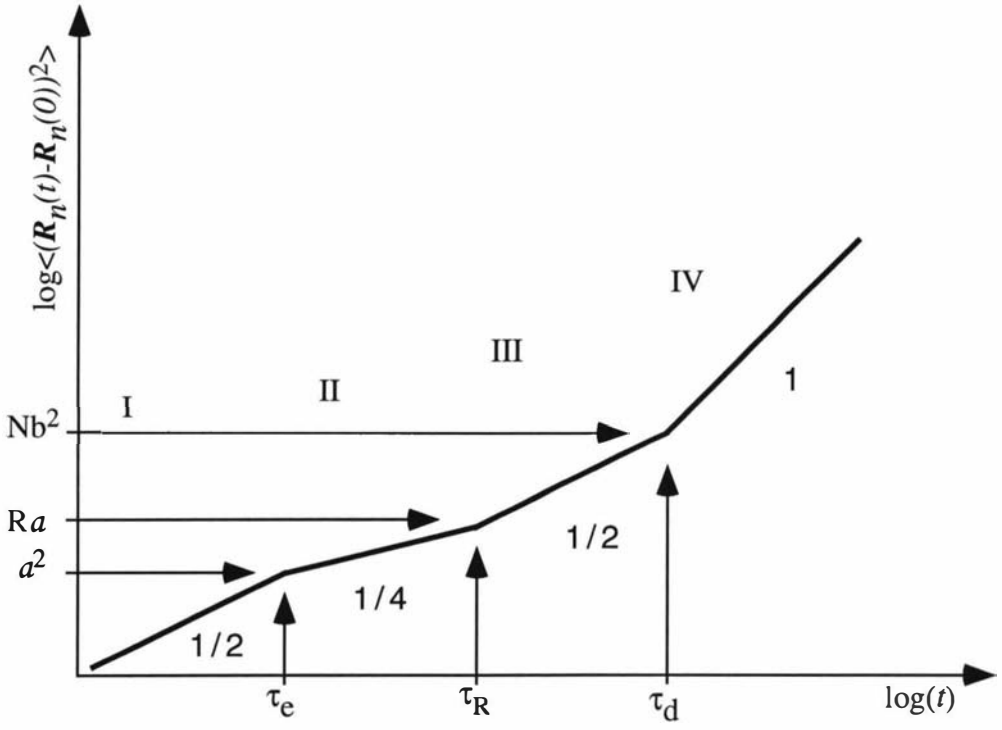

Figure 2.5[2]:
Schematic graph of regimes I to IV.

$$\sigma_{\alpha\beta}(t) = \int_{-\infty}^{t} G(t-t') \frac{d\gamma_{\alpha\beta}(t')}{dt} dt' \tag{2.38}$$

where $G(t-t')$ represents a "memory function". The same equation, after rearrangement under integration by parts, can be rewritten as[2]:

$$\sigma_{\alpha\beta}(t) = -\int_{-\infty}^{t} \frac{dG(t-t')}{dt} \gamma_{\alpha\beta}(t,t') dt' . \tag{2.39}$$

The memory function, $G(t)$, is known as the relaxation modulus, and represents the decay of the stress following a step strain. From a knowledge of the shear relaxation modulus of a particular material, stress-strain relations for any kind of linear experiment can be predicted provided the deformation is sufficiently small and/or sufficiently slow[11].

Under deformation flow, the stress, i.e. the tensorial pressure, $\sigma_{\alpha\beta}$ associated with a polymer in solution, can be expressed as:

$$\sigma_{\alpha\beta}(t) = \left(\frac{\partial v_{\alpha}(t)}{\partial r_{\beta}} + \frac{\partial v_{\beta}(t)}{\partial r_{\alpha}} \right) \eta_s + \sigma_{\alpha\beta}^{(p)}(t) + P\delta_{\alpha\beta} \tag{2.40}$$

where $\alpha,\beta,...$ are the Cartesian directions and $\frac{\partial v_{\alpha}}{\partial r_{\beta}}$ is a velocity gradient. The first term of the equation is the contribution of the solvent to the stress, were $\eta_s = \int G(t)dt$ is the viscosity of the solvent for the linear regime. The second term $\sigma_{\alpha\beta}^{(p)}$ represents the contribution of the polymer to the stress. This part of the stress comes from the force that one bead applies to another. Doi and Edwards show that this polymer contribution can be represented by an ensemble average on the product of the force acting on a segment n, and its displacement.

$$\sigma_{\alpha\beta}^{(p)} = -\frac{c_B}{N} \sum_{n=1}^{N} \left\langle F_{n\alpha} R_{n\beta} \right\rangle \tag{2.41}$$

where $F_m = \sum_n F_{mn}$ is the sum of the non hydrodynamics force acting on bead m, R_m is the position of bead m, c_B is the concentration of a bead and N is numbers of beads. In the continuous limit

$$\sigma_{\alpha\beta}^{(p)} = \frac{c_B}{N}\frac{3k_BT}{b^2}\int_0^N dn\left\langle \frac{\partial R_{n\alpha}}{\partial n}\frac{\partial R_{n\beta}}{\partial n}\right\rangle. \tag{2.42}$$

by using the same normal coordinates as in the Rouse and reptation model we get:

$$\sigma_{\alpha\beta}^{(p)} = \frac{c_B}{N}\frac{3k_BT}{b^2}\sum_p \frac{2p^2\pi^2}{N}\left\langle X_{p\alpha}(t)X_{p\beta}(t)\right\rangle. \tag{2.43}$$

The third term in equation 2.40 refers to the contribution of an isotropic pressure to the stress. In the case of a polymer solution there is always a competition between the first and second terms. In case of very dilute polymer solutions the first term dominates the equation since the hydrodynamic force is big. At higher concentrations the second term increases while the first term is unchanged. For semidilute, concentrated solutions and melts the second term is the only significant term in the equation.

In the case of polymeric liquids, the constitutive equation is quite complicated and generally non linear. However, when one applies a small deformation to the polymer the stress will be linearly dependent on $\dot{\gamma}(t)$ and can be written as:

$$\sigma_{\alpha\beta}^{(p)}(t) = \int_{-\infty}^{t} dt'\, G(t-t')\left(\dot{\gamma}_{\alpha\beta}(t') + \dot{\gamma}_{\beta\alpha}(t')\right) \tag{2.44}$$

where $G(t)$ is the shear relaxation modulus.

There are several ways to measure the relaxation modulus and each relates to the way the material is deformed. Presented here are three common deformations and their associated stress responses.

1. stepwise shear(figure 2.6a)[2]. This is a transient experiment in which the sample is deformed instantaneously at time $t = 0$ and then the response is recorded while relaxing back to the equilibrium state. The shear strain $\gamma(t)$ is given by:

$$\gamma(t)=\begin{cases}0 & t<0,\\ \gamma_0 & t>0,\end{cases} \tag{2.45}$$

For small deformation the corresponding stress is linear:

$$\sigma_{xy}(t)=\gamma_0 G(t). \tag{2.46}$$

This provides a direct determination of $G(t)$.

2. oscillatory shear (figure 2.6b)[2]. This is also a linear experiment in which the shear strain is alternating in constant frequency ω and the stress is changing accordingly.

$$\gamma(t)=\gamma_0\cos(\omega t)=\gamma_0\,\mathrm{Re}\left(e^{i\omega t}\right). \tag{2.47}$$

The response to this type of deformation defines the storage modulus $G'(\omega)$, loss modulus $G''(\omega)$, and the complex modulus $G^*(\omega)$,

$$\sigma_{xy}(t)=\gamma_0\left(G'(\omega)\cos(\omega t)-G''(\omega)\sin(\omega t)\right)=\gamma_0\,\mathrm{Re}\left(G^*(\omega)e^{i\omega t}\right) \tag{2.48}$$

where

$$G^*(\omega)=G'(\omega)+iG''(\omega) \tag{2.49}$$

and

$$G'(\omega)=\omega\int_0^\infty dt\sin(\omega t)G(t) \qquad G''(\omega)=\omega\int_0^\infty dt\cos(\omega t)G(t) \tag{2.50}$$

3. steady shear flow(figure 2.6c)[2,11]. In this case one applies a constant strain rate $\dot{\gamma}$. The stress during steady, sufficiently slow, flow is determined from:

$$\eta=\sigma_{xy}\frac{1}{\dot{\gamma}}. \tag{2.51}$$

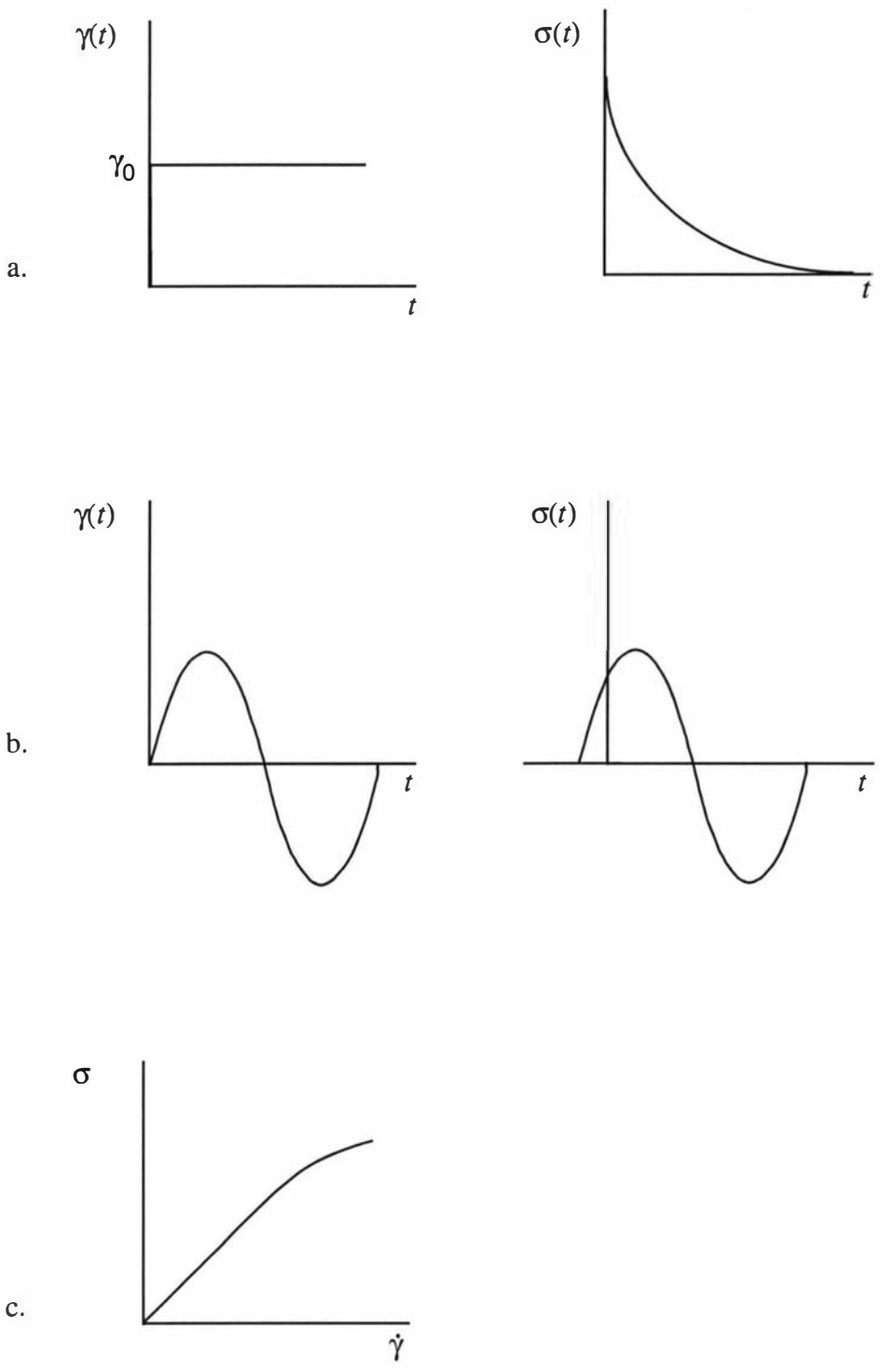

Figure 2.6:
Three rheology experiments, their shear strain and their stress response. a) stepwise shear b) oscillatory shear and c) steady shear flow.

Steady shear involves unbounded strain and is therefore highly non-linear. In the limit as $\dot{\gamma} \to 0$ however, linear response theory can be used. Since in semi-dilute and concentrated solutions the only term which contributes to the viscosity is due to the polymer, the viscosity in the limit $\dot{\gamma} \to 0$, can be expressed also by:

$$\eta = \int_0^\infty dt G^{(p)}(t). \tag{2.52}$$

We now turn to the rheological implications of the Rouse and reptation models. First, the Rouse model is discussed. Note that even though this model describes the dynamics of a polymer coil in dilute solution, it neglects the solvent interaction so in fact only the polymer term is considered as a contribution to the viscosity. According to the Rouse model[3]:

$$\langle X_{px} X_{py} \rangle = \frac{Nb^2}{6\pi^2 k_B T p^2} k_B T \int_{-\infty}^{t} dt' \exp(t'/\tau_R)\dot{\gamma}(t') \tag{2.53}$$

By substituting equation 2.43 and 2.44, one can extract the relaxation modulus $G^{(p)}(t)$:

$$G^{(p)}(t) = \frac{c_k}{N} k_B T \sum_{p=1}^{\infty} \exp(-2tp^2/\tau_R) \tag{2.54}$$

where τ_R is the Rouse relaxation time,

$$\tau_R = \frac{\zeta N^2 b^2}{3\pi^2 k_B T}. \tag{2.55}$$

Thus the zero shear viscosity is[2]:

$$\eta_0 = \int_0^t dt G(t) = \frac{c_k}{N} k_B T \frac{1}{2} \tau_R \sum_{p=1}^{\infty} p^{-2} = \frac{\pi^2}{12}\left(\frac{c_k k_B T}{N}\right)\tau_R = \frac{c_k \zeta}{36} N b^2. \tag{2.56}$$

This equation yields the scaling law:

$$\eta_0 \propto cM \tag{2.57}$$

where c is the polymer weight per unit volume:

$$c \equiv \frac{c_k M}{N N_A}. \tag{2.58}$$

The relaxation modulus can be directly measured by a step shear method. $G(t)$, and should change with time according to the different regimes the theory predicts. The first regime is on the time scale of $t \leq \tau_e$. At such short times the polymer segment does not feel the entanglements constraints and thus follows unconstrained Rouse dynamics. The relaxation modulus is similar to eq. 2.54, and approximated:

$$G(t) = \frac{c_k}{N} k_B T \int_0^\infty dp \exp\left(-2tp^2 / \tau_R\right) = \frac{c_k}{2\sqrt{2}N} k_B T \left(\frac{\tau_R}{t}\right)^{1/2}. \tag{2.59}$$

When $t \geq \tau_e$, the reptational behavior starts and the unconstrained Rouse model no longer can be applied. From this time onward two processes are in progress. The first one is the relaxation of the contour length from the deformed tube to the original equilibrium state, characterized by the relaxation time, τ_R, and the second process is the actual disengagement of the polymer segments from the deformed tube, characterized by the tube disengagement time, τ_d. However, in the linear regime i.e. when a small deformation (γ) is applied, only the tube orientation is deformed. The change of the contour length is negligible and as a consequence the viscoelasticity in this regime is governed only by the tube disengagement process (figure 2.7). The relaxation modulus of the disengagement process will be proportional to the fraction of the polymer coil, $\psi(t)$, which is still confined in the deformed tube at time $t > \tau_e$,:

$$G(t) = G_N^{(0)} \psi(t). \tag{2.60}$$

Where $G_N^{(0)}$ is the plateau modulus and $\psi(t)$ is:

$$\psi(t) = \sum_{p;odd} \frac{8}{p^2 \pi^2} \exp\left(-p^2 t / \tau_d\right) \tag{2.61}$$

with

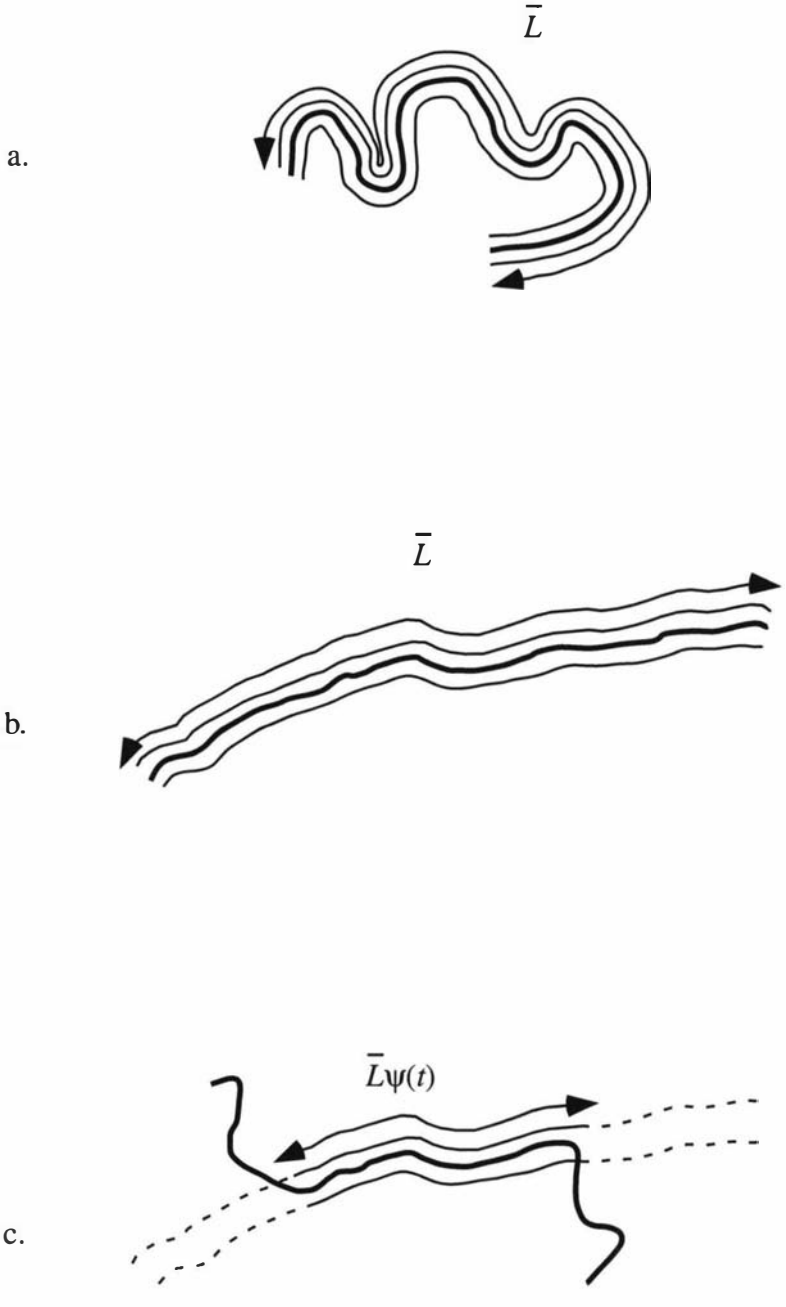

Figure 2.7:
a) The undeformed tube and b) the deformed tube. Note, the deformation is influencing only the orientation of the tube. The contour length remains constant at all time. c) the vicoelasticity is governed by reptative motion. Stress is relaxed as the deformed tube memory is lost.

$$\tau_d = \frac{\zeta N^3 b^2}{\pi^2 k_B T}\left(\frac{b}{a}\right)^2. \tag{2.62}$$

The zero shear steady state viscosity can be calculated:

$$\eta_0 = \int_0^\infty G(t)dt = G_N^{(0)} \int_0^\infty dt\psi(t) = \frac{\pi^2}{12} G_N^{(0)} \tau_d \tag{2.63}$$

and by assuming that $G_N^{(0)} \cong G(\tau_e)$, the plateau modulus can be expressed as:

$$G_N^{(0)} \cong G(\tau_e) \cong \frac{c_k}{N} k_B T \left(\frac{\tau_R}{\tau_e}\right)^{1/2} \tag{2.64}$$

and eq 2.59 can be written as:

$$G(t) \cong G_N^{(0)} \left(\frac{\tau_e}{t}\right)^{1/2}. \tag{2.65}$$

Replacing τ_e with $\tau_e \cong a^4\zeta / k_B T b^2$ one obtains

$$G_N^{(0)} \cong \frac{c_k b^2}{a^2} k_B T. \tag{2.66}$$

When a step shear instrument is not available, other methods can be applied. The tube disengagement time, the tube diameter and the plateau modulus can be obtained by measuring the storage modulus doing the oscillatory shear experiment. Combining equations 2.50, 2.60 and 2.65 gives the storage modulus (figure 2.8):

$$G'(\omega) = G_N^{(0)} \left(\frac{\pi}{2}\omega\tau_e\right)^{1/2} \qquad \text{for} \quad \omega\tau_e \geq 1 \tag{2.67}$$

$$= G_N^{(0)} \sum_{p:odd} \frac{8}{\pi^2}\frac{1}{p^2}\frac{\left(\omega\tau_d / p^2\right)^2}{1+\left(\omega\tau_d / p^2\right)^2} \qquad \text{for} \quad \omega\tau_e \leq 1 \tag{2.68}$$

One important parameter which can be obtained by knowing the plateau modulus, is the tube diameter, a. Since

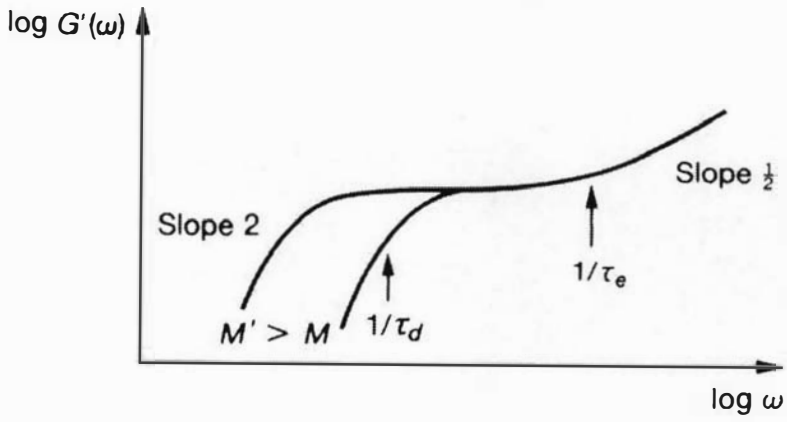

Figure 2.8[2]:
Theoretical results of the Doi-Edwards model for the storage modulus.

$$c_k b^2 = \frac{c_k}{N} N b^2 = \frac{c N_A}{M} N b^2 \tag{2.69}$$

eq. 2.66 can be written:

$$G_N^{(0)} \cong \frac{cRT}{M} \frac{Nb^2}{a^2}. \tag{2.70}$$

Experimentally the plateau modulus is often expressed by a characteristic molecular weight M_e, called the molecular weight between entanglements, which is defined by:

$$M_e = \frac{cRT}{G_N^{(0)}}. \tag{2.71}$$

Combining eq. 2.70 and 2.71:

$$a \cong \left(\frac{M_e}{M} N b^2 \right)^{1/2} \equiv \overline{R}_{M_e}. \tag{2.73}$$

Alternatively, the tube disengagement time can be calculated by measuring the viscosity in the steady shear flow experiment. According to the independent alignment assumption of the Doi and Edwards model[2]:

$$\eta \cong \eta_0 h^{IA}(\dot{\gamma}\tau_d) \tag{2.73}$$

and

$$\sigma_{xy} \cong G_e \dot{\gamma}\tau_d h^{IA}(\dot{\gamma}\tau_d) \tag{2.74}$$

$h^{IA}(\dot{\gamma}\tau_d)$ is the damping function. The relation between τ_d and $\dot{\gamma}$ can be obtained by comparison of the theoretical curve and experiment values (figure 2.9):

$$\tau_d \cong \frac{6}{\dot{\gamma}^*} \tag{2.75}$$

where $\dot{\gamma}^*$ is the shear rate at which the viscosity drops to $0.1\eta_0$.

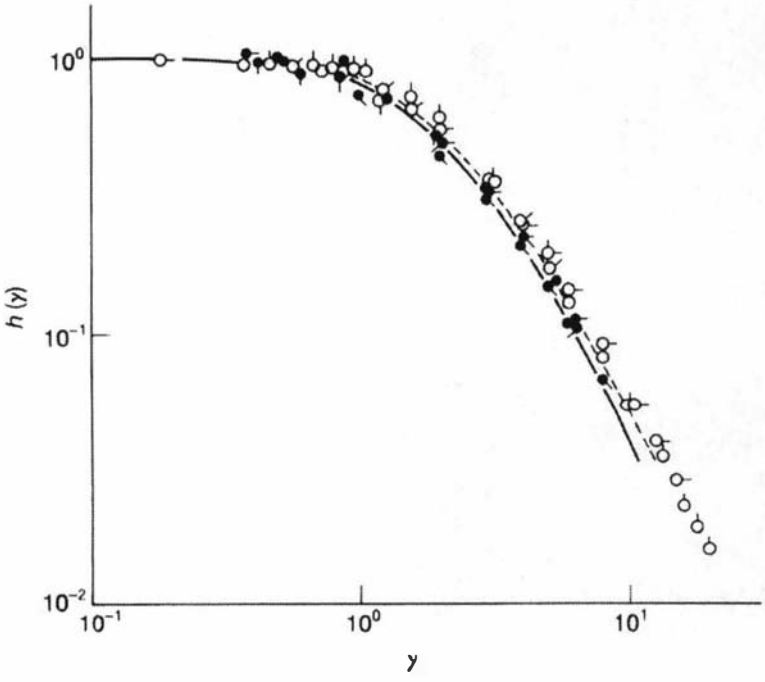

Figure 2.9[2]:
$h(\gamma)$ *vs* γ. Filled circles represent polystyrene of molecular weight 8.42×10^6 and the unfilled circles of 4.48×10^6. Directions of pips indicate concentrations which range from 0.02 g cm^{-3} to 0.08 g cm^{-3}. The dashed curve represents the results of the independent alignment approximation.

2.4 Concentration dependence

Polymer solutions are divided into three categories, namely dilute, semidilute and concentrated. Dilute solutions are characterized by low concentration in which the polymer segments on different molecules are well separated and only weakly interact. In dilute solution hydrodynamic interactions govern the polymer's dynamics and the Zimm[2] model applies. Semidilute solutions are characterized by a concentration in which the polymer segments overlap $(c > c^*)$ but still occupy a small volume fraction. Thus beyond a correlation length ξ, the excluded volume and the hydrodynamic interactions are screened and the polymer dynamics follow again the Rouse model[2]. The excluded volume screening length can be expressed as[12]:

$$\xi_c \approx b g^{\upsilon_c} \sim \varphi^{-\upsilon_c/(3\upsilon_c - 1)} \qquad (2.76)$$

where g is the number of Kuhn segments in the correlation length, φ is the polymer volume fraction and b is a Kuhn segment. $\upsilon_c = 1/2$ in case of θ solutions (in which the excluded volume interaction is screened and the chain is not swollen) and $\upsilon_c = 3/5$ in case of semidilute solutions where the chain is highly swollen.

In both, dilute and semidilute solutions, the fluctuations in the concentration are large. The concentrated region is the region in which fluctuations become small and a simple mean field theory[2] applies. In our discussion we will disregard the first and last groups and concentrate on the semidilute region and how the change of concentration influences some of the reptation parameters. Our goal is to derive the relationship between the concentration, the diffusion coefficient and the tube disengagement time. The key to understanding those relations lies in scaling both the microscopic parameter a (which is the mesh size between entanglement or the tube diameter)[12] and the end to end distance with concentration.

The end to end distance in the semidilute regime is swollen because of the excluded volume interactions. The statistical properties of the swollen state have been worked out by Flory[13] and as a result the end to end distance can be written according to equation 2.76. $\upsilon_c = 3/5$ and $b = \tau^{1/5} n^{1/5} a_m$ where n is the number of monomers size a_m in the Kuhn segment. $\tau = \dfrac{(T-\theta)}{T}$ is the reduced temperature. In the case of theta solvents there are no excluded volume interactions and any length scale follows a

Gaussian distribution thus $\upsilon_c = 1/2$ and $b = n^{1/2}a_m$. For convenience we assume that the number of monomers in ξ_c and ξ_H is identical. Note that ξ_H is a dynamical length which is used for calculation of the monomer friction coefficient and may be written:

$$\xi_H \approx bg^{\upsilon_H} \sim \varphi^{-\upsilon_H/(3\upsilon_c-1)} \tag{2.77}$$

Using the Kuhn segment concentration, $c_k = g/\xi_c^3$, where g is the number of Kuhn segments per correlation length, the distance between entanglements, a, can be written. Assuming a Gaussian distribution for the end-to-end distance which exceeds the screening length ξ_c:

$$a = \xi_c\left(\frac{N_e}{g}\right)^{1/2}. \tag{2.78}$$

The relation between a and c_k can be established by measuring the plateau modulus G_0[12]:

$$G_0 \approx \frac{kTc_k}{N_e} \tag{2.79}$$

N_e is the number of segment between entanglements and c_k is the number of Kuhn segments per unit volume. Eq. 2.79 can be rewritten as:

$$G_0 \approx \frac{kT}{a^2\xi_c}. \tag{2.80}$$

Typical measurements of the plateau modulus exhibit a power law dependence on the concentration:

$$G_0 \sim c^{\alpha} \tag{2.81}$$

where $\alpha \approx 2.3 \pm 0.2$[14,15].

Rubinstein, in his review on polymer dynamics[12], presents three possible models for the definition of a.

model 1[16]:

This model is based on the assumption that there is a constant number, n_{strand}, of entanglement strands (containing $\sim N_e$ Kuhn segments each) per entanglement volume where n_{strand} is on the order of 10. The numbers of entanglement strands in the mesh volume a^3 is:

$$n_{strand} = \frac{c_k}{N_e} a^3. \tag{2.82}$$

This equation leads to the dependency:

$$a \sim c_k^{-1/3} \sim \xi_c. \tag{2.83}$$

Model 2[17]:

The second model assumes constant number of binary contacts for strands. The probability of a given Kuhn segments (of size b) to be in contact with any other segments is proportional to the monomer concentration, $c_k b^3$. The number of binary contact for strands combined for N_e segments is:

$$c_k b^3 N_e = const \tag{2.84}$$

which leads to the following dependency:

$$a \approx \xi_c^{5/6} b^{1/6} \qquad \text{for good solvents} \tag{2.85}$$

and

$$a \approx \xi_c^{1/2} b^{1/2} \qquad \text{for theta solvents.} \tag{2.86}$$

Model 3[18]:

The basic assumption in the third model is that there is a constant number of binary contacts per entanglement volume, a^3. Since the number of segments per volume a^3 is $c_k a^3$ and the probability of binary contacts is $\sim c_k b^3$, the average number of binary contacts in volume a^3 is:

$$c_k^2 a^3 b^3 = const \tag{2.87}$$

which leads to:

$$a \sim c_k^{-2/3} \tag{2.88}$$

$$a \approx \xi_c^{8/9} b^{1/9} \qquad \text{for good solvents} \tag{2.89}$$

and

$$a \approx \xi_c^{2/3} b^{1/3} \qquad \text{for theta solvents.} \tag{2.90}$$

Apart from the dependency of a on concentration, we could also establish, from our experiments, the dependency of the tube disengagement time, τ_d, and the centre of mass diffusion, D_G. Taking the friction of a screening length "blob" as:

$$\zeta = 6\pi\eta_s\xi_H \tag{2.91}$$

and assuming Gaussian distribution for the end to end distance $R^2 = \left(\frac{N}{g}\right)\xi^2$, eq 2.27 and 2.31 give the relation between the tube disengagement time, center of mass diffusion and a[19]:

$$\tau_d = 3\left(\frac{N}{N_e}\right)\left(\frac{N}{g}\right)\xi^2 \frac{(N/g)6\pi\eta_s\xi_H}{3\pi^2 k_B T} = \left(\frac{N}{g}\right)^3 \xi_c^4 a^{-2} \frac{6\eta_s\xi_H}{\pi k_B T}$$

$$\sim M^3 a^{-2} c^{(4\upsilon_c+\upsilon_H-3)/(1-3\upsilon_c)} \tag{2.92}$$

and

$$D_G = \left(\frac{N}{g}\right)^{-2} \xi_c^{-2} a^2 \frac{k_B T}{18\pi\eta_s\xi_H} \sim M^{-2} a^2 c^{(2-\upsilon_H-2\upsilon_c)/(1-3\upsilon_c)}. \tag{2.93}$$

In order to establish those dependencies one should replace the parameter a in eq. 2.92 and 2.93 according to the three models.

Under model 1, the scaling of τ_d and D_G can be written:

$$\tau_d \sim M^3 c^{(2\upsilon_c+\upsilon_H-3)/(1-3\upsilon_c)} \tag{2.94}$$

and

$$D_G \sim M^{-2} c^{(2-\upsilon_H)/(1-3\upsilon_c)}. \tag{2.95}$$

Thus:

$$D_G \sim M^{-2} c^{-1.75} \quad \text{(good solvents)} \tag{2.96a}$$

$$D_G \sim M^{-2} c^{-3} \quad \text{(theta solvents)} \tag{2.96b}$$

$$\tau_d \sim M^3 c^{1.5} \quad \text{(good solvents)} \tag{2.96c}$$

$$\tau_d \sim M^3 c^3 \quad \text{(theta solvents)} \tag{2.96d}$$

Under model 2, the scaling of τ_d and D_G can be written:

$$\tau_d \sim \mathrm{M}^3 c^{(7\upsilon_c/3+\upsilon_H-3)/(1-3\upsilon_c)} \quad \text{(good solvents)} \tag{2.97a}$$

$$\tau_d \sim \mathrm{M}^3 c^{(3\upsilon_c+\upsilon_H-3)/(1-3\upsilon_c)} \quad \text{(theta solvents)} \tag{2.97b}$$

and

$$D_G \sim M^{-2} c^{(2-\upsilon_c/3-\upsilon_H)/(1-3\upsilon_c)} \quad \text{(good solvents)} \tag{2.98a}$$

$$D_G \sim M^{-2} c^{(2-\upsilon_c/3-\upsilon_H)/(1-3\upsilon_c)} \quad \text{(theta solvents)} \tag{2.98b}$$

thus:

$$D_G \sim M^{-2} c^{-1.5} \quad \text{(good solvents)} \tag{2.99a}$$

$$D_G \sim M^{-2} c^{-2.0} \quad \text{(theta solvents)} \tag{2.99b}$$

$$\tau_d \sim M^3 c^{1.25} \quad \text{(good solvents)} \tag{2.99c}$$

$$\tau_d \sim M^3 c^2 \quad \text{(theta solvents)} \tag{2.99d}$$

Under model 3, the scaling of τ_d and D_G can be written:

$$\tau_d \sim M^3 c^{(20\upsilon_c/9+\upsilon_H-3)/(1-3\upsilon_c)} \quad \text{(good solvents)} \quad (2.100a)$$

$$\tau_d \sim M^3 c^{(8\upsilon_c/3+\upsilon_H-3)/(1-3\upsilon_c)} \quad \text{(theta solvents)} \quad (2.100b)$$

and

$$D_G \sim M^{-2} c^{(2-2\upsilon_c/9-\upsilon_H)/(1-3\upsilon_c)} \quad \text{(good solvents)} \quad (2.101a)$$

$$D_G \sim M^{-2} c^{(2-2\upsilon_c/3-\upsilon_H)/(1-3\upsilon_c)} \quad \text{(theta solvents)} \quad (2.101b)$$

thus:

$$D_G \sim M^{-2} c^{-1.58} \quad \text{(good solvents)} \quad (2.102a)$$

$$D_G \sim M^{-2} c^{-2.33} \quad \text{(theta solvents)} \quad (2.102b)$$

$$\tau_d \sim M^3 c^{1.33} \quad \text{(good solvents)} \quad (2.102c)$$

$$\tau_d \sim M^3 c^{2.33} \quad \text{(theta solvents)} \quad (2.102d)$$

2.5 Modification of the Reptation theory

The assumptions behind the reptation model as described so far are somewhat simplistic. For example, according to this model, the polymer coils move inside a rigid static matrix. A more sophisticated approach would acknowledge the contribution of the medium dynamics to the chain relaxation process. Extensive experimental work on polymer coils in a semidilute solution has shown that the dependence of the diffusion coefficient and the tube disengagement time on the molecular weight is not as predicted by the reptation theory but closer to $M^{-2.4}$ and $M^{3.4}$[11,15,20,21] respectively. A number of modifications to the reptation theory have been suggested which bring either one of the scaling laws closer to the experimental observations, yet the relation between both observations and the theory is not fully understood. In this chapter I will review a few of the well known modifications.

2.5.1 *Contour length fluctuations*

The contour length of the primitive path is not constant but, in fact, fluctuates with time (see figure 2.10). It was suggested by Doi[22,23] that those fluctuations play an important role in various dynamical processes. Let s_n be the curvilinear coordinate of the n-th Rouse segment measured from a certain fixed point on the tube. The contour length of the primitive chain is time dependent and can be written as:

$$L(t) = s_n(t) - s_0(t). \tag{2.103}$$

The dynamics of s_n are described by the Langevin equation for the Rouse model:

$$\zeta \frac{\partial}{\partial t} s_n = \frac{3k_B T}{b^2} \frac{\partial^2}{\partial n^2} s_n(t) + f_n(t) \tag{2.104}$$

where:

$$\langle f_n(t) \rangle = 0 \qquad \text{and} \qquad \langle f_n(t) f_m(t') \rangle = 2\zeta k_B T \delta(n-m)\delta(t-t'). \tag{2.105}$$

The dynamics of the fluctuations appear in the boundary conditions. In the case of pure isotropic Rouse motion $\langle R_N - R_0 \rangle$ is equal to zero. However, this is not the case as far as the contour length fluctuations are concerned. Here one direction of translational motion is clearly favored (figure 2.11), since there are more possibilities for the polymer to diffuse outside the tube than inside.

Let the equilibrium of the contour length be given by:

$$\langle s_N - s_0 \rangle = \overline{L}. \tag{2.106}$$

The boundary conditions are:

$$\frac{\partial^2}{\partial n^2} \langle s_n \rangle = 0 \tag{2.107}$$

and

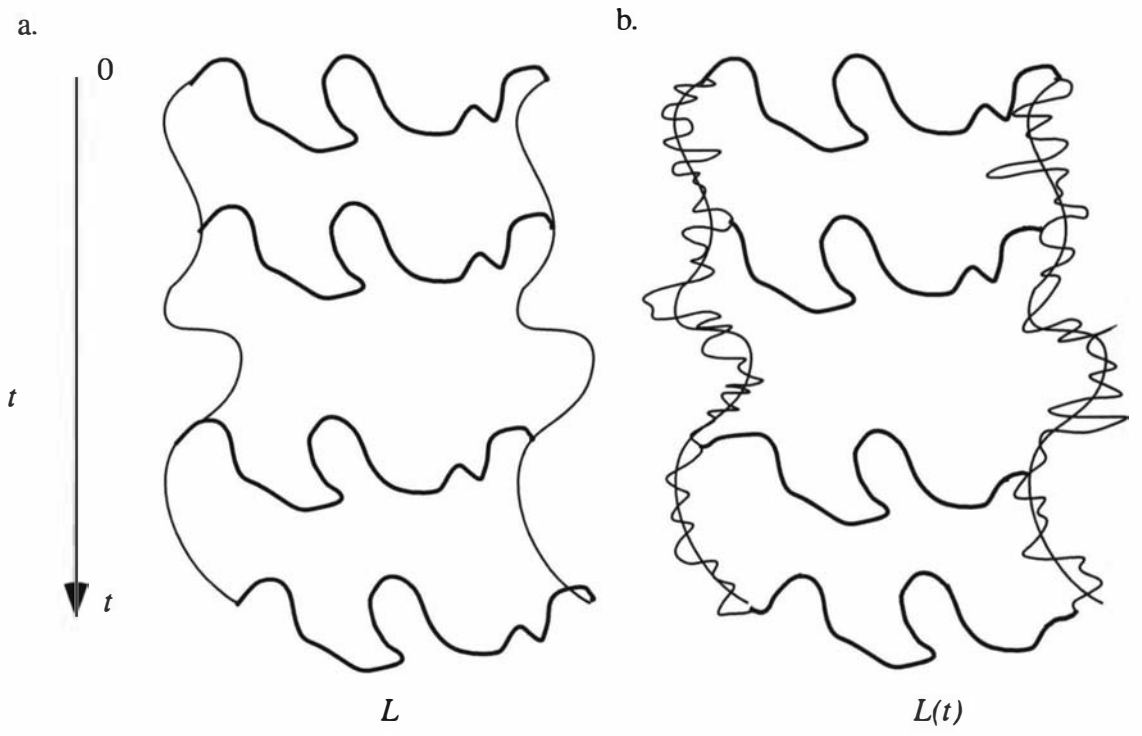

Figure 2.10:
The change in the contour length, L, with time. a) Classic reptation and b) contour length fluctuations.

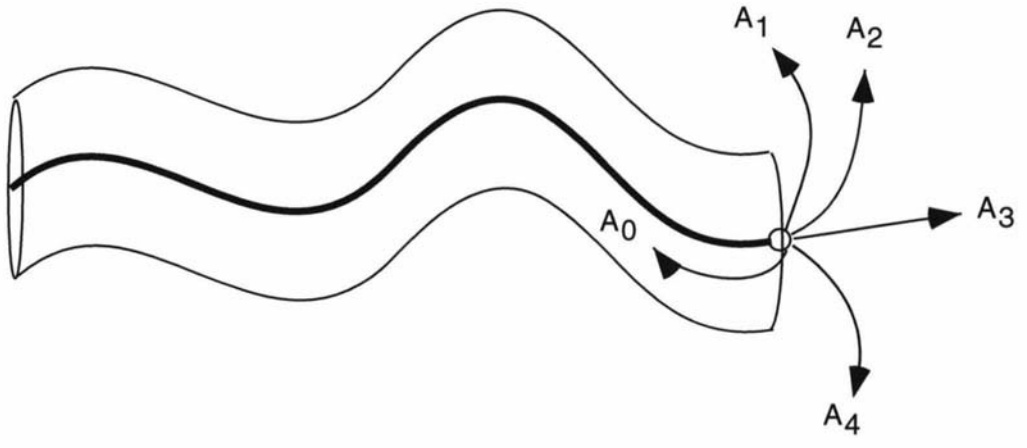

Figure 2.11[2]:
The probability for the polymer segments to diffuse out of the tube is higher than the probability to diffuse back into the tube.

$$\frac{\partial}{\partial n} s_n = \frac{\overline{L}}{N} \qquad \text{at} \qquad n=0 \text{ and } N. \tag{2.108}$$

To satisfy the Langevin equation with the new boundary conditions Doi uses different normal coordinates than were used in the simple Rouse model:

$$Y_0 = \frac{1}{N}\int_0^N dn s_n \tag{2.109}$$

$$Y_p = \frac{1}{N}\int_0^N dn \cos\left(\frac{p\pi n}{N}\right)\left(s_n - \frac{n\overline{L}}{N}\right) \qquad \text{for} \qquad p=1,2,\ldots, \tag{2.110}$$

so

$$s_n = Y_0 + 2\sum_{p=1}^{\infty} Y_p(t)\cos\left(\frac{p\pi n}{N}\right) + \frac{n\overline{L}}{N}. \tag{2.111}$$

The coordinate Y_0 represents the position of the 'curvilinear center of mass', and Y_p represents the fluctuation along the tube. The contour length of the primitive path is written as:

$$L(t) = s_N(t) - s_0(t) = \overline{L} - 4\sum_{p:odd} Y_p(t) \tag{2.112}$$

and the contour length fluctuation is:

$$\left\langle \Delta L^2 \right\rangle = \left\langle L^2 \right\rangle - \overline{L}^2 = \frac{8Nb^2}{3\pi^2}\sum_{p:odd}\frac{1}{p^2} = \frac{Nb^2}{3}. \tag{2.113}$$

Since this equation describes the variation in the contour length caused by the fluctuations, it is only natural that those fluctuations will influence the tube disengagement time. The tube disengagement time of a non fluctuating chain is given approximately by the time it takes for a chain to move the distance $\overline{L}$.

$$\tau_d^{(NF)} \cong \frac{\overline{L}^2}{D_c}. \tag{2.114}$$

For the case of a fluctuating chain the tube disengagement can occur sooner, when the polymer segment reaches the distance $\bar{L} - \Delta\bar{L}$, $\left(\Delta\bar{L} = \langle \Delta L^2 \rangle^{1/2}\right)$. Thus the tube disengagement time for a fluctuating chain, according to Doi, is:

$$\tau_d^{(F)} \cong \left(\bar{L} - \Delta\bar{L}\right)^2 / D_c \cong \tau_d^{(NF)}\left(1 - \frac{X}{\sqrt{Z}}\right)^2 \qquad (2.115)$$

where X is numerical constant on the order of 1.47. Note, Z is the number of steps in the primitive path and it is proportional to N. Equation 2.115 leads to the relation $\tau_d \sim M^{3.4}$ for a limited range of molecular weights[24].

2.5.2 *Double Reptation*

The Double Reptation model, suggested by des Cloizeaux[25], uses the same parameters of the classic Doi & Edwards model of single reptation. The difference between the two models is in the concept that every stress point, which was created by the entanglements, is influenced by a motion of two polymers and not only one as in the classic reptation model.

At a stress point p two polymers are entangled (figure. 2.12). Those stress points are distributed randomly all over the polymer melt. The stress point p can be relax if either one of the two polymer chains will reptate along the tube and release it. Unlike the reptation theory, where the relaxation modulus is proportional to the fraction of a polymer chain still in the tube at time t, in the double reptation model the modulus is proportional to the product of the fraction of the two polymers which are entangled in this stress point. The probability that the polymers A and B, that were entangled at point p at time equal to zero, will be still entangled at time t, is proportional to $\psi_A(t)\psi_B(t)$. Thus the fraction of unrelaxed stress at time t is given by:

$$m_d(t) = \sum_{A,B} \varphi_A(t)\varphi_B(t)\psi_A(t)\psi_B(t) = \left[m_s(t)\right]^2 \qquad (2.116)$$

where d stand for double reptation and s for single reptation. φ_A is the volume fraction of polymers with a molecular weight M_A $\left(\sum_A \varphi_A = 1\right)$. Since for single reptation:

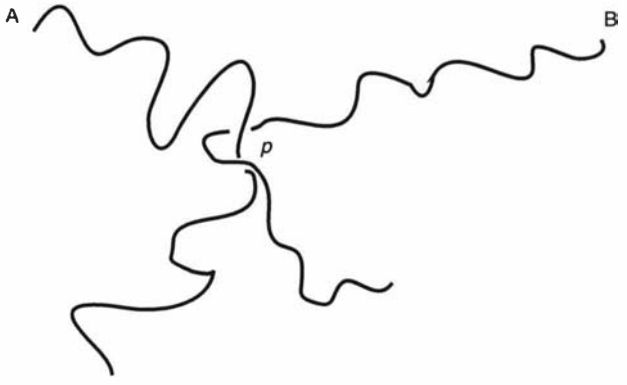

Figure 2.12[25]:
The double reptation model. *p* is a stress point created by polymer A and B. The only way the stress point can be released is if either polymers, A or B, will reptate away.

$$\psi_A(t) \propto \exp[-t/\tau_d] \tag{2.117}$$

for double reptation the probability function will be $[\psi_A(t)]^2$[25]. Introducing the double reptation correction to the stress relaxation function:

$$G(t) = G_N^{(0)} m_d(t) = G_N^{(0)} [m_s(t)]^2. \tag{2.118}$$

Eq. 2.118 gives a better fit, yet not perfect, to the data acquired by Rubinstein and Colby[26] (figure 2.13). Des Cloizeaux continued to develop the model in various directions[27-29]. Note that while double reptation may be helpful in describe stress relaxation, the model is less relevant in the case of diffusion, where single chain motion is most significant.

2.5.3 *Reptons*

The "repton" model[24] is a discretized version of the reptation model. Rubinstein, provides a more accurate treatment of the tube length fluctuations than Doi, and the resulting scaling laws are in better agreement with experiments. In the model the entangled chains, instead of being restricted by a rigid matrix, are confined by the primitive path of other polymer coils surrounding it. Consider one polymer coil in an entangled environment. The entanglements points which confine this coil form cells, each of which stores unentangled polymer loops (figure. 2.14a). The polymer loops inside the cells are divided into segments (called reptons) and the number of reptons in each cell is proportional to the length of the unentangled loop stored in it. The primitive path of that chain is a line connecting the center of those cells. In figure 2.14b we can see that the polymer chain from 2.14a can be seen as 7 reptons in form of 4 clusters. The system can be visualized by one dimensional directed random walk figure 2.14c.

The axioms of the repton model are:

1. The chain never vacates a site in the middle of a cluster.
2. From each cell the chain can move to z sites, so for a cell located at the end of the chain there are z-1 possibilities to occupy an empty cell site and only one possibility to occupy an already occupied site.

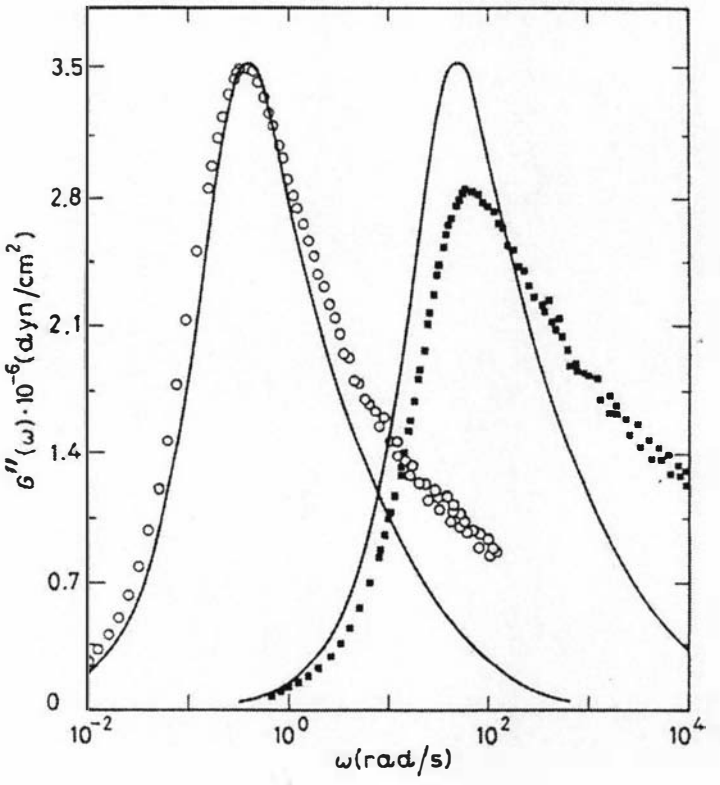

Figure 2.13[28]**:**
Simulation fit of loss modulus data obtained by applying "double reptation" principle to the Doi-Edwards model. Opened circles are data for M_L=355000; filled squares are data for M_s=70900[26].

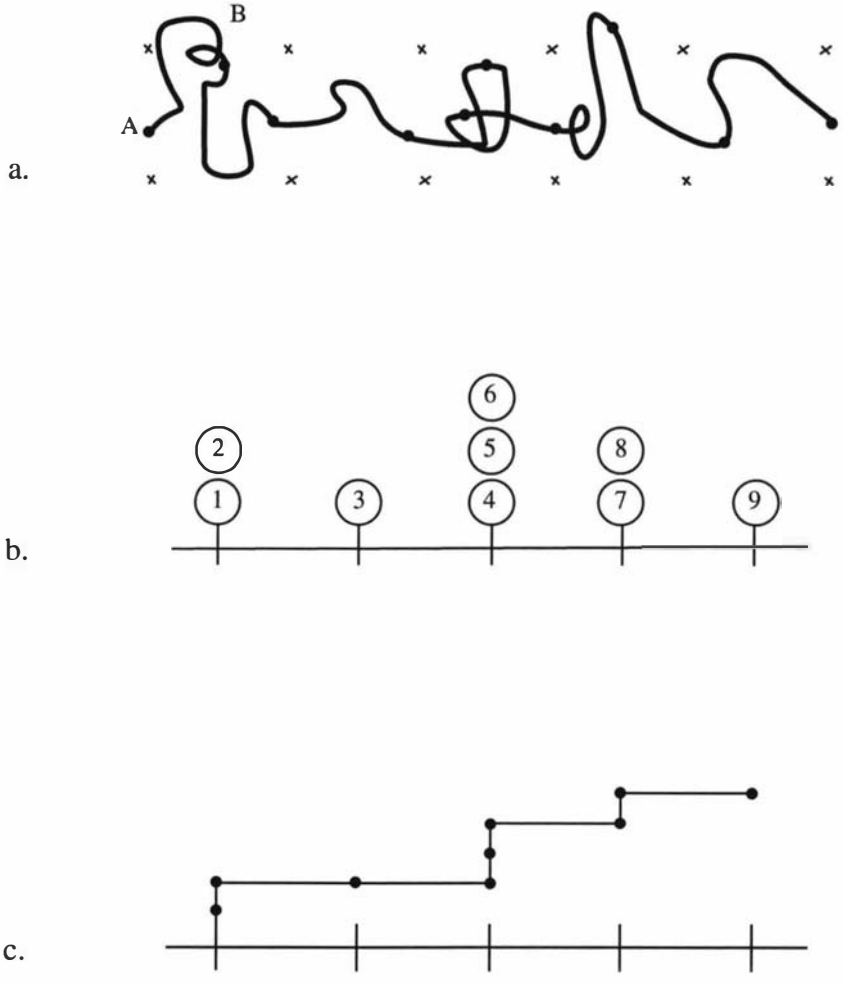

Figure 2.14[24]:
The repton model. a) A polymer coil in an entangled environment. The environment is divided into cells which contains polymer loops. Those loops are divided into segments (filled dots). b) The polymer chain from a can be seen as 9 reptons in form of 5 clusters. c) Directed random walk of the polymer coil.

3. The probability of a repton hoping between neighboring occupied sites is $1/z$, while the probability of hopping onto an empty site is $(z\text{-}1)/z$.

The calculation of the average cluster size $\langle L \rangle$ is carried out by looking at a cluster made from N reptons occupying K sites ($K = 1,2,...,N$). The probability for N reptons to occupy K sites is:

$$P(K,N) = \frac{(z-1)^{K-1}(N-1)!}{z^{N-2}(K-1)!(N-K)!} \tag{2.119}$$

thus $\langle L \rangle$:

$$\langle L \rangle = \sum_{K=1}^{N} KP(K,N) = N - (N-1)/z. \tag{2.120}$$

From axioms 1 & 2 the probability of an attempted repton jump to succeed can be calculated:

$$J = \left[2(z-1)/z^3\right]\left\{1 + 2(z-1)/N\right\}. \tag{2.121}$$

The one dimensional diffusion coefficient of center of mass is given by:

$$\begin{aligned} D_G &= \frac{\langle (x_{c.m.}) \rangle}{2\tau_m} = \frac{\left\langle \left(\frac{1}{N} \sum_{n=1}^{N} x_n \right) \right\rangle}{2\tau_m} = \frac{\left\langle \frac{1}{N^2} \sum_{n,m} x_m x_n \right\rangle}{2\tau_m} = \\ &= \frac{1}{N^2} \frac{\sum_{n,m} \langle x_m x_n \rangle}{2\tau_m} = \frac{1}{N^2} \frac{\sum_{n} \langle x_n \rangle^2}{2\tau_m} = \frac{1}{N^2 2\tau_m} \sum_{1}^{N} Ja^2 \end{aligned} \tag{2.122}$$

thus

$$D_G = (z-1)a^2 / z^3 N\tau_m + O\left(N^{-2}\right). \tag{2.123}$$

This result suggest a greater dependence on molar mass of the center of mass diffusion for shorter reptons clusters.

$$D_G \sim N^{-2-o(1/N)} \tag{2.124}$$

a is the average cell size and τ_m is the average microscopic time between attempted hops. This equation represent the one-dimension curvilinear diffusion coefficient in a tube.

From eq. 2.121 & 2.122 one can estimate the time it take the cluster to diffuse its own length :

$$\tau_z \cong \langle L \rangle^2 / D_z \cong z(z-1)N^3\tau_m . \tag{2.125}$$

The stress relaxation function is determined by the set of site which are still occupied between time 0 and time t. The number of the sites which are always occupied is the difference between the furthest propagator in the right end of the cluster, $x_R(t)$, and the furthest propagator to the left of the cluster, $x_R(t)$. The stress relaxation function is the fraction of unvacated sites

$$G(t) \approx \langle x_R(t) - x_L(t) \rangle / N \tag{2.126}$$

averaged over different time histories. The zero-shear-rate viscosity is equal to the integral of the stress-relaxation function:

$$\eta_0 = \int_0^\infty \mu(t)dt \sim N^{3.4} . \tag{2.127}$$

2.5.4 *Constraint Release*

The models which fall into this category consider a relaxation mechanism additional to reptation alone, namely the tube renewal process[30-33]. Constraint release theory takes into consideration the ability of a "breathing" matrix to relax chains at any point on the primitive path (and not only in the ends), each model having a slightly different dependency between the two process. In this section, I will explain the constraint release model introduced by Graessley as a representative of this family of models.

According to the constraint release model two independent processes are occurring, the reptation of the tagged chain and the reptation of the medium (tube

renewal process). The tube disengagement time, in this case, is a sum of those two relaxation pathways. Let us view the tube as an ensemble of cells, where each cell length is a one step of the primitive path, a. Each cell bounded by z_0 neighboring chains, contains z $(z < z_0)$ constraints, which are going through the same process of reptation as the tagged chain. The constraint release mechanism is in fact the temporary removal of part of those neighboring chains. Removal of chains along the primitive path allows the tagged chain to jump into an adjacent cell, thus altering the path locally. We can see now that the probability of chain movement will depend in each case on the disposition of the adjoining portions of its primitive path. The local jump distance is the path step length a, and the average time between jumps is $2\tau_w$, where τ_w is the mean waiting time for release of a constraint which allow a jump that not changing the path length. By using the fraction of initial primitive path steps which are still occupied (defined by Doi & Edward[2]), τ_w can be calculated:

$$\tau_w = \int_0^\infty [\psi(t)]^z dt = \frac{8}{\pi^2} \sum_{p:odd} \frac{1}{p^2} \exp\left(-p^2 t / \tau_d\right). \tag{2.128}$$

This equation can be written as:

$$\tau_w = \Lambda(z)\tau_d \tag{2.129}$$

where

$$\Lambda(z) = \left(\frac{8}{\pi^2}\right)^z \sum_{\substack{p_1 \\ :odd}} \cdots \sum_{p_z} \frac{1}{p_1^2 + p_2^2 + \cdots + p_z^2} \frac{1}{p_1^2 \cdot p_2^2 \cdot \cdots \cdot p_z^2} \cong \left(\frac{\pi^2}{12}\right)^z. \tag{2.130}$$

The diffusion of the center of mass is influenced by two parallel independent processes, the constraint release and the pure reptation. The diffusion coefficient of the constraint release part is expressed in terms of the jump frequency:

$$D_G = \frac{1}{6} \overline{\Delta R}^2 \phi \tag{2.131}$$

ΔR is the spatial displacement produced by a jump, and $\overline{(\Delta R)}^2$ is the long time average of ΔR. ϕ is the jump frequency. For the constraint release case:

$$\overline{(\Delta R)^2} = \frac{a^2}{Z^2} \tag{2.132}$$

and

$$\phi = \frac{Z}{2\tau_w} \tag{2.133}$$

Thus the diffusion coefficient associated with constraint release is:

$$D_G = \frac{1}{12}\frac{a^2}{Z\tau_w}. \tag{2.134}$$

However, this equation should be rearranged in order to bring together the two effects, constraint release and reptation.

As already mentioned the contour length of the polymer is $L = Za$ and the tube disengagement time is, $\tau_d = L^2/\pi^2 D_C$. By substituting these two relations and eq. 2.129 in eq. 2.134 one gets[33]:

$$D_G(N) = \frac{\pi^2}{12}\frac{1}{\Lambda Z^3} D_C. \tag{2.135}$$

In polymer blends τ_w strongly depends on the matrix size. Thus, for a polymer matrix with Z_s steps on the primitive path, the constraint release contribution to diffusion will be:

$$D(N, N_s) = \frac{\pi^2}{12}\frac{1}{\Lambda Z_s^3} D_C(Z). \tag{2.136}$$

As already known from the reptation theory the diffusion coefficient of center of mass is given by:

$$D_G = \frac{D_c}{3Z}. \tag{2.137}$$

Thus the overall center of mass diffusion of a polymer segment can be expressed:

$$D_G(Z, Z_s) = \left[\frac{1}{3Z} + \frac{\pi^2}{12\Lambda Z_s^3}\right] D_C(Z). \tag{2.138}$$

As one can see from the above equation, for sufficiently large matrix polymer the constraint release is negligible and even in a case of self diffusion $(Z = Z_s)$ the constraint release process should not play a significant role. This was shown experimentally by Green and Kramer[34]. Their data indicate that constraint release effects are insignificant in the case of a polymer surrounded by identical length chains, i.e. for the polymer melts and semidilute solutions considered in this thesis. They also showed experimentally that for sufficiently small matrix molecules the constraint release process changes the dynamics of the polymer system, as the topology of the tube is being modified on a time scales less than τ_d.

2.5.5. *Reptation and contour length fluctuations*

The last model discussed in this chapter is very recent and was suggested by Milner & McLeish[35]. The reptation and contour length fluctuation model is based on a theory of star polymer dynamics[36], which was extended to linear polymers by treating them as a two branched star. The model acknowledges two processes which are contributing to relaxation of the polymer configuration. These are the fast relaxation of the contour length fluctuation and the slow relaxation due to reptation. The contour length fluctuation is essentially a retraction and sliding of the arms from the old configuration to a new one, a process whose scales as $\sim N^4$. Any section of the polymer which cannot meet the retraction process over the tube disengagement time will then be relaxed via reptation, whose characteristic time scales as $\sim N^3$. Since the contour length fluctuation process decreases with the polymer length, for large N the polymer will principally follow the reptation dynamics.

In the Milner Mcleish model, the stress relaxation function $G(t)$ is a sum of all process involved, retraction, reptation and free Rouse motion for distances smaller than the entanglement dimension.

$$G(t) = G_{retract}(t) + G_{reptate}(t) + G_{Rouse}(t). \tag{2.139}$$

These authors show that their model leads to:

$$\eta \sim N^{3.4}. \tag{2.140}$$

2.6 Polymer-Mode-Coupling theory[4]

As mentioned in the previous chapter, the reptation theory uses a simple mean field approach, and relies on the assumption that entanglement interactions with surrounding polymers serve to effectively confine each chain in a static "tube". This simple model can be used to derive all dynamic parameters of polymers in solutions and melts. In most cases this theory agrees quite well with the experimental data. Over the years several researchers have suggested various theories for polymer dynamics[37-41], each of which were derived from general Langevin equations[42-44], but none of those theories predicted the reptation "finger print" (a range of time over which the mean square displacement scales as $t^{1/4}$). More recently Schweizer et al[4] developed a microscopic statistical dynamical theory of entangled macromolecular fluids, Polymer-Mode-Coupling. This theory is the first which qualitatively predicts "reptation like" mean-square displacement *vs* time scaling laws. However, unlike reptation, the theory lacks a defined quantitative character in which one can derive key dynamic parameters.

Polymer-Mode-Coupling (PMC) focuses on deriving effective equations of motion for a single tagged polymer dissolved in a macromolecular fluid matrix. The bead and spring Gaussian chain is used to model the polymer chain and it is assumed that the polymer dynamics arise from the site-site interaction which can occur either between sites on the same chain or with sites on the surrounding chains. The real dynamics of a polymer coil inside a polymer matrix involves the coupling of every site to all the other interacting sites and results in a N-body tensorial memory function which cannot be solved. However, a "pre-averaging" or mean field cage approach was adopted by Schweizer and the potential of the mean force assumed to be harmonic.

These approximations lead to the following Langevin equation, the "generalized Rouse" form:

$$\zeta_0 \frac{\partial r_\alpha}{\partial t} + \int_0^N d\gamma \int_0^t d\tau \Gamma_{\alpha\gamma}(t-\tau) \frac{\partial r_\gamma(\tau)}{\partial \tau} = K_s \frac{\partial^2 r_\alpha}{\partial \alpha^2} + f_\alpha(t) + F_\alpha^Q(t) \qquad (2.141)$$

where ζ_0 is the "bare" friction coefficient, $\Gamma_{\alpha\gamma}(t)$ is an $N \times N$ matrix which describes the ensemble-averaged statistical correlation between the total force exerted at $t = 0$ by all the matrix polymer on tagged polymer segment γ at later time t, K_s is the spring constant, $f_\alpha(t)$ is the white noise random force and $F_\alpha^Q(t)$ is the projected fluctuating "random force" on the segmental scale. Note, equation 2.141 is similar to the Langevin equation derived for Rouse model, with an additional two terms which represent the influence of surrounding matrix on the tagged polymer chain, $\Gamma_{\alpha\gamma}(t)$ and $F_\alpha^Q(t)$. This shows the cross over from isolated coil to a polymer coil which is confined in a polymeric matrix. The simplest model which solves the problem of tagged polymer coil inside a polymeric matrix is the "renormalised Rouse model" (RR)

The renormalised Rouse theory[45] is a crude simplification of the polymer dynamics, which assumes that a four body excluded volume force is enough to represent entanglement. This model fails to describe the dynamics of a "physical" entangled polymer system and is valid only for short range motion and/or for small polymer chains. However, RR theory describes the intermediate regime between the pure Rouse dynamics and the long range cooperative motion of the polymer coil. The RR simplification of the generalized Rouse equation comes through the memory function:

$$\Gamma_{\alpha\gamma}(t) \cong \delta_{\alpha,\gamma} N^{-1} \sum_{\alpha,\gamma=1}^{N} \Gamma_{\alpha\gamma}(t) \equiv \delta_{\alpha,\gamma} \Delta\zeta(t) \qquad (2.142)$$

where:

$$\Delta\zeta(t) \propto \zeta_0 \psi (\tau_0 / t)^{-3/4} = \zeta_0 \left(\rho \sigma^3 g^2(d) S(0)\right) (\tau_0 / t)^{-3/4} \qquad \text{for } \tau_c << t << \tau_R \qquad (2.143)$$

were ψ is a dimensionless structural parameter, σ is a segment length, $g(d)$ is the *inter*molecular pair correlation function, $S(0)$ is the collective liquid structure factor and

τ_c defines the crossover between Rouse to RR regions. As a consequence, the segmental averaged mean square displacements scale as:

$$\phi(t) = \left\langle \left(r - r(t)\right)^2 \right\rangle \propto t^{3/8} \tag{2.144}$$

and the center of mass mean square displacement is:

$$\phi_{CM}(t) = \left\langle \left(R_{CM} - R_{CM}(t)\right)^2 \right\rangle \propto t^{3/4}. \tag{2.145}$$

As mentioned, the RR theory valid only at short range motion or small polymer chains. The Mode-Mode-Coupling[4,46,47] (MMC) theory deals with the problem of highly entangled long chains. It incorporates slow variables which enter through the dynamical memory function. These slow variables arise from the entanglements which create an effective cage inducing a strong cooperative motion of the N segments of the tagged polymer. Unlike reptation, where only the chain ends can diffuse freely, the MMC theory allows free diffusion of any two segments, regardless of their position on the chain, where the rest $N-2$ segments accordingly cooperatively diffuse. The general Langevin equation for the entangled state can be written:

$$\zeta_0 \frac{\partial \vec{r}_\alpha}{\partial t} + \int_0^t d\tau \Sigma(t-\tau) \frac{\partial \vec{r}_\alpha(\tau)}{\partial t} + \int_0^t d\tau M(t-\tau) \frac{\partial}{\partial \tau} \frac{\partial^2 \vec{r}_\alpha(\tau)}{\partial \alpha^2} = K_s \frac{\partial^2 \vec{r}_\alpha(t)}{\partial \alpha^2} + \vec{f}_\alpha(t) + \vec{F}_\alpha^Q(t). \tag{2.146}$$

This equation is similar to the generalized Rouse equation with two additional caging forces: $\Sigma(t)$ is the "diffusion" memory function which describes a time delayed, uniform drag on each segment, and $M(t)$ is the "viscoelastic" memory function which describes a time-delayed force sensitive to the rate of change of the elastic spring force with time. This force strongly modifies conformation and stress relaxation, and describes the history of changing polymer shape or orientation.

The memory functions relax via three relaxation channels: center-of-mass diffusion of the tagged polymer, tagged polymer internal mode dynamics or shape fluctuations and collective matrix relaxation. Those channels are roughly parallel to reptation, contour length fluctuation and constraint release. The relaxation channels are not independent parallel channels and must be described in terms of statistical

correlations of the entanglement forces which are in turn influenced by multiple structural length scale and time-dependent decay channels.

Schweizer separates the center of mass motion, $R_{CM}(t)$, from the motion of segments, $r(t)$. The mean square displacement of a polymer coil inside a polymeric matrix for the Rouse, RR and MMC theories can be summarized as follow:

$$\begin{aligned}
\beta\zeta_0\left\langle \left(R_{CM}(t)-R_{CM}(0)\right)^2\right\rangle &\sim t/N && \text{for } t << \tau_c \\
&\sim t^{9/16}/N && \text{for } \tau_c << t << \tau_R \\
&\sim t^{3/4}/N^{11/8} && \text{for } \tau_R << t << \tau_{RR} \\
&\sim t/N^2 && \text{for } t >> \tau_{RR}
\end{aligned} \qquad (2.147)$$

$$\begin{aligned}
\beta\zeta_0\left\langle \left(r(t)-r(0)\right)^2\right\rangle &\sim t^{1/2} && \text{for } t << \tau_c \\
&\sim t^{9/32}/N^{1/4} && \text{for } \tau_c << t << \tau_R \\
&\sim t^{3/8}/N^{7/16} && \text{for } \tau_R << t << \tau_{RR} \\
&\sim Dt \sim t/N^2 && \text{for } t >> \tau_D \sim N^3
\end{aligned} \qquad (2.148)$$

The quantity measured by NMR, and that which should be compared with the reptation prediction (eq. 2.36) is the segmental displacement represented by the equations 2.148. The time dependent exponents are quite in close agreement with the anomalous diffusion exponents found in the reptation theory and experimentally cannot be differentiated. The MMC molecular weight dependence prediction is different than the reptation prediction for the $t^{1/4}$ regime. In this regime, reptation predicts no dependency on molecular weight yet, as shown later, our experiments show a clear dependency. However, since the MMC theory at this point does not offer a quantitative equation for the mean square displacement (as the reptation model offers), it was impossible for us to compare the mean square displacements found in our experiments to the MMC theory. Nevertheless, Kimmich et al[48-50], who conducted NMR measurements on polymer melts found this theory to be in good agreement with their experiments.

3

BASIC THEORY OF NMR

When nuclei possessing a magnetic moment and angular momentum are placed in a large static magnetic field a splitting in their Zeeman energy levels occurs[51]. The population distribution of the spins on those energy levels, in thermal equilibrium, follows the Boltzmann distribution and leaves an excess of spins in the lowest level. In consequence the spin ensemble exhibits a net magnetization. Nuclear Magnetic Resonance (NMR) is a technique which utilizes the magnetization of the spins to detect resonant transitions between the Zeeman energy levels. During Nuclear Magnetic Resonance experiment, the spins are disturbed and various responses of the spin system may be recorded before the ensemble returns to its thermal equilibrium state[52-55].

3.1 Semi-Classical description of NMR

NMR can be described both by means of a full quantum mechanical treatment and by a semi-classical approach. In this chapter I will give a brief overview using the semi-classical description. The semi-classical treatment provides a convenient way to visualize the simple physical properties of the spin system. However, this method fails to describe many phenomena and especially those phenomena which involve interactions between spins, such as quantum mechanical evolution under the influence of the scalar spin-spin interaction and the dipolar interaction. However, the majority of the thesis concerns spin evolution in the presence of magnetic field gradients for which the semi-classical description is both useful and valid. Later, where discussing spin-diffusion, it will be necessary to reconsider the spin dynamics from a quantum mechanical perspective. At this point we give a simple semi-classical overview. The interaction of the angular momentum vector, $\boldsymbol{I}$, and the magnetic moment, μ, of the nuclei with the magnetic field can be expressed by Newton's second law as:

$$\frac{d\boldsymbol{I}}{dt} = \mu \times \boldsymbol{B}_0 = \tau \tag{3.1}$$

τ is the magnetic torque acting on the dipole moment. Because $\boldsymbol{I}$ and μ are parallel $(\mu = \gamma \boldsymbol{I})$ equation 3.1 predicts a precession of the spins around B_0, the static magnetic field. The change of the magnetic moment with time can be written as:

$$\frac{d\mu}{dt} = \mu \times \gamma B_0. \tag{3.2}$$

The frequency of the precession is called the Larmor frequency and can be expressed by:

$$\omega_0 = -\gamma B_0 \tag{3.3}$$

ω_0 varies from nucleus to nucleus depending on the gyromagnetic ratio γ. Note also that the molecular orbital surrounding a nucleus results in a slight magnetic shielding effect so that the magnetic field and hence the Larmor frequency experienced by the nucleus will vary slightly (within a few ppm) depend on the chemical surroundings and structure.

In this thesis we shall be concerned with spins in nuclei for which the z-component of the magnetic moment may exist in one of two eigen-states with eigenvalues:

$$\mu_z = \pm\frac{1}{2}\gamma\hbar. \tag{3.4}$$

Thus when an ensemble of such spins is placed in the field B_0, the spins precess with either their z component of the magnetic moment parallel or antiparallel to the magnetic field (figure 3.1a). Since there is no particular preferable direction in the x-y plane their phases are distributed uniformly around the z axis. The population excess in the lower energy level can be represented as a vector along the direction of B_0 (figure 3.1b).

3.1.1 *The rotating frame*

The Larmor frequency of most of the nuclei is on the order of hundreds of MHz, depending on the magnetic field strength. In most cases the spectral information of interest, is in the range of $10 - 10^4$ MHz on either side of this frequency. In order to simplify theoretical calculations the spin system is usually analyzed using a rotating Cartesian frame which rotates at ω about the direction of the magnetic field (the z-axis). In the rotating frame eq. 3.2 takes the form:

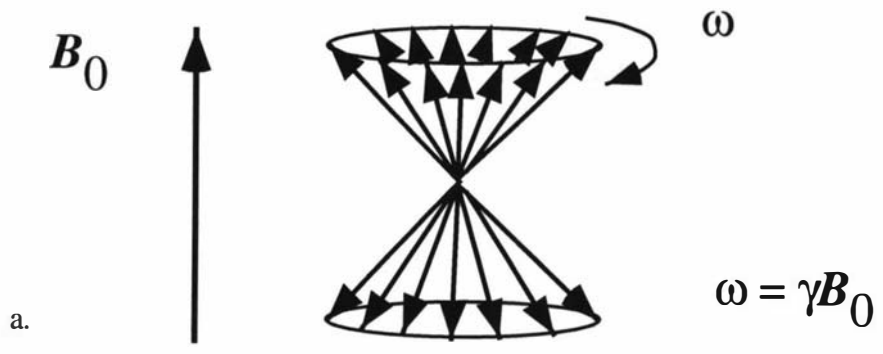

a.

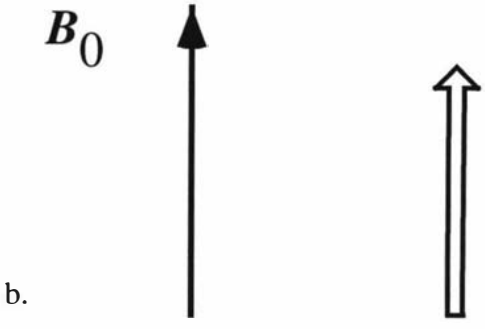

b.

Figure 3.1:
The behavior of spins in the presence of magnetic field. a) Spins system of I=1/2 precesses around the magnetic field. b) Since there is a population excess in the direction of the magnetic field the magnetization can be represented as one spin vector.

$$\frac{d\mu}{dt} = \gamma\mu \times \left(B_0 + \frac{\omega}{\gamma} \right) \hat{k}. \tag{3.5}$$

Where $\boldsymbol{B_0} = B_0\hat{k}$ and $\hat{k}$ is the unit vector on the z-direction defined by $\boldsymbol{B_0}$. Taking ω as $\omega_0 = -\gamma B_0$:

$$\frac{d\mu}{dt} = 0. \tag{3.6}$$

Clearly when the spin system and the frame rotate at the same frequency the spins can be treated as a static system.

3.1.2 *rf pulse*

In order to observe the nuclear spin precession by means of an induced emf in a receiver coil, the spin magnetization must acquire a non zero component in the x-y plane, the so called detection plane. This can be achieved by tilting the magnetization from equilibrium with an rf pulse. The rf pulse is a burst of alternating magnetic field B_1, produced by the rf coil which surrounds the sample inside the probe, whose direction which is perpendicular to B_0, and whose frequency is on the order of the Larmor frequency. Using the usual $\hat{i}$ and $\hat{j}$ unit vector to describe the x-y plane we may write:

$$\boldsymbol{B}_1(t) = \hat{i}\, 2B_1 \cos\omega t = B_1\left(\hat{i}\cos\omega t + \hat{j}\sin\omega t\right) + B_1\left(\hat{i}\cos\omega t - \hat{j}\sin\omega t\right) \tag{3.7}$$

Thus the linearly polarized field can be decomposed into two circularly polarized components, one of which rotates in the same sense as the spin precession. The counter-rotating rf field can be ignored provide $\gamma B_1 << \omega_0$, a situation which applies throughout the work represented in this thesis.

The effect of the rf pulse on the magnetization in the rotating frame of frequency ω, and with the x-axis defined by the direction of $\boldsymbol{B_1}$, is (figure 3.2):

$$\frac{d\mu}{dt} = \gamma\mu \times \left[\left(B_0 + \frac{\omega}{\gamma} \right) \hat{k} + B_1\hat{i} \right]. \tag{3.8}$$

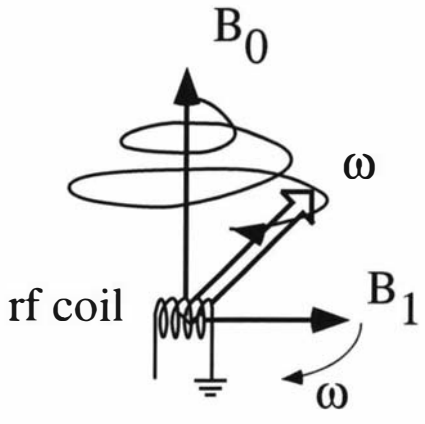

Figure 3.2:
The influence of an rf pulse on the magnetization

When B_1 is on resonance, $\omega = -\omega_0$:

$$\frac{d\mu}{dt} = \gamma\mu \times \left[(B_0 - B_0)\hat{k} + B_1\hat{i}\right] = \gamma\mu \times \boldsymbol{B}_1. \tag{3.9}$$

As one can see, by applying rf pulse on resonance, the magnetization will precess around B_1 and can be tilted from the z axis by any polar angle θ. The tipping angle, θ, depends on the pulse duration, t_p, according to $\theta = \gamma B_1 t_p$.

3.1.3. *Detection*

Once the rf pulse is finished B_0 is again the only magnetic field applied, so that the spins continue to precess around the z-axis in the laboratory frame. However, if $0 < \theta < \pi$, there will be a component of magnetization normal to z. Consequently the precession results in a fluctuating magnetization in the coil surrounding the sample (this coil is the same antenna used to produce the transverse B_1 field). This fluctuation due to precession of magnetization induces an alternating current in the rf coil which may be amplified, heterodyne detected and the resulting audio difference signal digitized and computed. The observed transient decays due to spin relaxation and is known as a Free Induction Decay (FID).

3.1.4. *Spin lattice and spin-spin relaxation process*

Spin lattice or longitudinal relaxation is the process by which the magnetization returns to the z axis after an rf pulse. The effect of applying rf pulses to the spin system is to change the energy level populations. For example, a $\frac{\pi}{2}$ pulse equalizes the population while a π pulse inverts it. After such disturbances the system tends to return to thermal equilibrium by releasing the excess energy to the mechanical degrees of freedom of the surrounding medium. The medium, considered to be a thermal reservoir, is assumed to be in thermal equilibrium at all time[56]. In the semi-classical picture the relaxation mechanism is assumed to be exponential:

$$\frac{dM_z}{dt} = \frac{M_0 - M_z}{T_1} \tag{3.10}$$

where M_0 is the magnetization at thermal equilibrium and T_1 is the spin lattice relaxation time. The solution to eq. 3.10 for the special case of $\frac{\pi}{2}$ pulse is:

$$M_z = M_0\left(1 - e^{-t/T_1}\right). \tag{3.11}$$

The relaxation time, T_1, depends on many parameters such as chemical structure, the size of the molecule and the viscosity of the surrounding medium. However, this relaxation process is usually long compared with other spectroscopic times of interest and is typically in the range of 0.1 to 10 seconds for protons in dielectric materials[57].

Unlike the longitudinal relaxation process, there is no energy transfer to the surrounding medium during the spin-spin or transverse relaxation process but a coherence loss in the *x-y* plane. Once tipped to the *x-y* plan the spin magnetization starts to decay as the spins start losing their phase coherence while precessing about B_0. This process is completed once the magnetization is distributed randomly around the *z* axis at which point no signal can be detected. In the absence of any other spin interaction the transverse relaxation time must equal the longitudinal relaxation time, considering that no signal can be detected once the spin system reached thermal equilibrium. However, in most cases other spin-spin interactions (such as dipolar interactions) determine the relaxation time. In the semi-classical model the transverse relaxation process is taken to be exponential as well:

$$\frac{dM_{x,y}}{dt} = -\frac{M_{x,y}}{T_2} \tag{3.12}$$

which for the case of a $\frac{\pi}{2}$ pulse leads to the result:

$$M_{x,y}(t) = M_0 e^{-t/T_2} \tag{3.13}$$

T_2 values are usually in the range of 10 μm to 10 s[57].

3.2 Spin echo and stimulated echo experiments.

Once the spins precess in x-y plane their coherence is lost gradually and the detectable magnetization decays. There are two coherence loss processes involved, one due to inhomogeneous broadening which is reversible, and one due to stochastic processes which are irreversible and which contribute to homogeneous broadening of the spectrum. To describe those processes we use two different relaxation terms, T_2^*, and T_2. T_2^* is the time take the spins to lose their coherence due to both inhomogeneous and homogeneous broadening. T_2 is the time constant for irreversible decay. The signal loss due to inhomogeneous broadening can be recovered by means of special pulse sequence which have the effect of reversing the sign of the spin interaction and which leads to so called "echoes". We shall be concerned with two simple versions which reverse Zeeman broadening, namely, the spin and stimulated echo.

The spin echo experiment, suggested by Hahn in 1950[58], (figure 3.3a) consists of two pulses. The first pulse is 90° and tips the magnetization to the x-y plane (figure 3.3b), following which the spins dephase for a time τ. Then a 180° pulse is applied. This pulse inverts the direction of the precession of the spin (figure 3.3d), and after a time equal to τ an echo is formed (figure 3.3e). The echo attenuation at the time of the echo arises solely from T_2 and can be written as[55]:

$$A(2\tau) = A(0)\exp\left(-\frac{2\tau}{T_2}\right). \tag{3.14}$$

Note that in the absence of the echo formation by the 180° rf pulse, if the spins were allowed to dephase in an inhomogenous magnetic field for a period 2τ after a 90° pulse the FID signal attenuation would be given by:

$$A(2\tau) = A(0)\exp\left(-\frac{2\tau}{T_2^*}\right). \tag{3.15}$$

The spin echo experiment can be used not only for the obvious purpose of measuring the transverse relaxation time, T_2, but for many other applications, among them diffusion measurements[59,60] which will be explained in the following chapter. The spin-echo experiment can be used as long as the experimental time is shorter or on the order of T_2. For $\tau >> T_2$ no signal can be recovered.

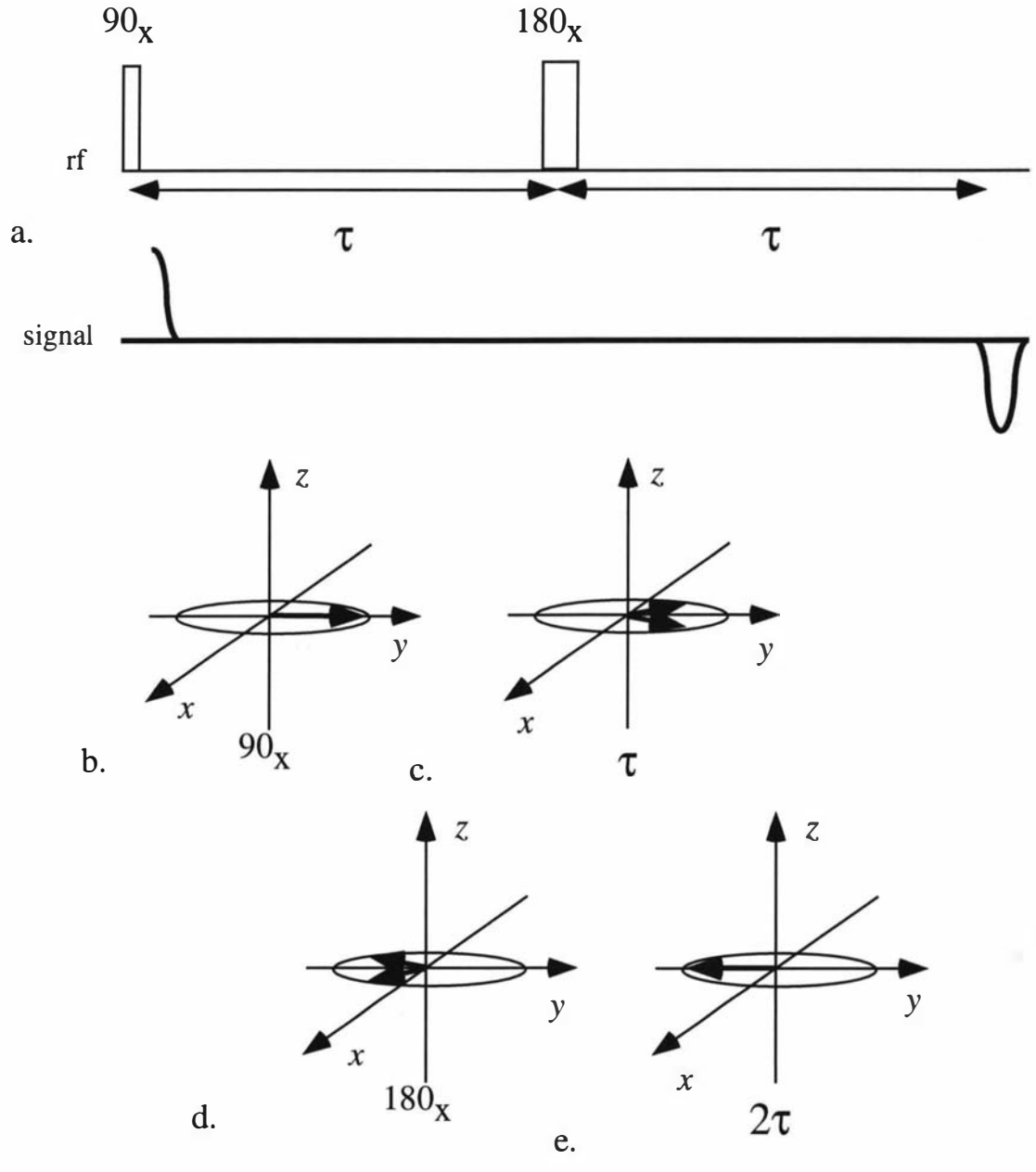

Figure 3.3:
a) The spin echo pulse sequence. b) The first 90° pulse tips the magnetization to the *x*-*y* plane c) The spins dephase for a time τ. d) 180° pulse inverts the directions of the spins. e) The echo is formed at a time equal to 2τ.

When the required experimental time for magnetization observation exceeds the transverse relaxation time, for example, in diffusion measurements with long diffusion times, one needs to use a technique which stores the magnetization out of the x-y and along the z-axis. In this case the experiment will be T_1 weighted. The stimulated echo is an example of such an experiment. The stimulated echo experiment (figure 3.4a) consists three 90° pulses. The first pulse tips the magnetization to the x-y (figure 3.4b) plane for time τ, during which some transverse coherence is lost (figure 3.4c). The second pulse stores the memory of this transverse phase distribution in the z direction (figure 3.4d) permitting evolution of the spin system under the T_1 influence. The third 90 degree pulse tips the magnetization back to the x-y (figure 3.4e) plane to form an echo at time τ (figure 3.4f).

Since the stimulated echo experiment involves three 90° pulses, it is capable of generating a complex pattern of echoes. Up to four echoes can occur in the acquisition window. The unwanted echoes can be eliminated by using a small magnetic field gradient pulse between the second and third pulse and by an effective phase cycling in which both the rf and acquisition phases are altered in a predetermined pattern. Another fact to be considered is the loss of magnetization transferred to zero and double quantum coherence, neither of which are directly detectable in the rf coil. However, the observable magnetization following the stimulated echo experiment is simply related to the various terms used in the pulse sequence and can be written as:

$$A(\tau_1 + 2\tau_2) = 0.5A(0)\exp\left(-\frac{\tau_2}{T_1} - \frac{2\tau_1}{T_2}\right). \tag{3.16}$$

Note that the stimulated echo experiment is also used to see a cross correlation effects in the spin system, these effects will be discussed on the spin diffusion chapter.

3.3 Translational motion of spins

3.3.1 *Diffusion measurement in the presence of continuous magnetic field gradient*

Spin echo experiments, in theory, perfectly refocus all Zeeman precessions of the spins so that the only attenuation observed is that due to the transverse relaxation process. We now consider what happens when spins translational motion occurs in the

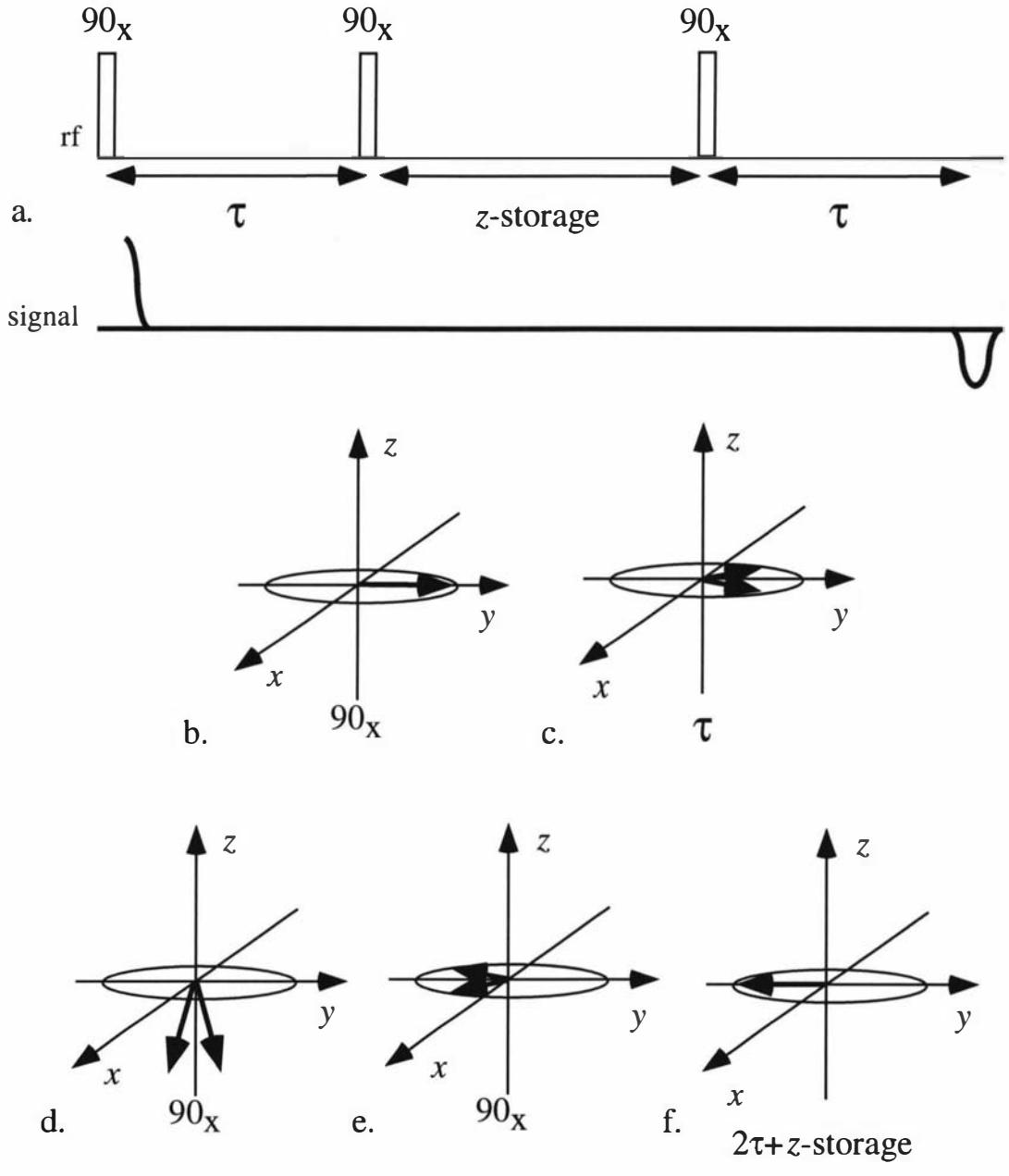

Figure 3.4:
a) The stimulated echo pulse sequence. b) The first 90° pulse tips the magnetization to the *x*-*y* plane c) The spins dephase for a time τ. d) The second 90° pulse stores the magnetization in the *z* direction. e) The third 90° pulse tips the magnetization back to the *x*-*y* plane. f) The echo is formed at a time equal to 2τ+*z*-storage.

presence of a magnetic field gradient. In reality, magnetic field gradients are always present while conducting an NMR experiment. The gradient may come, for example, from inhomogeneities in the static magnetic field, or diamagnetic susceptibility variation due to the structure and shape of the sample. These variations would not matter if the molecules which contain the nuclear spins remain stationary, because the Larmor frequency of the spins will not change during the experiment and the spin echo would be capable of perfect refocusing. But in liquids, where Brownian motion always exists, the diffusion effect must be taken into account and, in fact, we can use the additional dependency due to diffusion as a means to measure diffusion coefficient. The influence of self-diffusion on the spin echo amplitude was mentioned in Hahn's original paper on spin echoes[58] and was calculated a few years later by Carr & Purcell[60]. During the spin echo experiment, and because of the field gradient, spins experience different magnetic fields as they move and as a consequence precess at different Larmor frequencies in each time period of the experiment. The various precessions can be only partially refocused with the 180° pulse, and motion can result in a phase shift which can affect the amplitude of the echo.

In order to simplify the mathematical treatment of the diffusion process, it is described as a succession of random discrete hops in one dimension, the direction of the magnetic field gradient. The following discussion follows the formalism used by Carr and Purcell[60]. Let the mean time between the hops be τ_s and the mean square displacement of every hop, in one dimension, be ξ. The path over which the spins travel after n hops is a one dimensional random walk:

$$Z(n\tau_s) = \sum_{i=1}^{n} \xi a_i \tag{3.17}$$

a_i is a random number equal to ± 1. Z is the z-axis displacement of molecules from their respective origin. The mean square displacement of the spin is:

$$\overline{Z^2(n\tau_s)} = \sum_{i=1}^{n}\sum_{j=1}^{n} \xi^2 \overline{a_i a_j}. \tag{3.18}$$

The horizontal bar represents the ensemble average. When $i \neq j$ $\overline{a_i a_j}$ is zero, but for $i = j$ $\overline{a_i a_j} = 1$. Eq. 3.18 can be replaced with:

$$\overline{Z^2(n\tau_s)} = \sum_{i=1}^{n} \xi^2 \overline{a_i^2} = \xi^2 \sum_{i=1}^{n} 1 = n\xi^2. \tag{3.19}$$

By defining the self-diffusion coefficient as:

$$D = \frac{\xi^2}{2\tau_s} \tag{3.20}$$

the one dimensional mean square displacement can be written:

$$\overline{Z^2(t)} = 2Dt \tag{3.21}$$

or for three dimensions:

$$\overline{R^2(t)} = 6Dt. \tag{3.22}$$

The influence of self-diffusion on the magnetization coherence due to magnetic field gradient, G, can be calculated[57]. We will calculate the phase shift occur due to diffusion of spin, start at the position $z = 0$, in the direction of the gradient. The Larmor frequency in the presence of constant magnetic field gradient is:

$$\omega(n\tau_s) = \gamma B_0 + \gamma G \sum_{i=1}^{n} \xi a_i \tag{3.23}$$

and the angle acquired in that time is:

$$\phi(t) = \omega(n\tau_s) n\tau_s = \gamma B_0 n\tau_s + \sum_{m=1}^{n} \gamma G \tau_s \xi \sum_{i=1}^{m} a_i. \tag{3.24}$$

The first part of the equation is common to all spins and describes the Larmor frequency due to the static magnetic field. The second part of the equation is the part which interests us since it contains the information about the coherence loss.

$$\Delta\phi = \gamma G \tau_s \xi \sum_{i=1}^{n} (n + 1 - i) a_i. \tag{3.25}$$

The phase modulation due to the field gradient is:

$$\overline{\exp(i\Delta\phi)} = \int_{-\infty}^{\infty} P(\Delta\phi)\exp(i\Delta\phi)d(\Delta\phi). \tag{3.26}$$

Eq. 3.26 shows the signal attenuation due to the translational motion at time t. According to the central limits theorem the phase distribution function is Gaussian:

$$P(\Delta\phi) = \left(2\pi\overline{\Delta\phi^2}\right)^{1/2} \exp\left(-\Delta\phi^2 / 2\overline{\Delta\phi^2}\right) \tag{3.27}$$

combining equations 3.26 and 3.27 gives:

$$\overline{\exp(i\Delta\phi)} = \exp\left(-\overline{\Delta\phi^2} / 2\right). \tag{3.28}$$

By squaring eq. 3.25 and eliminating the cross terms we get:

$$\begin{aligned} \overline{\Delta\phi^2} &= \gamma^2 G^2 \tau_s^2 \xi^2 \sum_{i=1}^{n} (n+1-i)^2 \\ &= \gamma^2 G^2 \tau_s^2 \xi^2 \sum_{j=1}^{n} j^2 \\ &= \frac{1}{3}\gamma^2 G^2 \tau_s^2 \xi^2 n^3 \end{aligned} \tag{3.29}$$

by replacing $n\tau_s$ with t and the signal attenuation due to diffusion can be expressed[57]:

$$\overline{\exp(i\Delta\phi)} = \exp\left(-\frac{1}{3}\gamma^2 G^2 D t^3\right). \tag{3.30}$$

The calculations above can be visualized by figure 3.5. The figure shows a triangle which represents the one dimensional phase evolution in time. The starting point of the figure is just after the 90° pulse where the spins start their evolution in the presence of magnetic field gradients. The spins can hop either to the positive or negative direction acquiring a phase shift according to the direction of each hop. The total phase shift acquired by the end of the experiment is the sum of all the individual a_i values. Since it is a random walk, the average phase shift over long time will sum to 0. As shown in eq. 3.29 the first non zero term is the mean squared phase shift. As one can see the net phase shift is the area under the triangle.

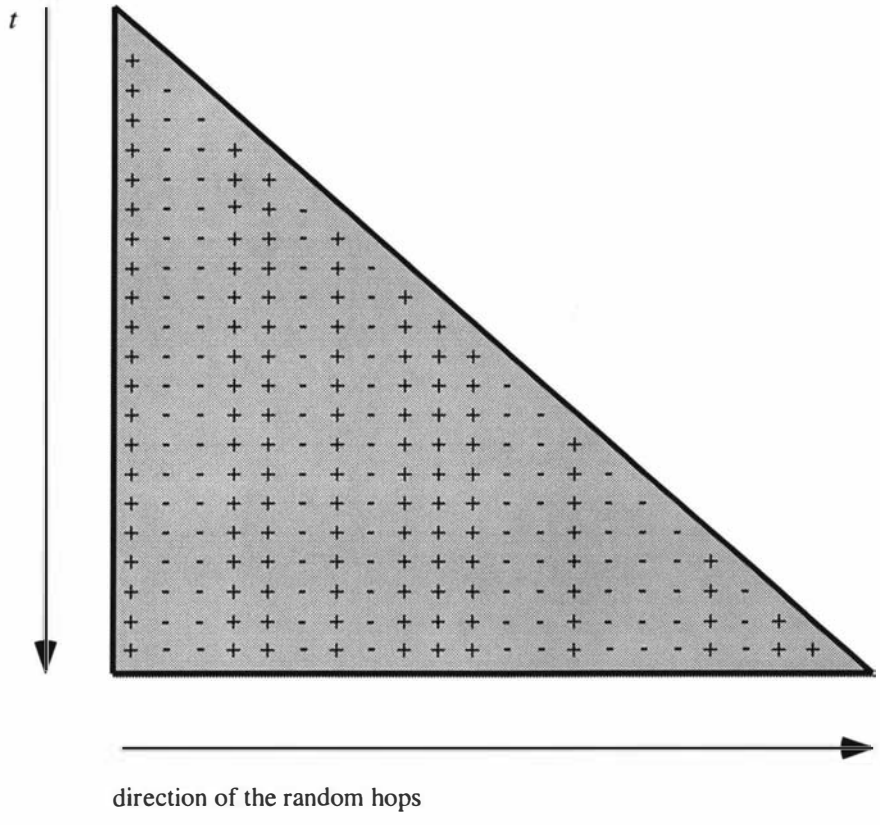

Figure 3.5[57]:
Cumulative phase diagram in which the spins evolve in the presence of magnetic field gradient. The spins can acquire either positive or negative phase according to the direction of the motion. Each row represent a time interval. The + and - signs represent the a_i parameter. Summing horizontally and vertically is equivalent to the double sum in eq. 3.24.

In the spin echo experiment the 180° pulse inverts the sign of the phase. The effect of this 180° pulse is illustrated in figure 3.6. All the phases which accumulated in the first part of the experiment change signs in the second part, which causes partial phase cancellation. The part that contributes to the phase shift in the spin echo experiment, (when squared), is the shaded triangle. As one can see, the area under this triangle is double the area of the triangle acquired in the first part of the experiment. Thus the echo at time $2t$ is:

$$\overline{\exp(i\Delta\phi)} = \exp\left(-\frac{2}{3}\gamma^2 G^2 D t^3\right). \tag{3.31}$$

By knowing the gradient strength the diffusion coefficient can be calculated.

3.3.2 *Pulsed Gradient Spin Echo experiment*

Diffusion measurements with a constant natural field gradient are rather limited. This becomes apparent when one needs to measure motion of very slow molecules such as polymers, where a high magnetic field gradient is needed rather than a weak background gradient. Furthermore, when a steady gradient is deliberately applied the NMR spectrum is greatly broadened leading to the need for large bandwidth rf pulse and large bandwidth data acquisition. The latter requirement greatly degrades the signal-to-noise ratio. In the case of very dilute samples the loss of signal due to acquisition with constant gradient can make diffusion measurements impossible.

Stejskal and Tanner, in 1965, suggested using a pulsed magnetic field gradient to spread the magnetization[59]. By placing a short pulse of high magnetic field gradient on each side of the 180° pulse of the spin echo experiment (figure 3.7a) the spins rapidly acquire a large phase shift which enables one to differentiate between neighboring spins. Unlike the continuous gradient method, the pulsed gradient experiment is more flexible in that one can vary either the pulse duration (δ), the gradient strength or the interval between the two gradient pulses (Δ), depending on the instrument limitations. Moreover, the T_2 relaxation can be kept independent of the diffusion process and the acquisition is made in a relatively homogenous magnetic field. One can visualize this experiment using the phase geometry method of the previous section (figure 3.7b). In a perfectly homogeneous magnetic field, the signal attenuation in the PGSE experiment is[59]:

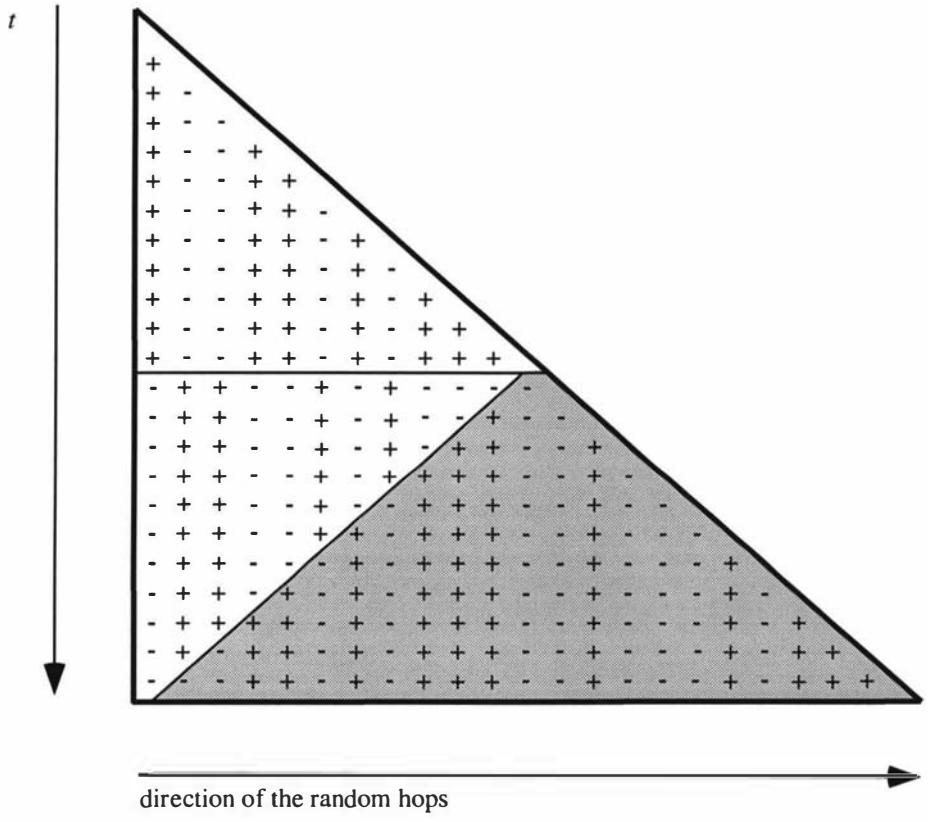

Figure 3.6[57]:
Cumulative phase diagram for the spin echo experiment. The 180° rf pulse canceled part of the phase which was accumulated in the experiment, thus the total phase shift is only the area under the shaded triangle.

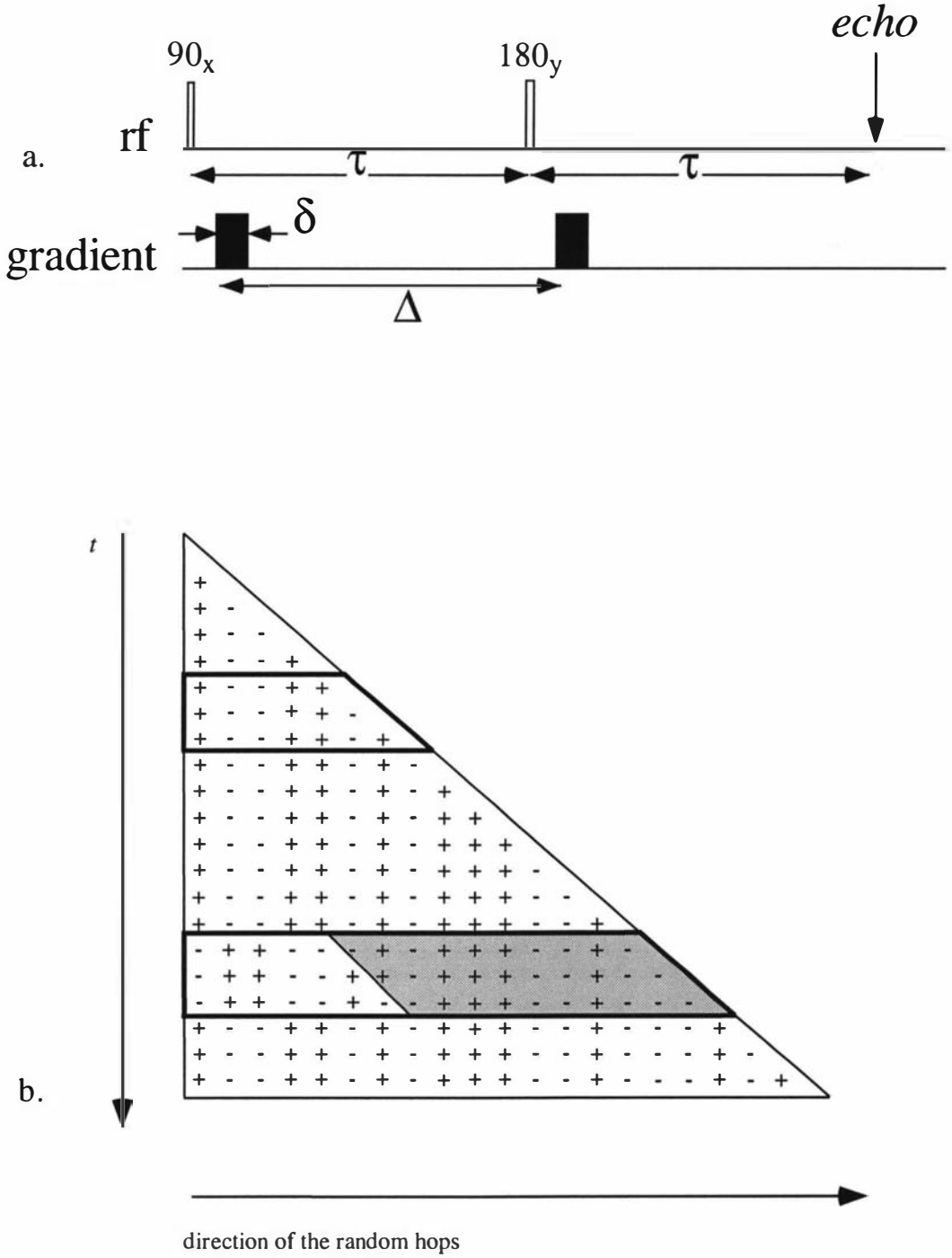

Figure 3.7:
a) PGSE-NMR pulse sequence and b) the PGSE-NMR experiment cumulative phase diagram[57].

$$A(2\tau) = A(0)\exp\left(-\frac{2\tau}{T_2} - (\gamma G\delta)^2 D\left(\Delta - \frac{\delta}{3}\right)\right). \tag{3.32}$$

By repeating the experiment with and without the gradient pulses and dividing the resulting echo, one gets the attenuation only due to the translational motion:

$$A(G)/A(0) = \exp\left(-\gamma^2 G^2 \delta^2 D(\Delta - \delta/3)\right). \tag{3.33}$$

For narrow gradient pulses $(\delta << \Delta)$ equation 3.33 can be written:

$$\begin{aligned} A(G)/A(0) &= \exp\left(-\gamma^2 G^2 \delta^2 D\Delta\right) \\ &= \exp\left(-\frac{1}{2}\gamma^2 G^2 \delta^2 \langle Z^2 \rangle\right) \end{aligned} \tag{3.34}$$

where $\langle Z^2 \rangle = 2D\Delta$. In the finite gradient pulse case $\Delta - \frac{1}{3}\delta$ may be taken to be an effective or reduced diffusion time $\Delta_r = t$.

In the case of an inhomogeneous static magnetic field, which produces a significant additional constant field gradient G_0 an additional factor is needed[59]:

$$\begin{aligned} A(2\tau) = A(0)\exp\left(-\frac{2\tau}{T_2} - (\gamma G\delta)^2 D\left(\Delta - \frac{\delta}{3}\right)\right) \times \exp\left(-\frac{2\gamma^2 G_0 D\tau^3}{3}\right) \\ \times \exp\left(-\gamma^2 G G_0 D\delta\left(t_1^2 + t_2^2 + \delta(t_1 + t_2) + 2\delta^2/3 - 2\tau^2\right)\right) \end{aligned} \tag{3.35}$$

where t_1 is the time between the rf pulse and the beginning of the first gradient pulse and t_2 is the time between the end of the second gradient pulse and the echo. The G_0 effect is negligible when the gradient pulse is two orders of magnitude larger than G_0, which is the case in this thesis.

In the stimulated echo experiment the first gradient pulse occurs after the first rf pulse and the second gradient pulse after the third rf pulse(figure 3.8). The echo attenuation in that experiment can be written as:

$$A(2\tau_1 + \tau_2) = A(0)0.5\exp\left(-\frac{\tau_2}{T_1} - \frac{2\tau_1}{T_2} - (\gamma G\delta)^2 D(\Delta - \delta/3)\right). \tag{3.36}$$

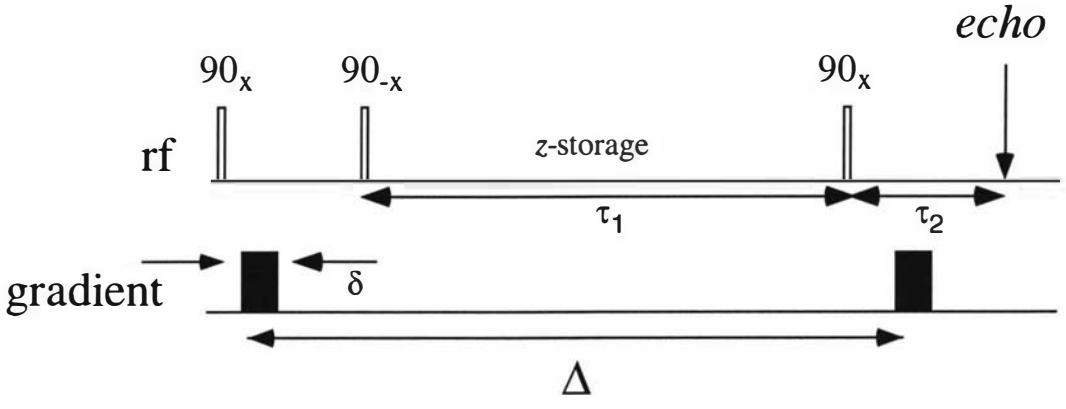

Figure 3.8:
PGSTE-NMR pulse sequence.

By taking a ratio of the echo signal with and without gradients we get the echo attenuation as in eq. 3.33, meaning the same attenuation as for the spin echo experiment.

Finally, it should be noted that it is customary to write the integrated pulse area factor δG in terms of a scattering wavevector $q = (2\pi)^{-1}\gamma\delta G$. Thus one may write the fundamental normalized echo attenuation expression as[57]:

$$\begin{aligned} E(q) &= \exp\left(-4\pi q^2 Dt\right) \\ &= \exp\left(-2\pi q^2 \left\langle Z^2 \right\rangle\right) \end{aligned} \quad . \tag{3.37}$$

3.3.3 *Double PGSE*

A wide range of materials, such as porous media[61,62], liquid crystals[63] and biological tissues[64,65] are structurally anisotropic and as a result the diffusive motion of molecules within those materials will also be anisotropic. PGSE pulse sequences are widely used to detect this anisotropy[61-63,66]. By performing the measurements of diffusion using different gradient directions, the various components of diffusion can be obtained. However, the standard PGSE method is limited to detecting only a *macroscopic* anisotropy. Materials which are structurally anisotropic but whose anisotropic axes are randomly (isotropically) distributed in space, such as polymer melts and semidilute solutions, cannot be examined by such a simple PGSE experiment since the resulting diffusion coefficients will have the same value regardless of the direction of the gradients.

In order to detect such anisotropy one can use a Double-PGSE experiment[57] (figure 3.9). This particular pulse sequence is used in various applications such as a flow compensation experiments[67] and for measuring the eccentricities and symmetries of confining cavities[62,68]. In this thesis we used the method in order to attempt to detect the anisotropic motion of polymers in semidilute solutions. The pulse sequence consists of two sequential single PGSE experiments in which the first PGSE labels the spin motion in one direction while the second set allows a correlation to either the perpendicular direction or the same direction of motion (depending on whether the second gradient set is in the same direction as the first set or in the perpendicular direction). As a result, the attenuation, which is detected after the second gradient set, includes information about the spin history over the whole experimental time. Note, that

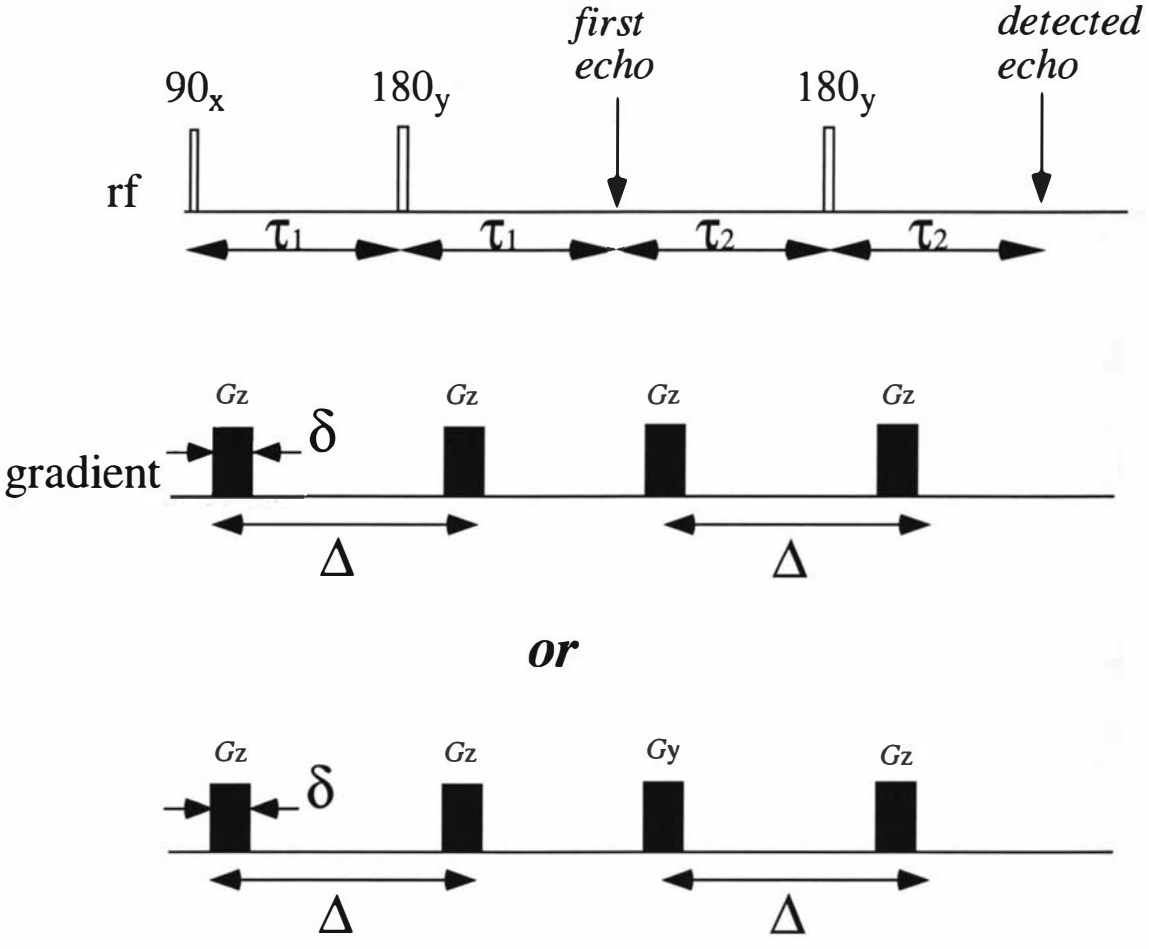

Figure 3.9:
Double-PGSE pulse sequence.

that every detected echo is a two dimensional correlation experiment which is projected into one dimension. Allowing that the local effective diffusion coefficient of each molecule is $D_{\parallel}$ and $D_{\perp}$ respectively with respect to the orthogonal gradients, the echo attenuation detected in the double PGSE experiment can be written.

$$\begin{aligned} A(G)/A(0) &= \left\langle \exp\left(-\gamma^2 G^2 \delta^2 D_{\parallel}(\Delta - \delta/3)\right) \exp\left(-\gamma^2 G^2 \delta^2 D_{\parallel}(\Delta - \delta/3)\right) \right\rangle \\ &= \left\langle \exp\left(-2\gamma^2 G^2 \delta^2 D_{\parallel}(\Delta - \delta/3)\right) \right\rangle \end{aligned} \tag{3.38}$$

or

$$\begin{aligned} A(G)/A(0) &= \left\langle \exp\left(-\gamma^2 G^2 \delta^2 D_{\parallel}(\Delta - \delta/3)\right) \exp\left(-\gamma^2 G^2 \delta^2 D_{\perp}(\Delta - \delta/3)\right) \right\rangle \\ &= \left\langle \exp\left(-\gamma^2 G^2 \delta^2 (D_{\parallel} + D_{\perp})(\Delta - \delta/3)\right) \right\rangle \end{aligned} \tag{3.39}$$

where $\langle \cdots \rangle$ is an ensemble average over the molecules and must take account of the isotropic angular distribution of $D_{\parallel}$ and $D_{\perp}$. As we will show, provided $D_{\parallel} \neq D_{\perp}$, even an isotropic distribution will result in a different echo attenuation in the case of the two PGSE encoding.

The difference in the resulting echo attenuation between the two experiments gives an insight regarding the nature of the anisotropy. The experiment thus distinguishes local and macroscopic anisotropy. Local anisotropy is reflected by $D_{\parallel} \neq D_{\perp}$ with respect to some local direction and materials which are locally anisotropic will show no difference between the two PGSE encoding. Macroscopic anisotropy is reflected by an anisotropic distribution of local directors. Materials which are locally anisotropic but macroscopically isotropic will give identical echo attenuation for a simple pulse pair PGSE experiment, whatever the direction of the gradient, but a different result for the two orthogonal encodings of the double-PGSE experiment.

3.3.4. *Stabilization of the echo*

The major limitation to diffusion measurement concerns the mismatch between the two gradient pulse areas. When the gradient pulses do not match, the phase refocussing process is either incomplete or passes the refocussing point, depending on

which of the two pulses is bigger. As a result one gets a faulty, inconsistent, phase spread which artificially increases the echo attenuation and, because of interaction with the background gradient, results in shift of the position of the echo with the acquisition time window.

The reason for the shift is that the residual background gradient acts to make up the excess or deficit in the pulse mismatch, so that the echo condition, $\int G^*(t)dt = 0$ applies where the effective gradient G^* has opposite sign on each side of the 180° rf pulse. As a rule of thumb, in order to measure a diffusion coefficient smaller than 10^{-15} m^2 s^{-1} the gradient pulses must match down to at least 1 ppm. This accuracy is very hard to achieve and requires a very stable current supply with minimal fluctuations and minimal mains hum. Three problems arise when the echo shifts during the experiment. First, when the echo shifts randomly between two scans, the accumulation of data, necessary for signal averaging, is not possible (figure 3.10a). Furthermore, even when the mismatch is consistent and the shift occurs between different values of gradient pulses, i.e. accumulation of signal in one dimension is possible but there will generally be a shift between the experiment in the second dimension. In other words, as the gradient pulse area is incremented the degree of the time shift will change since the pulse mismatch will depend on gradient pulse area. This means that it is not possible to predict the position of the echo center for the purpose of starting the data acquisition (figure 3.10b).

One way of avoiding this problem is to start the acquisition early and obtain the entire echo envelope. But this procedure will not help when T_2 relaxation effects are significant. In this case the different echoes are centered at different places in the T_2 relaxation envelope. The problem of random pulse area mismatch and their treatment has been discussed by P. Callaghan[57]. One method of overcoming this is known as PGSE-MASSEY[69]. However, in this chapter we will discuss the case that is relevant to this thesis which is the second problem, namely that of a non random mismatch. In order to overcome a *small* mismatch between the two gradient pulses one should carry out the PGSE experiment in the presence of a small background gradient and instead of starting the acquisition from the top of the echo, acquire the echo complete (figure 3.10c). However, it is essential that the residual echo shift should be so small that there is no significant change in position in the T_2 envelope. By acquiring the complete echo one is no longer susceptible to small shifts as regards the echo complete, but the effect of the echo center being shifted from the sampling origin leads to a frequency dependent phase shift in the Fourier transform spectrum. Thus, following F.T. one

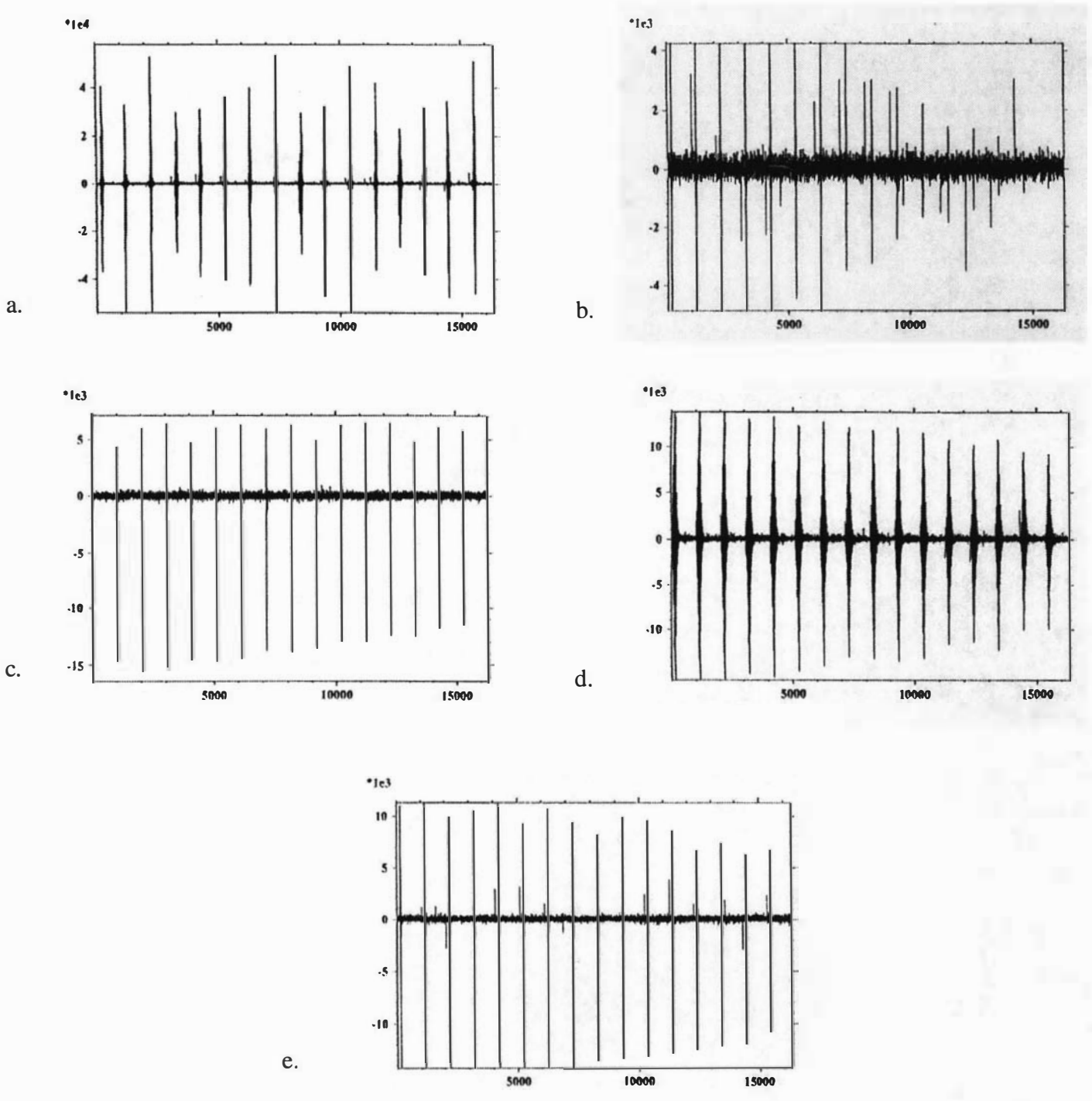

Figure 3.10:
Echo attenuation of a PGSE-NMR experiments. The vertical axis in the (attenuated) signal amplitude, while the horizontal axis is the aquisition data points each separated by 20 μs: a) Attenuations resulting from a random shift of the echo between two scans. b) Attenuations resulting from a consistent mismatch of the gradient pulse. The echo shift occurs between different values of gradient pulses. c) Attenuation resulting when the acquisition start at the top of the echo. d) Attenuation resulting from acquiring the complete echo. e) Attenuation resulting from acquiring the complete echo in the presence of background gradients.

should calculate the magnitude of the spectrum. Of course the use of a background gradient significantly decreases the echo envelope width which help ensure that the whole echo appears in the acquisition window (figure 3.10d). The role of the background gradient in ensuring correct echo refocusing is shown in (figure 3.10e).

4
INSTRUMENTATION

The need to measure the motion of high molecular weight polymers in semidilute solutions requires an ability to measure diffusion coefficients on the order on 10^{-16} m^2 s^{-1}. These measurements require a high magnetic field gradient and highly accurate magnetic field gradient pulses. Those two requirements are hard to achieve and involved building new equipment and considering problems resulting from high current output and mechanical vibrations. This chapter describes the NMR hardware which was used, the problems that were encountered and the solutions which were applied during the work on this thesis.

4.1 The features of the NMR instrument

The NMR instrument used in this thesis comprised a super-conducting vertical wide bore magnet, along with a Bruker AMX 300 NMR spectrometer and a micro-imaging probe. The strength of the magnetic field is 7.05 T, in which the proton's Larmor frequency is 300 MHz. Home built rf coils and gradient coils were attached to the tuning stage of the commercial micro-imaging probe. Those coils will be discussed in the next chapter. Figure 4.1 shows the block diagram of the NMR spectrometer system[57].

4.2 Data acquisition and processing

As mentioned in section 3.3.4, in order to overcome the instrument limitation we had to acquire the complete echo signal and take the magnitude of the Fourier transform spectrum. The number of points in the acquisition window was 2048, 1024 for the imaginary and 1024 for the real part of the spectrum. This was sufficient for the spectral resolution required in this experiment. After the data was acquired it was transferred by ftp to a Macintosh quadra 650 computer and processed with the "PGSE-magnetude-∂-var" software. The "PGSE-magnitude-∂-var" software was written by Andrew Coy[70] and was designed to first Fourier transform the echo data, take the modulus spectrum, integrate the data within a spectral window, and subtract a baseline from a pre-determined spectral region. The program divides the amplitude of this integrated signal by that from the first experiment echo. The resulting attenuation factors are plotted as log(echo attenuation) against q^2 and the resulting mean square

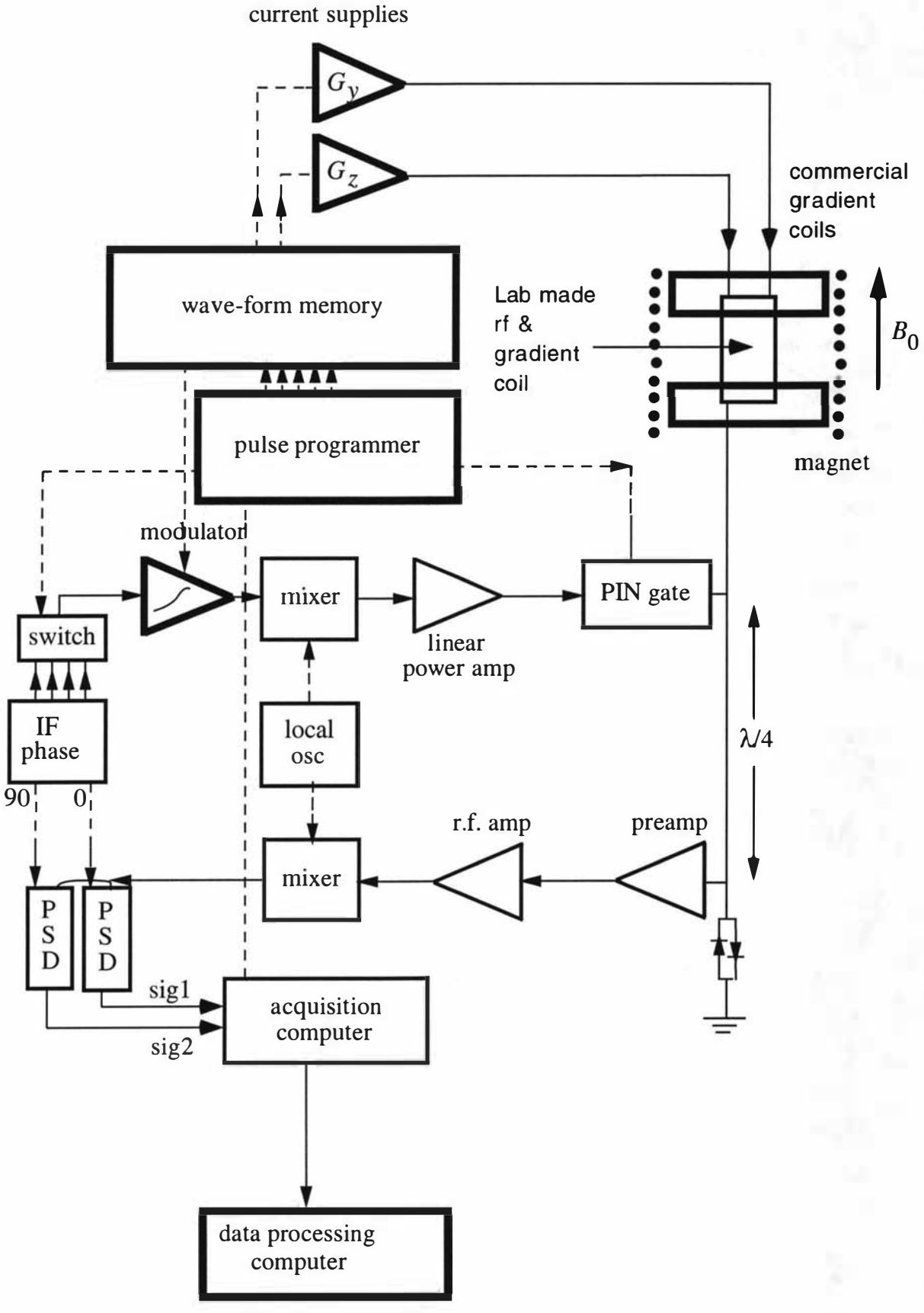

Figure 4.1[57]**:**
Schematic representation of the NMR spectrometer. Note, in our standard experimental setup the gradient cables were soldered directly to the home built gradient coil while the commercial microimaging gradient coils were used only as support to help avoid mechanical vibration.

displacement and diffusion coefficients calculated by linear regression. An example for the program parameter display is shown in figure 4.2.

4.3 The gradient coil

Most PGSE NMR experiments are performed using gradient amplitudes on the order of a few T m^{-1} with a very few researchers reporting work carried out at around 10 T m^{-1}[71-77]. In most cases however the mean squared displacements being measured are quite large (> 10^{-7} m). In order to test the reptation theory one should able to measure motion of high molecular weight polymer solution on the scale of a few hundred angstroms. The time over which their displacement can be measured by NMR is limited to a maximum of a few seconds by spin relaxation and to a minimum of a few ms, by the need to allow for eddy current decay following gradient coil current switching. For NMR time scales on the order of ms to seconds, the desired distance scale corresponds to diffusion coefficients on the order of $10^{-15} - 10^{-16}$ m^2 s^{-1}. This is at the lower limit ever achieved by PGSE NMR. In this work we report on the lowest ever diffusion coefficient measured using this technique. Such measurements require a high performance gradient coil. In particular the coil used to produce large gradients on the order of several 10's T m^{-1}. One feature which needs to be considered is that we will want a gradient pulse duration somewhat smaller than the diffusion time if we are to satisfy the narrow pulse approximation on which the analysis is based[57]. Since the diffusion time, Δ, in our experiment can go down to a few milliseconds we find that we need to produce gradients in excess of 20 T m^{-1}.

One solution to the problem of how to generate large magnetic field gradients is offered by the stray field method of Kimmich and co-workers[72]. When a steady gradient is used in combination with a stimulated echo rf pulse sequence, the effect is to cause the effective gradient to be non-zero only during the periods of transverse magnetization evolution (*i.e.* single quantum coherence) and zero during periods of *z*-storage (*i.e.* polarization). By utilizing the stray field in the outer bore of a superconducting magnet it is possible to achieve 20 T m^{-1} without difficulty, and in the case of a specially constructed Maxwell pair superconductor[73], around 200 T m^{-1}. However the stray field method suffers from three principal defects. First, there is a loss of spectral resolution due to the need to acquire the signal in the presence of the gradient. Second, the rf excitation of the spins and subsequent acquisition in the presence of the gradient implies that only a narrow slice of sample will participate and

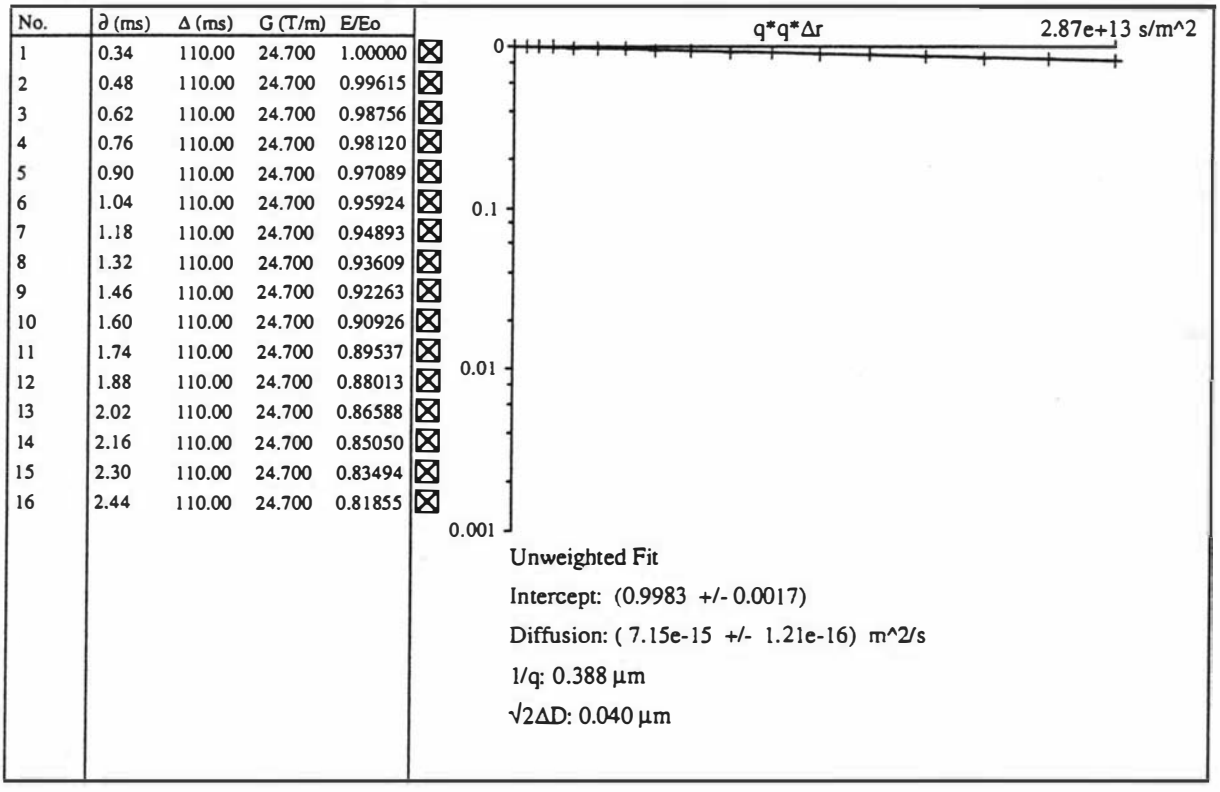

Figure 4.2:
The output of the program "PGSE-magnitude-∂-var". 4.96% 15.4×10^6 dalton Polystyrene in a deuterated toluene, Δ=110 ms .

that the signal must be detected at wide spectral width, both effects causing a severe reduction in available signal-to noise ratio. Finally, the inability to control the magnitude of q except by varying the duration of transverse magnetization evolution makes it difficult to separate the influence of relaxation, dipolar dephasing and gradient dephasing, thus leading to some ambiguity in data interpretation unless special steps are taken to elucidate these effects.

The second solution to the problem involves the design and building of a high gradient coil for use in the PGSE experiment. A 1.2 T m^{-1} A^{-1} gradient coil was designed, built and used in previous high spatial resolution experiments for an older 60 MHz ^{1}H-NMR probe in an electromagnet based spectrometer[71]. Using the same quadrupole design we have built a one channel (G_z) gradient coil[78] and a two (G_y, G_z) channel gradient coil of 1.65 and 2.4 T m^{-1} A^{-1} respectively, which can be incorporated in the 300 MHz ^1H NMR probe of our wide-bore superconducting magnet. A photograph of the coil assembly is shown in Figure 4.3b and 4.4b. The schematic layout of the coils is shown in Figure 4.3a and 4.4a. The one channel coil comprises a quadrupolar array with 23 turns per bundle, each bundle being wound between two holes drilled in supporting posts. The 0.36 mm diameter enameled copper wires, while under tension, are initially free standing, but subsequently potted in epoxy (Araldite, Ciba-Geigy) which penetrates the bundle and once set, provides mechanical support. At the array center a three turn 4 mm diameter solenoidal rf coil is wound around a horizontal glass supporting tube, thus providing a 3 mm diameter sample space. The 90^o pulse time of this coil at 50W and 300 MHz is 4 μs. The gradient coil has an inductance of 15.3 μH and a resistance of 0.8 Ω.

The two channel coil comprises a quadrupolar array with 27 turns per bundle, the horizontal structure being the G_z-channel and the diagonal structure, the G_y-channel. The diameter of the enameled copper wires is 0.254 mm, and the wire bundles were potted in epoxy (Araldite, Ciba-Geigy) in the same manner the one channel coil. The solenoidal rf system differs from the one channel coil only in the number of turns on the coil, which is four, and the duration of the 90° pulse, which is 4.5 μs. The gradient coil has an inductance of 37 μH on the G_z-channel and 31 μH on the G_y-channel and a resistance of 1.9 Ω and 1.5 Ω respectively.

Figure 4.5b-d shows the calculated gradient distribution over the 2.0 mm inner diameter of the sample tube space. The uniformity is very good, with a standard

a.

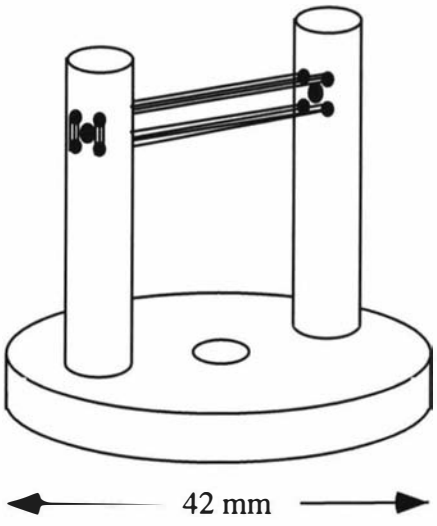

b.

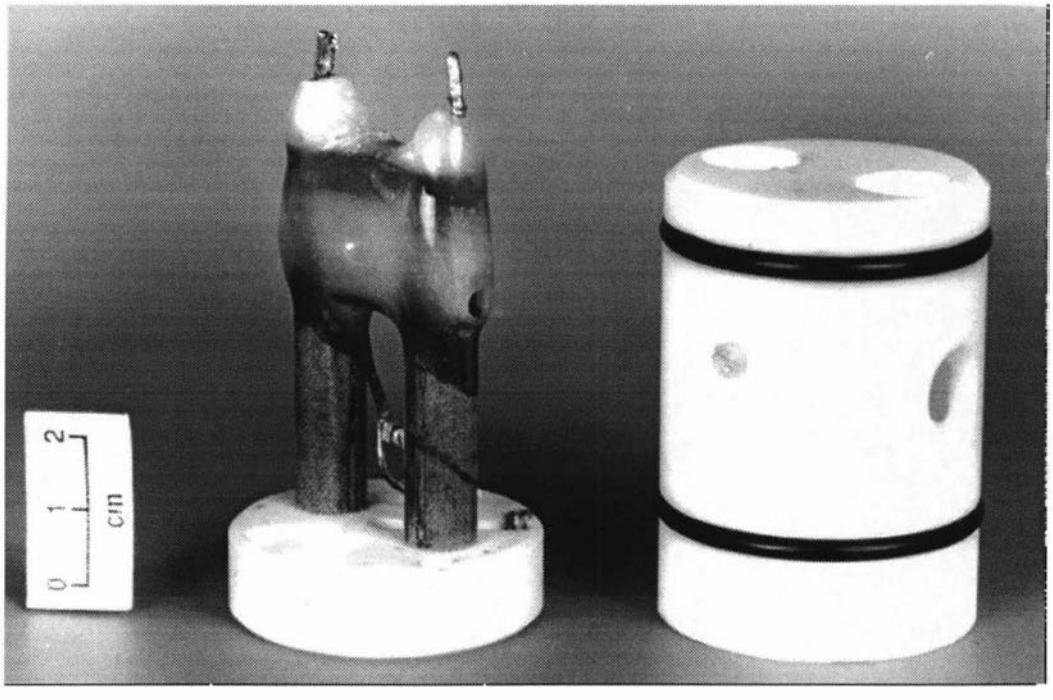

Figure 4.3[78]:
a) Schematic diagram of the one channel gradient coil assembly. b) Photograph of coil assembly and mechanical cowling.

a.

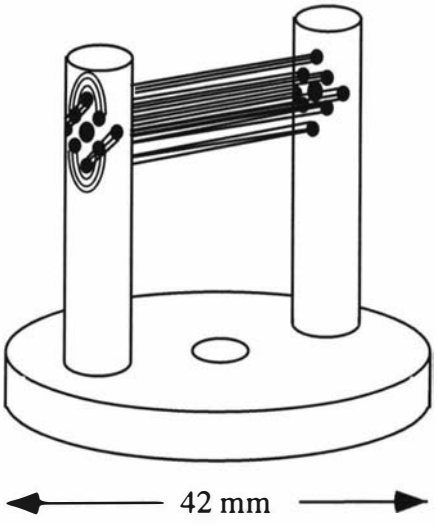

b.

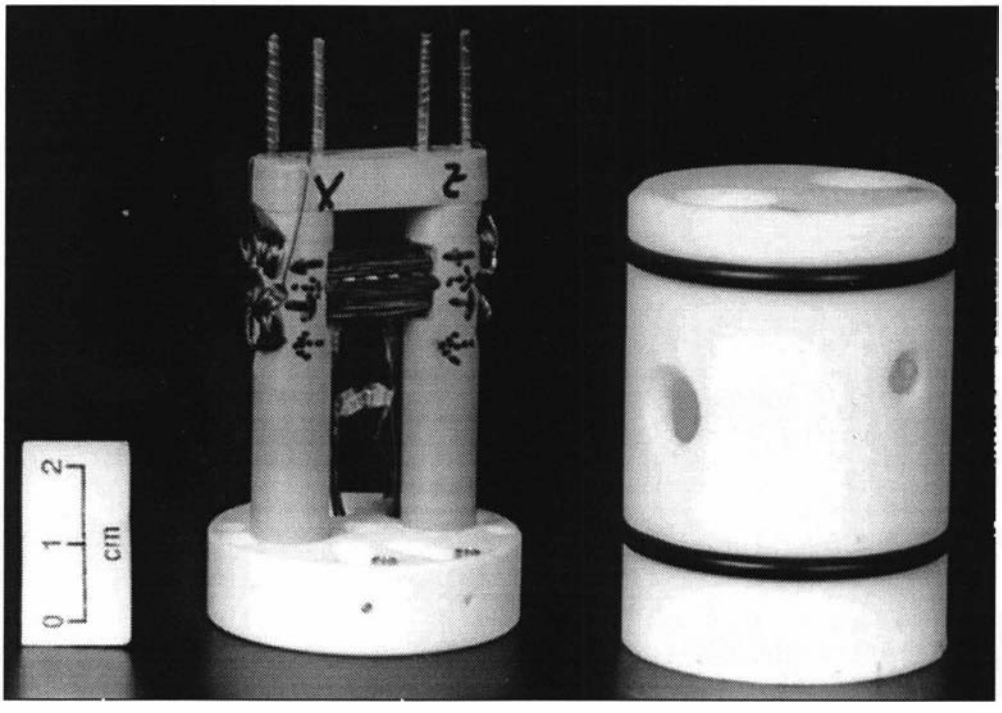

Figure 4.4:
a) Schematic diagram of the two channels gradient coil assembly. b) Photograph of coil assembly and mechanical cowling.

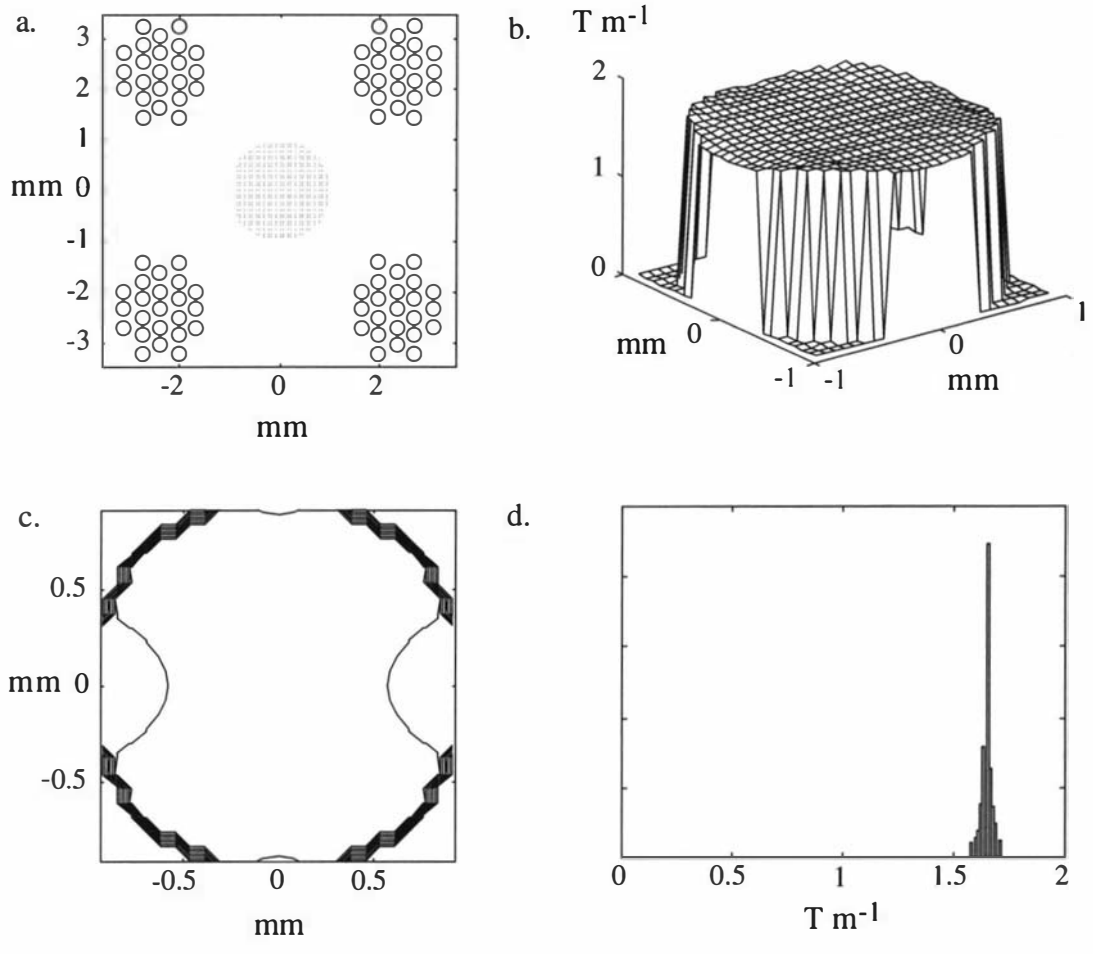

Figure 4.5[78]**:**
a) Layout of the wire bundle of the one channel gradient coil in relation to the sample space of 2 mm diameter shown in cross-section. b) Stackplot profile of gradient across sample space. c) Contour map of gradient distribution across sample space. d) Histogram of gradient distribution across 2 mm diameter sample space.

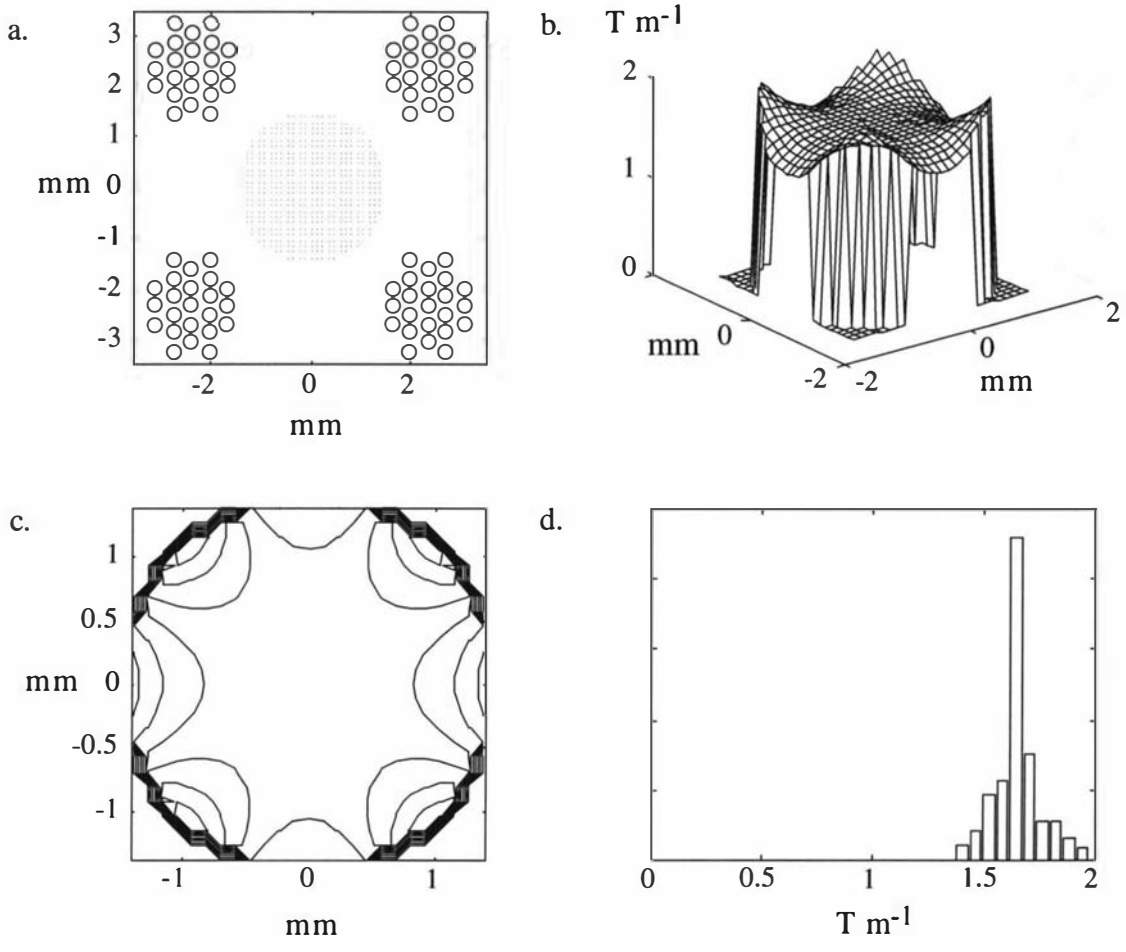

Figure 4.6[78]:
As for figure 4.5, but for a 3 mm diameter sample space.

deviation of 2.5%. By comparison, the uniformity is somewhat poorer over a 3 mm diameter as shown in figure 4.6b-d, the standard deviation being 8%. The mean gradient strength is 1.65 T m^{-1} A^{-1} on the one channel coil, 2.4 T m^{-1} A^{-1} on the z-coil and on the y-coil

There is a general maxim concerning PGSE NMR which can be summarized as follows[78]. *All artefacts cause excess echo attenuation, never reduced echo attenuation. All PGSE NMR systems have a lower limit of mean squared displacement below which artefactual attenuation exceeds diffusive attenuation.* In consequence the diagnostics to be used in testing a PGSE NMR system should be based on the use of a sample for which the mean squared displacements of the spins are as small as possible. We use a very high molecular weight semi-dilute polymer sample (4.96% w/v $20x10^6$ daltons polystyrene in deuterated toluene) in which the segmental mean squared displacements over the PGSE time Δ are exceedingly small (~ 100 $\mathring{A}$) for Δ on the order of T_2 (around 35 ms). Because the echo attenuation due to diffusive motion is small, attenuation due to spurious effects become dramatically obvious. By this means we are able to progressively improve the system.

The first problem to be overcome concerned that due to mechanical motion of the coil set, an effect not obvious at 1.4 T but very important in a 7 T environment. To this end a Teflon cowling was designed with locking screws which sits tightly around the gradient coil assembly. The cowling is shown in the photograph in figures 4.3b, 4.4b. The cowling is then held firmly inside the bore of the Bruker micro-imaging gradient coil assembly by means of two rubber o-rings. The current leads which enter the bore from above are well-supported in the vicinity of the coil so that no whiplash motion is transferred. Finally, the sample tube is securely located in the bore of the rf tube by means of Teflon tape. Each of the these steps was found to be crucial to the operation of the system at the required spatial resolution. The second problem concerned the choice of power supply and will be clarified in the next chapter.

As mentioned in chapter 3, for an ensemble of molecules undergoing unrestricted Fickian self-diffusion, the distribution of mean-squared displacements will be Gaussian and so

$$E(q) = \exp\left(-2\pi^2 q^2 \left\langle Z^2 \right\rangle\right). \tag{4.1}$$

An example of such Gaussian behavior is shown in figure 4.7 for the a 4.96% solution of 1.57×10^6 daltons polystyrene in per-deuterated toluene. This experiment was performed with Δ=1000 ms and G=14.85 T m^{-1} and with q varied by changing the pulse duration, δ. The mean squared displacement, $\langle Z^2 \rangle$, is on the order of 5000 $\mathring{A}$ for this example.

In the case of slow diffusion, in particular the internal modes of high polymers, the motion is non-Fickian and equation 4.1 cannot be used. In general, for any stochastic displacement distribution $E(q) = \langle \exp(i2\pi qZ) \rangle$ and the Taylor expansion for E gives:

$$E(q) \approx 1 - \frac{1}{2}(2\pi q)^2 \langle Z^2 \rangle + \frac{1}{12}(2\pi q)^2 \langle Z^4 \rangle - \ldots \qquad (4.2)$$

so that the semi-logarithmic plot $\ln(E)$ *vs* q^2 will be approximately linear down to attenuation values of around 0.8, and yield the mean squared displacement $\langle Z^2 \rangle$ directly.

As an example of how small a diffusion coefficient may be measured using our apparatus we shown in figure 4.8 the echo attenuation plot for a 23.58% solution of 3×10^6 daltons polystyrene in the same deuterated toluene solvent. The value obtained is 7.5×10^{-16} m^2 s^{-1}. To our knowledge this value is lower by a factor of 3 than any published value obtained using NMR field gradient methods.

4.4 Power supply

When the goal is to achieve a resolution of 100 $\mathring{A}$, one needs not only a strong gradient coil but also a power supply which will be able to produce high yet very stable current pulses. All active current sources have noise and hum. At 100 $\mathring{A}$ resolution the matching required in the gradient pulse areas is on the order of 10 ppm, a level below that normally measurable by electronic means, but easily detectable in the diagnostic

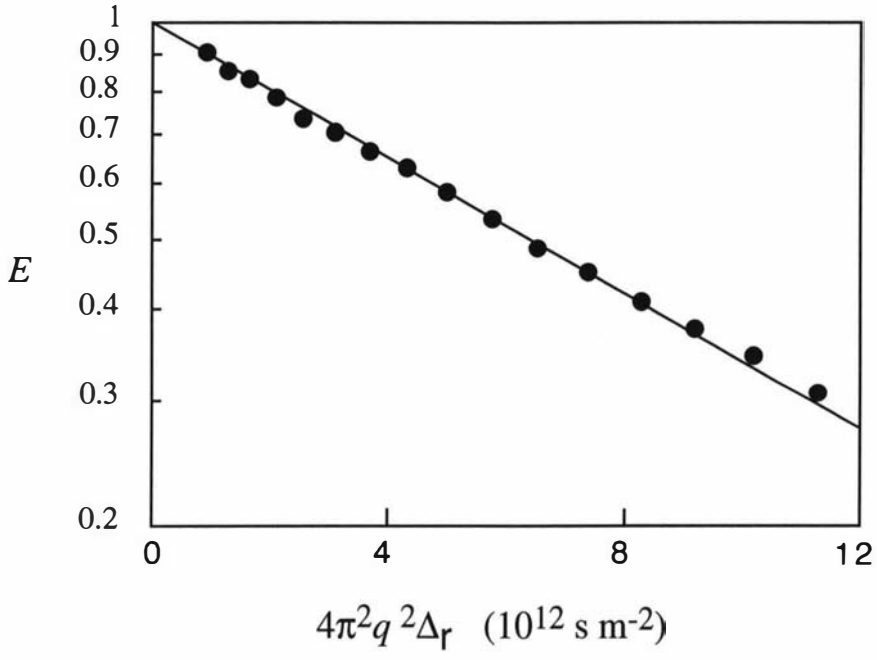

Figure 4.7[78]:
Echo attenuation plot for a sample of 4.96% w/v 1.75×10^6 daltons polystyrene in deuterated toluene for a diffusion time Δ=1000 ms. The experiment was performed by keeping G constant at 14.75 T m^{-1} and varying the pulse duration δ.

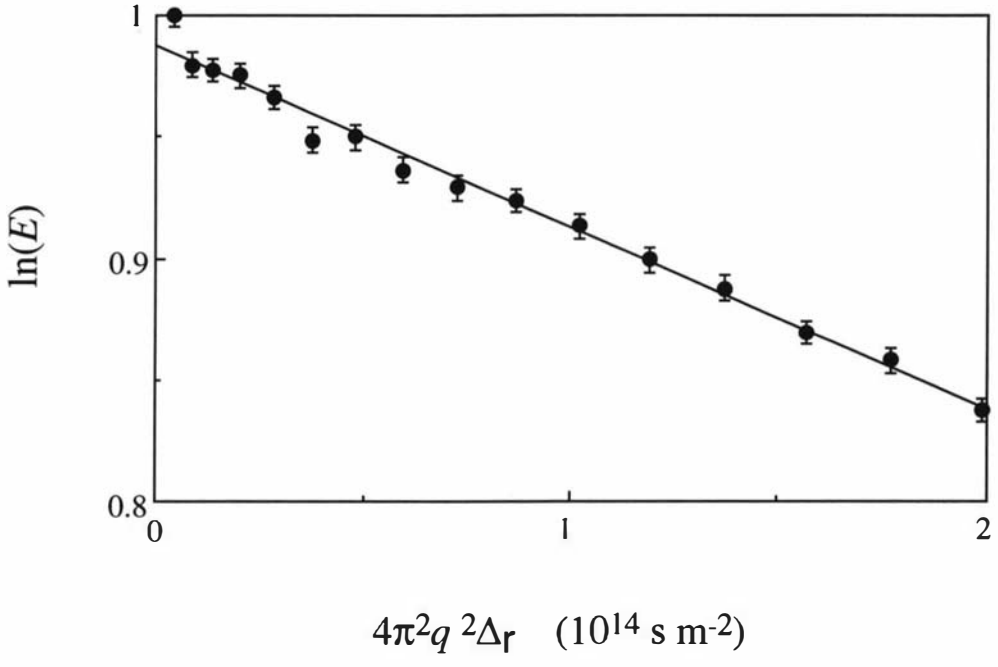

Figure 4.8[78]:

Echo attenuation plot for a sample of 23.58% w/v 3.0×10^6 daltons polystyrene in deuterated toluene for a diffusion time Δ=1000 ms. The experiment was performed by keeping G constant at 24.75 T m^{-1} and varying the pulse duration δ. Note that the diffusion coefficient thus obtained is 7.5×10^{-16} m^2 s^{-1}.

PGSE NMR signal. Of a range of well-known commercial power supplies which we have compared (Kepco, Techron 7570 and Bruker B-AFPA 30 and 40 with external loop compensation), only one of the Bruker B-AFPA 30 series (internal loop compensation) proved of sufficient quality. These systems are unusual in their use of toroidally wound transformers whose stray mains frequency fields are very small. We have found however that these supplies respond best when the current pulse is ramped on the leading and trailing edges using around 20 steps each of a few microseconds duration, thus giving a controlled rise and fall time on the order of 100 μs (figure 4.9). We achieve this by means of the gradient waveform memory control in the Bruker AMX-300 micro imaging accessory.

Finally, we note that the use of a few dummy gradient pulses applied just before the PGSE pair significantly improved the performance of the system at the highest spatial resolution limit. We attributed this effect to the settling of the power supply into a steady state mode of current delivery. This settling is probably due to the current sensing resistor in the power amplifier reaching thermal equilibrium. When high current is demanded the current sensing resistor warms up slightly due to its own power dissipation and its resistance increases. The amplifier calibration is therefore altered and this results in a second gradient pulse slightly smaller than the first.

4.5 Dual gradient apparatus

As described in chapter 3.3.3 we used the Double PGSE experiment in order to directly detect the local anisotropic motion associated with reptation dynamic. The experiment is constructed from a repeated pair of PGSE gradients pulses. This double-PGSE method consists of a sequence of four *identical* gradient pulses, two in one direction and two in same or in orthogonal direction. In order to stabilize the current output to the gradient coil, in addition to the PGSE gradient pulses several dummy gradient pulses are applied. These dummy pulses are applied before the start of the experiment (i.e. the application of the 90° rf pulse) in order to bring the current sensing resistor in the power supply to thermal equilibrium. The need for identical gradient pulses amplitude forced us to use only one power supply to drive the current in both pair of pulses. In the case where the first pair was applied to the G_z coil and the second to the G_y coil, it was necessary to re-route the current. Normally in NMR imaging experiments, where this kind of gradient accuracy is not required, each gradient

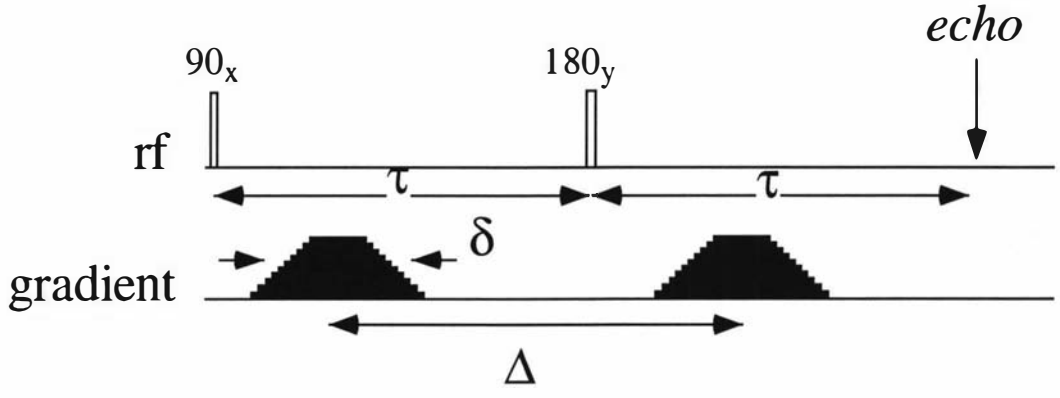

Figure 4.9:
Schematic diagram of the PGSE experiment pulse sequence with the ramped gradient pulses.

direction is driven by its own separate power supply. In order to be able to use only one power supply in this experiment, a special switching box was designed and built by Mr. Robin Dyktsra from the electronic workshop. The switching box is designed to channel the current from the power supply to one coil at a time. The switching between the channels is controlled by external TTL pulses from the spectrometer.

The use of background gradients in this experiment was not an easy task. In the single PGSE experiment the background gradient was produced by the same gradient coil used for the gradient pulses. The only way to use the same coil for the background gradient and the pulses in the double-PGSE experiment is to give a background gradient in one channel at a time. This means that when the direction is to be switched from z to x half of the experiment will be conducted in the presence of z background gradient and the other half will be conducted in the presence of the y background gradient. In this case, it is very important to ensure that the switching between the two gradients happens at the top of the first echo, so that the signal from the first part of the experiment is completely refocused. Without this perfect timing the second gradient channel will not be able to refocus the signal in the second cycle and the signal will be dephased. Since our echo is shifting a little bit between experiments and there is no simple way to monitor and switch the gradients on time and the two background gradients need to be present at all times. In order to achieve this a separate power supply was connected to the commercial micro-imaging z and y gradient coil to give constant background gradients of 0.023 T m^{-1}. The background current was controlled by an external TTL line from the spectrometer. Figure 4.10 shows a block diagram of the dual gradient apparatus.

4.6 Disaster, safety and other aspects

4.6.1 *Safety fuses*

The coil described in chapter 4.3, unfortunately, can no longer be used. A software error which did not send the turn off command to the power supply allowed a constant current to flow in the gradient coil. Unlike the 30-BAPA, the 40-BAPA series power supply, which was used during this particular event, did not have protection fuses inside and as a result the coil burned out, and so a replacement coil with the same features was built. After one software error too many in which the commercial Bruker gradient coil was also damaged, external safety fuses were introduced to the system. 2 amp motor rated HRC cartridge 10x38 mm fuses manufactured by Gould, were

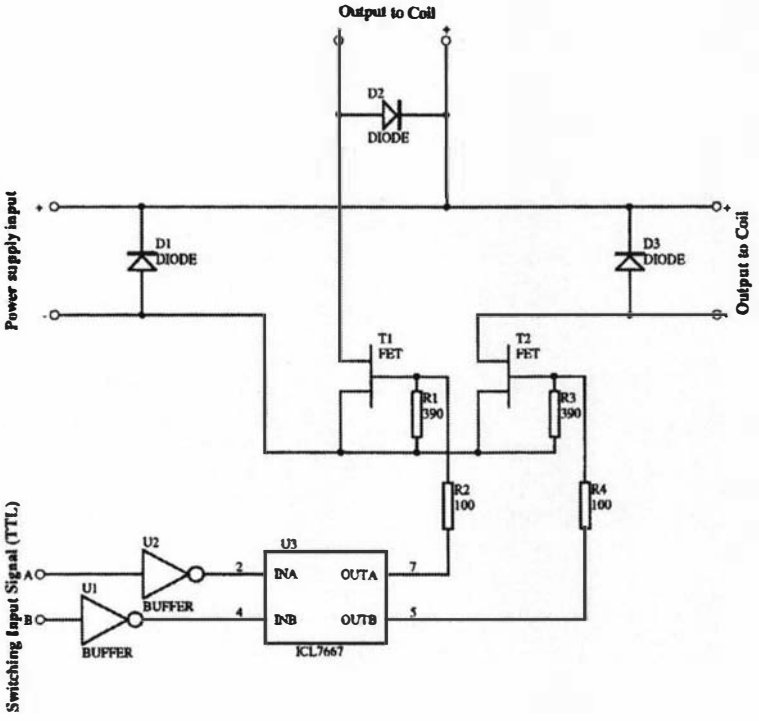

Figure 4.10:
Schematic diagram of the switching box.

connected in series to each power supply. These thermal sensitive fuses can withstand high transient current.

4.6.2 *Resistors box*

When the experiment required a large gradient value and hence a large current output from the power supply, it was found that the gradient amplifier would shut down due to excessive internal power dissipation. When the load resistance is small the output voltage from the power supply needs to be small and the power supply has to drop a large voltage internally. As a result excessive power is dissipating internally. A way to avoid this problem is to dissipate more power externally by putting a suitable resistor in series with the load. In order to achieve this, a resistor box was connected to give a total load of 3 ohms in the case of the two channel gradient coil and 2 ohms in the case of the one channel coil.

In the two channel coil set up, the resistor box was connected in series between the power supply and the switching box. In this particular experiment the resistor box also provided another function as protection to the power supply in case something happened to the switching box. For example, if the switching box burnt out during the experiment and produced a short circuit across the power supply, the resistor box helps to limit the current.

4.6.3. *Screened cables*

Half way through this work we started to pick up electromagnetic interference from the surrounding environment. The source of that pick up was unknown but the reason we could receive it lay in the geometric layout of the leads. Our gradient coils are connected to the power supply by long cables which are soldered to the gradient coil and stretched to the power supply from the top of the magnets. Those cables served as an antenna which was sensitive to radio frequency pickups. One consequence of this interference was a sharp random spike in our spectrum. We solved this problem by using screened cables.

5
NMR RESULTS

The main purpose of this thesis was to experimentally test the validity of the reptation theory. The PGSE-NMR method is the primary technique which we used for this purpose. In the previous chapter we described all the modifications which were made to our NMR system, in order to be able to measure diffusion coefficients on the order of 10^{-16} m^2 s^{-1}. This chapter presents those PGSE-NMR results along with a discussion of fits to the reptation theory.

5.1 Materials and methods

All the polymer samples used in this work were obtained from Polymer Laboratories, Church Stretton, Shropshire, UK, and their details are shown in Table 5.1. These polymers were dissolved in >99% deuterated toluene (Aldrich, Milwaukee, WI, USA), and were allowed to equilibrate for at least two months before transfer to 3.0 mm NMR tubes which were made at the glass workshop, following which they were sealed and allowed to equilibrate for several weeks. The polymer samples used for the concentration dependence experiments were made in the same way and their details are shown in Table 5.2.

Most of the experiments were performed at a controlled laboratory temperature of 27 °C. A typical set of echo attenuation data of stimulated-echo experiment at any short observation time Δ involved 16 values of q, with 16 signal averages, the time required per run being 40 minutes. In the spin echo experiments, where a delay of 20 s to 60 s between each acquisition was required in order to minimize any gradient coil heating effects, we used 8 scans and each measurement took few hours. The samples were inserted into the rf coil using Teflon tape to secure them against mechanical vibration and the entire probe assembly was heavily damped to minimize vibration.

The T_2 and T_1 of the polystyrene aromatic protons were approximately 70 ms and 800 ms respectively at the 4.96% concentration used in the majority of our work. It was not possible to carry out spin echo diffusion measurements with Δ values in excess of 45 ms and stimulated echo experiments in excess of 3 s. In both types of experiments when the extremes of time were being investigated, signal averaging was considerably extended, for example by taking many hours to acquire 16 q-values each with 128 acquisitions.

M_p	$\frac{M_w}{M_n}$	c (w/v)	c^* (w/v) $\frac{M_p}{N_A R^3}$	R $\left(\mathring{A}\right)$ (known)	D_G ($m^2\ s^{-1}$) (fitted)	a $\left(\mathring{A}\right)$ (fitted)	Z $\frac{R^2}{a^2}$	τ_d (s) $\frac{R^2}{3\pi^2 D_G}$	τ_R (s) $\frac{\tau_d}{3Z}$
20.0×10^6	1.30	4.96%	0.11%	3488	2.4×10^{-16}	210	279	17	2×10^{-2}
15.4×10^6	1.30	4.96%	0.12%	3061	3.4×10^{-16}	200	234	9.3	1×10^{-2}
10.2×10^6	1.25	4.96%	0.15%	2491	6.8×10^{-16}	300	69	3.1	1×10^{-2}
8.42×10^6	1.17	4.96%	0.16%	2263	1.1×10^{-15}	300	57	1.7	1×10^{-2}
6.5×10^6	1.12	4.96%	0.18%	1986	1.9×10^{-15}	300	43	7.1×10^{-1}	5×10^{-3}
4.0×10^6	1.06	4.96%	0.23%	1560	7.0×10^{-15}	300	27	1.2×10^{-1}	1×10^{-3}
3.04×10^6	1.04	4.96%	0.27%	1360	1.6×10^{-14}	300	20	3.9×10^{-2}	7×10^{-4}
1.95×10^6	1.04	4.96%	0.34%	1089	4.4×10^{-14}	300	13	9.1×10^{-3}	2×10^{-4}
1.57×10^6	1.06	4.96%	0.37%	977	1.1×10^{-13}	300	11	2.4×10^{-3}	9×10^{-5}

Fits for molar masses below 8.42×10^6 insensitive to tube diameter and a is set to 300 $\mathring{A}$.

Table 5.1:

Parameters relevant to the molar mass dependence of segmental diffusion at fixed concentration.

M_p	c (w/v)	D_G ($m^2\ s^{-1}$) (fitted)	a ($\mathring{A}$) (fitted)	Z $\frac{R^2}{a^2}$	τ_d (s) $\frac{R^2}{3\pi^2 D_G}$	τ_R (s) $\frac{\tau_d}{3Z}$
3.04×10^6	4.96%	1.6×10^{-14}	300	20	3.9×10^{-2}	7×10^{-4}
3.04×10^6	10.48%	1.2×10^{-15}	200	39	4.4×10^{-1}	4×10^{-3}
3.04×10^6	16.64%	6.6×10^{-16}	180	43	7.2×10^{-1}	6×10^{-3}
3.04×10^6	23.58%	2.5×10^{-16}	160	51	1.7×10^{-0}	1×10^{-2}

Table 5.2:

Parameters relevant to the concentration dependence of segmental diffusion at fixed molar mass.

Figure 5.1 shows a typical spin echo attenuation plot. In all the data shown in this thesis, t is taken as the reduced time $\Delta_r = \Delta - \frac{\delta}{3}$, a distinction which is only significant for $\Delta < 10\,\text{ms}$ and at the largest values of q used. (While this correction assumes Fickian diffusion we emphasize that the use of Δ_r can be justified given that the correction is small, and given the scatter in the data obtained for values of $\Delta < 10\,\text{ms}$, a consequence of the fact that the echo attenuations which could be achieved at these short values of Δ (and hence δ) were less than in the case of the data shown in figure 5.1 and the error in fitting for $\langle Z^2 \rangle$is consequently greater.

5.2 Fitting the tube/reptation model

Figure 5.2 shows a family of curves, $\langle Z^2 \rangle$ vs t, for nine different molar masses ranging from $1.57\text{x}10^6$ daltons to $20\text{x}10^6$ daltons, all at 4.96% in per deuterated toluene. It is immediately apparent that these $\langle Z^2 \rangle$ vs t data cover a range of scaling regimes $\langle Z^2 \rangle \sim t^{\alpha}$ where α lies between 0.25 and 1, as can be seen in the tangents plotted in figure 5.2. We next test whether these data are consistent with the Doi-Edwards theory by attempting to fit them with equation 2.36, the single closed form expression for $\langle Z^2 \rangle$ which encompasses regimes II through IV.

One crucial parameter to be determined is the end-to-end length for each molar mass, which varies (for $c > c^*$). The coil radius in infinite dilution is $R^{(0)} \cong N^{\upsilon} b$ and the overlap concentration is taken as:

$$c_k^* \cong \frac{N}{\left(R^{(0)}\right)^3} \cong \frac{N^{1-3\upsilon}}{b^3}. \tag{5.1}$$

Above c_k^* excluded volume interactions play a role at a length scale below the screening length but above the screening length the chain is Gaussian. Consequently it is concentration dependent and can be written,

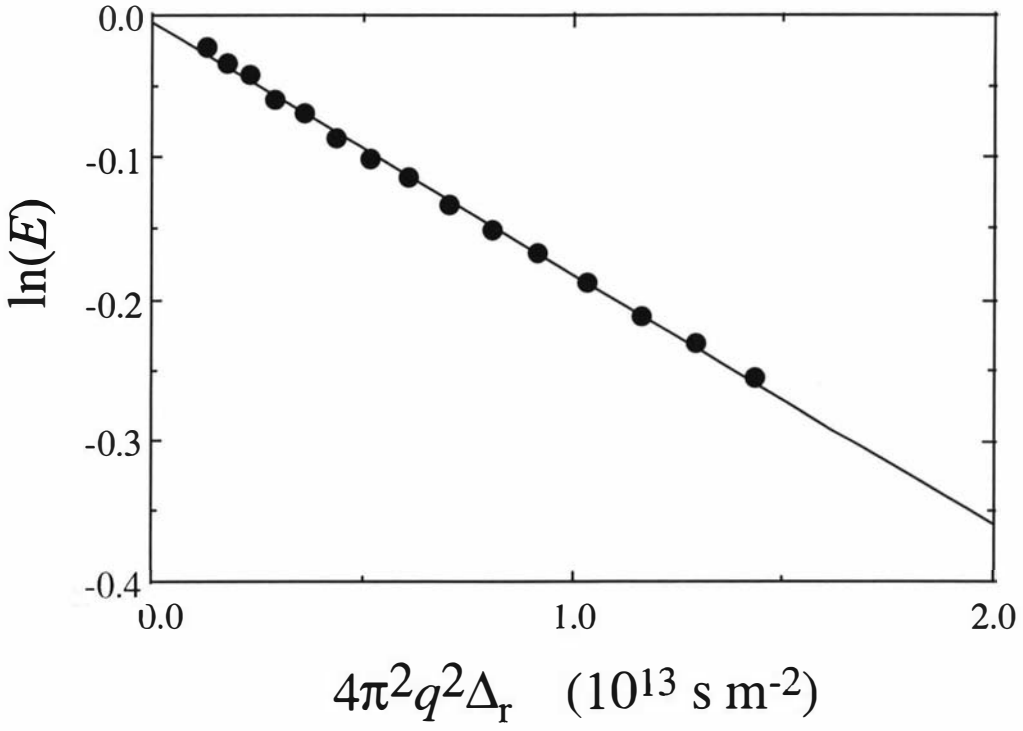

Figure 5.1[19]:
Stimulated echo attenuation for a 4.96% (w/v) sample of 3.04×10^6 daltons polystyrene in deuterated toluene at 25° C for Δ=900 ms and δ ranging between 0.25 and 1.0 ms at fixed G=14.9 T m^{-1}. The straight line is a fit assuming first order Gaussian behavior at low q and yields the mean squared displacement $\langle Z^2 \rangle$.

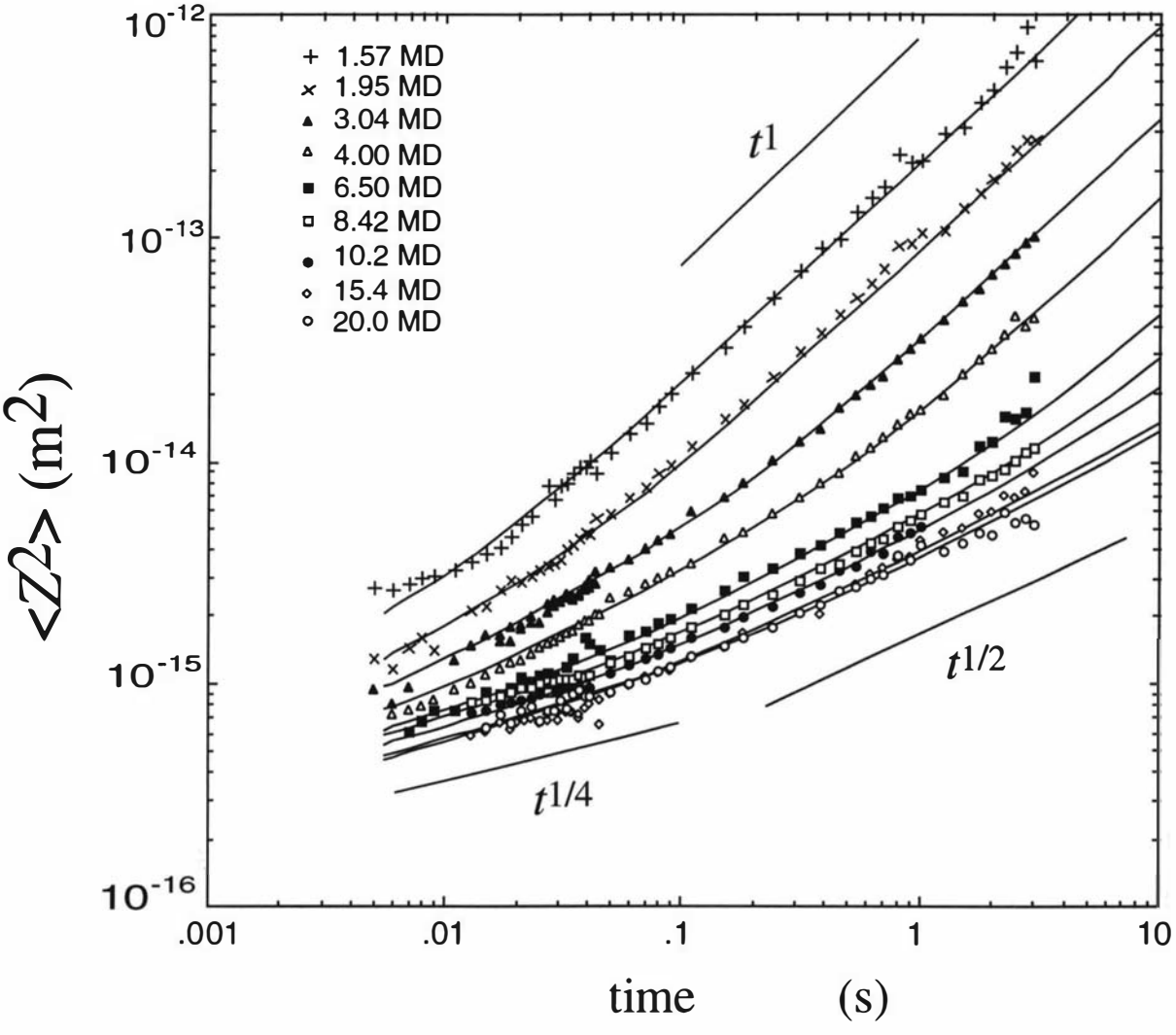

figure 5.2[19]**:**
log ($\langle Z^2 \rangle$) *vs* log(t), for nine different molar masses (see legend for molar mass labels) where, in the case of the $10x10^6$, $15x10^6$, and $20x10^6$ dalton polymers, the small spin diffusion correction has been made to the stimulated echo experiment data set. Asymptotic scaling exponents are shown in the straight line tangents. Clear $t^{1/4}$ to $t^{1/2}$ and $t^{1/2}$ to t^1 transitions are apparent as the changing molar masses sweep the Rouse and tube disengagement time across the NMR window. The data are fitted to eq. 2.36 using the two parameters τ_d and a as given in Table 1.

$$R = R^{(0)}\left(\frac{c_k}{c_k^*}\right)^x = N^{\upsilon} b\left(\frac{c_k b^3}{N^{1-3\upsilon}}\right)^x . \qquad (5.2)$$

Let the screening length ξ_c consist of g Kuhn segments. Thus

$$R = N^{\upsilon} b\left(\frac{c_k b^3}{N^{1-3\upsilon}}\right)^x \cong \left(\frac{N}{g}\right)^{1/2} \xi_c \qquad (5.3)$$

hence

$$\upsilon + (1-3\upsilon)x = \frac{1}{2} \quad i.e. \quad x = \frac{1-2\upsilon}{2(1-3\upsilon)}. \qquad (5.4)$$

Since in good solvents $\upsilon = 3/5$, as a consequence of eq. 5.3, the end to end distance of our sample was scaled as[2]:

$$R = R^{(0)}\left(\frac{c}{c^*}\right)^{-1/8} . \qquad (5.5)$$

This concentration scaling has been confirmed directly by neutron scattering measurements[79] for polystyrene in CS_2. These measurements also define the relationship[80] between the polymer radius of gyration at any ratio (c/c^*) with its radius in dilute solution, at the same time defining c^* for polystyrene at a known molar mass and dilute solution coil radius. The dilute solution coil radius, $R^{(0)}$, is calculated from measured value of R_G for $1.56\text{x}10^6$ daltons polystyrene in toluene from light scattering[81] to be 1300 $\mathring{A}$. Consequently we are able to calculate all our polymer end-to-end lengths in terms of the neutron scattering model and find R at c=5% to be 975 $\mathring{A}$ for $1.57\text{x}10^6$ daltons ($c^* \approx 0.5$ %) and values are determined by $R \sim N^{1/2}$ for all higher masses.

It is clear that our fitting procedure requires only two parameters, namely the long range center of mass diffusion coefficient, D_G (or equivalently, the set of disengagement times, τ_d), for the set of molar masses, and the tube diameter, which should, ideally, be independent of molar mass. We have freely varied both D_G and a for each molar mass in order to best fit the data. Figure 5.2 shows the corresponding

fits for the entire family of curves while the values of τ_d and a used in these fits are given in Table 5.1. The data fitting was made with MATLAB program which can be viewed in appendix A

As an internal consistency check we can test whether the disengagement times (or D_G) values have the expected molar mass scaling and whether $a \sim M^0$. Figure 5.3 shows the τ_d and D_G scaling behaviors, which are found to be close to $\tau_d \sim 3.4$ and, as a consequence, $D_G \sim -2.4$. The tube diameter is only relevant in the fits to the largest four molar masses where the $\langle Z^2 \rangle \sim t^{1/4}$ behavior is apparent. It is clear that the mean squared displacements in the $t^{1/4}$ regime (II) of different molar masses do not quite coincide as predicted by the pure reptation theory, and the consequential variation in fitted a values is shown in Table 5.1.

5.3 Concentration dependence.

The family of $\langle Z^2 \rangle$ *vs* t data for the concentration dependence measurements is shown in figure 5.4. This lower molar mass was chosen so that we could access the widest possible range of concentration within the $\langle Z^2 \rangle$ *vs* t sensitivity limits of our apparatus. Also shown in figure 5.5 are the dependencies on concentration of the best estimates for a, D_G and τ_d obtained from these fits. Our data is consistent with $\tau_d \sim c^{2.1}$ and $D_G \sim c^{-2.5}$. Nemoto et. al. showed a clear dependency of the monomer friction on concentration[82] which makes it difficult to directly ascribe these exponents to the values as shown in the three concentration dependence models for good solvent in chapter 2.4. In the case of the tube diameter the fits in figure 5.4 are fairly insensitive to a at the lowest concentration but more sensitive at the three higher concentrations where the $t^{1/4}$ region is approached. While one cannot ascribe great significance to the observed scaling shown in figure 5.5a, the best fit yields $a \sim c^{-0.3}$, although it is clear that the exponent could be anywhere in the range from -0.1 to -0.8.

5.4 Discussion

It is immediately apparent from figure 5.2 that the predictions of the Doi-Edwards tube model for mean squared segmental displacements fit the NMR data very

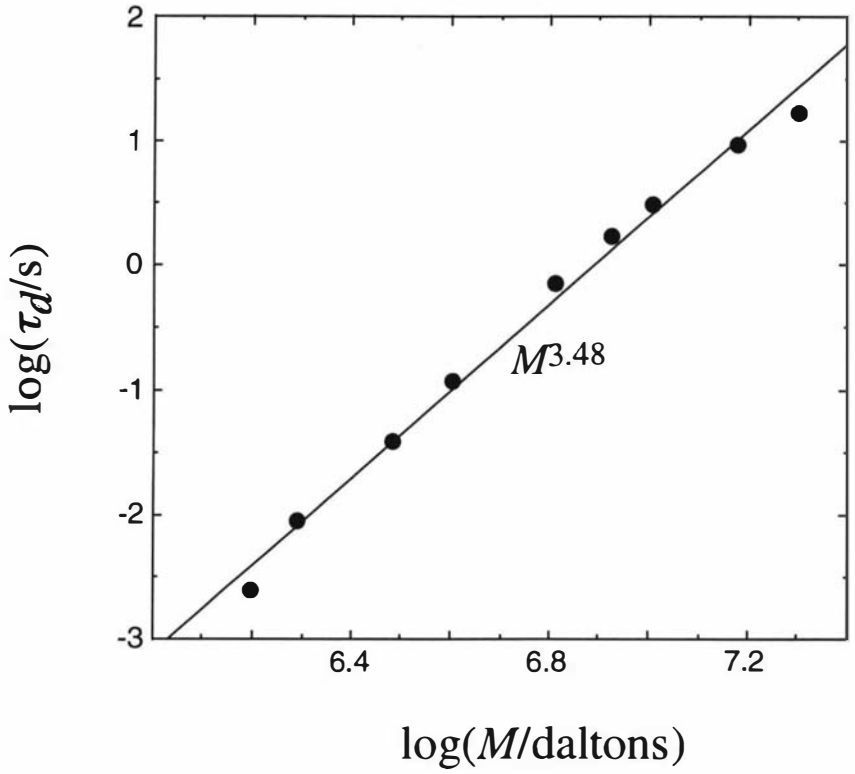

a.

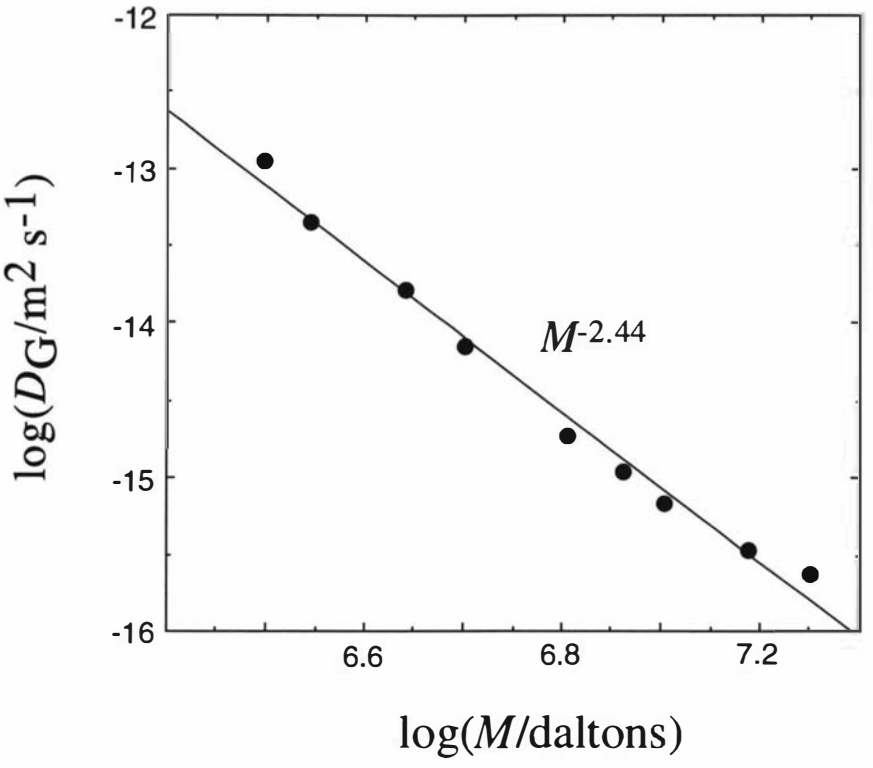

b.

Figure 5.3[19]:
a) τ_d and b) D_G scaling behaviors results from fits shown in figure 5.2. Note that 3.5 and -2.4 scaling exponents are found.

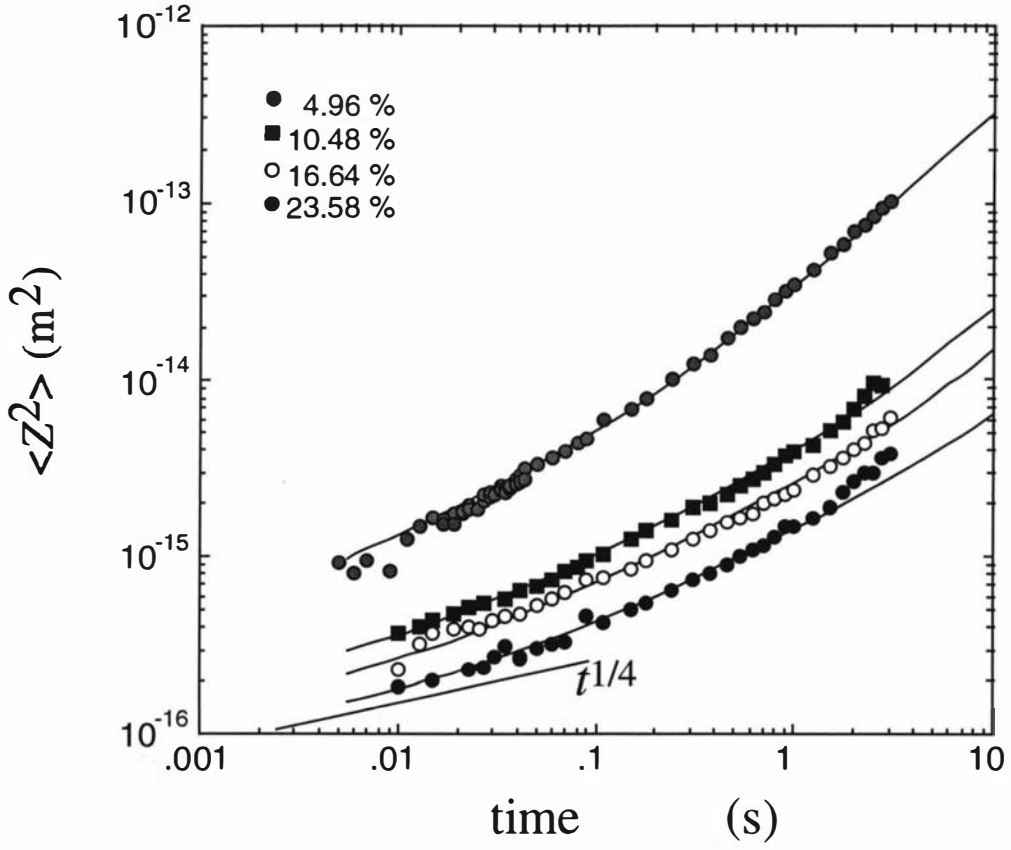

Figure 5.4[19]**:**

Concentration dependence for log ($\langle Z^2 \rangle$) *vs* log(t) at fixed molar mass (3.04×10^6 daltons) for polystyrene in deuterated toluene (solid circles, 23.58%; open circles, 16.64%; solid squares 10.48%; and dashed circles, 4.96% w/v). The fits shown use the Doi-Edwards model (eq. 2.36).

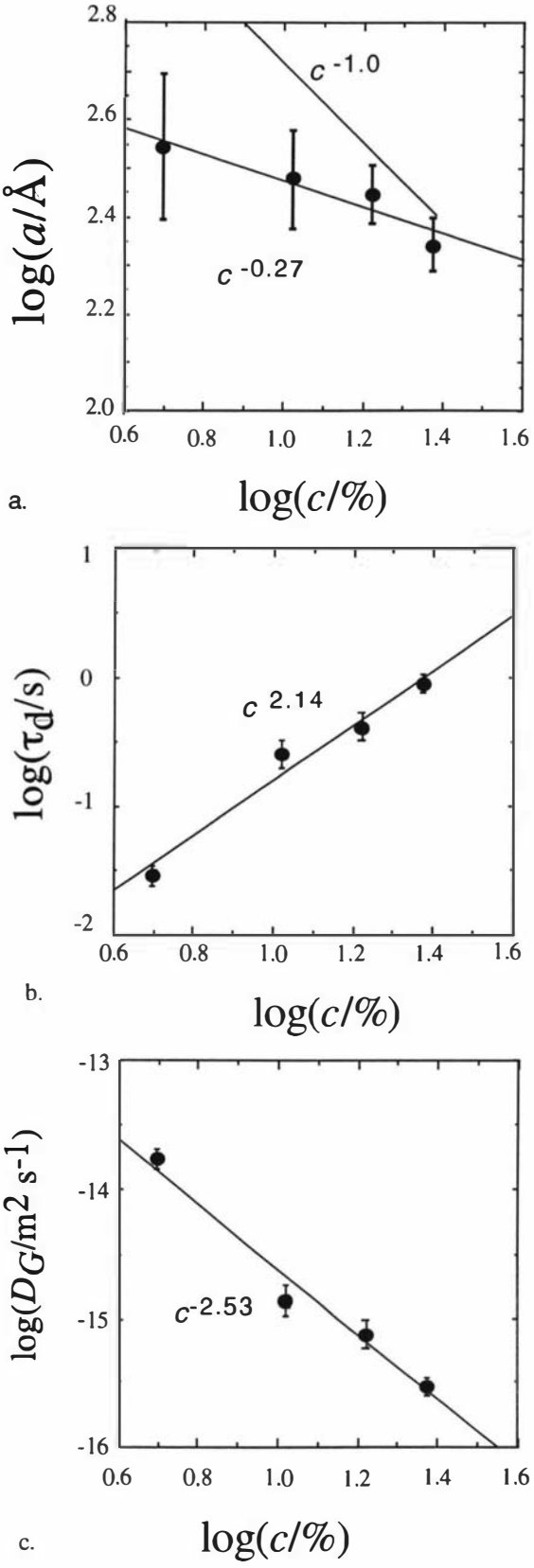

Figure 5.5:
Concentration dependencies of a) the tube diameter, b) the tube disengagement time, and c) the self-diffusion coefficient.

well indeed. In particular, the predicted transitions from $\langle Z^2 \rangle \sim t^1$, to $t^{1/2}$ to $t^{1/4}$ are all observed. To this extent the data would also be consistent with the mode-mode coupling model of Schweizer, for which very similar scaling regimes are predicted. Therefore we cannot regard our data as conclusively distinguishing in any way between these two very different theoretical models. However, Doi-Edwards theory makes specific predictions about the absolute values of mean squared segmental displacements based on just two adjustable parameters, namely the tube diameter and the intrinsic diffusion coefficient. Furthermore, the reptation theory is the only one which predicts, in first approximation, a quantitative scaling between the diffusion and the molecular weight of the polymer. We have therefore chosen to test this model by attempting to fit our entire family of $\langle Z^2 \rangle$ *vs* t data with a minimum of parameters. It is important to emphasize that the tube diameter only directly appears in the polymer mean-squared displacements once we reach the $t^{1/4}$ scaling regime (II). Above that, in regions III and IV, the segmental displacements are described once D_G (and the known polymer end-to-end length) is fixed. Thus only the first three or four values of a shown in Table 5.1 have particular significance.

The higher molar masses of 8.42 to 20×10^6 daltons all exhibit behavior consistent with the proximity of, or onset of $t^{1/4}$ scaling and for these the fit to a is important. Here we observe a weak dependence of a on M. While the idea of a tube diameter which depends (albeit weakly) on molar mass is not part of the strict reptation model, such a phenomenon has been proposed[83] based on the role of constraint release due to contour length fluctuation in surrounding chains. In the $t^{1/4}$ regime it is expected that this will lead to a tube diameter which increases weakly as the proportion of the chain located in the end region increases, *ie* as molar mass decreases.

When we turn to the scaling of tube disengagement time, and center-of-mass diffusion rate with molar mass (figure 5.3) we observe scaling exponents whose magnitudes are clearly in excess of 3.0, and 2.0. This behavior is quite consistent with both the proposal by Rubinstein[12] in which contour length fluctuations aid the tube renewal process relevant to self-diffusion, and with the proposal by Lodge[84,85] and co-workers, that in semi-dilute solutions, local concentration fluctuations leads to tube renewal in a manner similar to contour length fluctuation in a melt. For molar masses from 6.5 million and below, where the value for the tube diameter does not significantly enter the fitting process, the disengagement times provide the sole fitted parameter and follow a molar mass scaling close to $\tau_d \sim M^{3.4}$ (and, as a consequence,

$D_G \sim M^{-2.4}$). While the tube diameter provides another adjustable parameter in the larger molar mass fits, we would point out that the fitted τ_d values are essentially independent of a because they are dominated by the behavior at longer times. Looking closely at figure 5.3. one could notice that there seams to be a transition of τ_d (and D_G) from the semi-dilute behavior of 3.4 (and -2.4) to the classical 3.0 (and -2.0) exponents at the two highest molar masses investigated here. In either the Lodge or Rubinstein picture, such a trend would be expected as the mechanism for tube renewal is restricted to fluctuations around the vicinity of the chain end, and the proportion of the chain so involved will always decrease with increasing M.

The concentration scaling of D_G found on first analysis appear quite different from that found in previous studies[86] of polymers in good solvents, in which exponents with a magnitude well in excess of 1.75 have been observed[82]. Our results shows scaling behavior closer to the theta solvent regime. The reason for the discrepancy may either lie in the dependency of the monomer friction on concentration or in the dimension of the screening length ξ_c. For convenience, in our theoretical section we assumed that: a) $\xi_c \approx \xi_H$ and b) the friction coefficient does not change with concentration. In reality the monomer friction coefficient does change with concentration[2], in part this effect has been ascribed to a differing length scale dependence of hydrodynamic and static exponents[87].

Another reason for discrepancy might rise from the scaling parameter of the excluded volume screening length, $\xi_c = bg^{\upsilon_c}$. ξ_c defines a blob diameter in which within this blob the polymer behaves as an isolated coil in a dilute solution. υ_c is the parameter which ensures that the polymer segments will not be at the same coordinates at the same time and as a result $\upsilon_c = 3/5$. However, in order that the excluded volume effect will be significant enough to govern the coil's dynamics, the blob size should be sufficiently large that the polymer chain will be long enough and flexible enough, to permit a folding back of the coil on its own path. In the cases of distances which are shorter than the "fold back distance", $1/2 \le \upsilon_c < 3/5$. When the polymer solution is sufficiently concentrated but still semidilute, the polymer blob size may become sufficiently small to lead to a concentration dependence closer to that of a theta solvent than a good solvent[87].

The weak dependence of tube diameter on concentration falls in the range of the three model predictions. These predict exponents for good (and theta) solvents of -3/4

(-1), -5/8 (-1/2) and -2/3 (-2/3) respectively for models I, II and III. However, because of our large experimental error, one cannot use our data to discriminate between these models. But it is clear that the various tube diameter predictions are basically consistent with our measurement.

6
RHEOLOGY RESULTS

The subject of entangled polymer rheology along with its description in terms of the reptation theory was reviewed in section 2.3. This chapter describes the results of a series of rheology experiments on semidilute polymer solutions. These were conducted in order to provide a basis for comparison between the same reptation parameters obtained from different methods. In particular we seek to compare the key reptation parameters, the tube disengagement times and tube diameters.

6.1 Materials and methods

3.9×10^6 daltons, $M_w / M_n = 1.05$ polystyrene, manufactured by Polymer Laboratories, Church Stretton, Shropshire, UK was used for the rheometric measurements. This molecular weight was chosen to be as close as possible to the molecular weight used in the NMR measurements of concentration dependence. In order to preserve the same features of the samples used in the NMR section, the polymer was dissolved in >99% deuterated toluene (Aldrich, Milwaukee, WI, USA). Eight samples of 4.96%, 4.99%, 10.02%, 10.48%, 14.00%, 14.09%, 17.7% and 23.58% (w/v) concentration were prepared. The four samples 4.96%, 10.48%, 14.09% and 23.58% were allowed to equilibrate for five months at room temperature while the rest of the sample were equilibrated for one month at 37°C. This shorter equilibration at higher temperature was needed in order to repeat and augment the measurements during the final month of the experimental work.

All mechanical deformation measurements were made using the cone-and-plate cell of a Rheometrics Scientific model SR-5000 rheometer. The cone diameter was 25 mm and the nominal cone angle was 0.1 radian. The experiment were conducted in a saturated atmosphere of toluene to minimize evaporation and a constant temperature of 25°C. A photograph of this apparatus along with a close-up of the cell is showed in figure 6.1.

Two sets of experiments were performed: oscillatory shear and steady shear flow. Both experiments were stress controlled. In the oscillatory shear experiment which probes the linear viscoelastic response, the stress was 100 dyn cm^{-2} and the frequency ranged between 0.1 rad s^{-1} to 500 rad s^{-1} for the 4.96%, 10.48% and 14.09% samples and between 0.05 rad s^{-1} to 500 rad s^{-1} for the 4.99%, 10.02%, 14.00%, 17.7% and 23.58% samples. In the steady flow experiment which probes the non-

a.

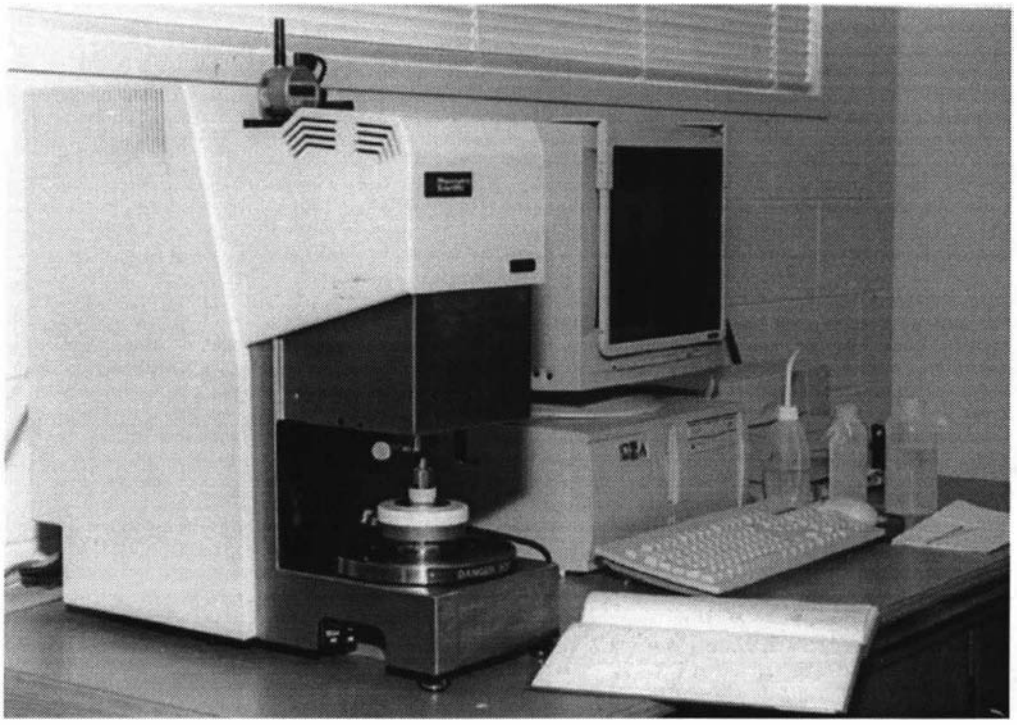

b.

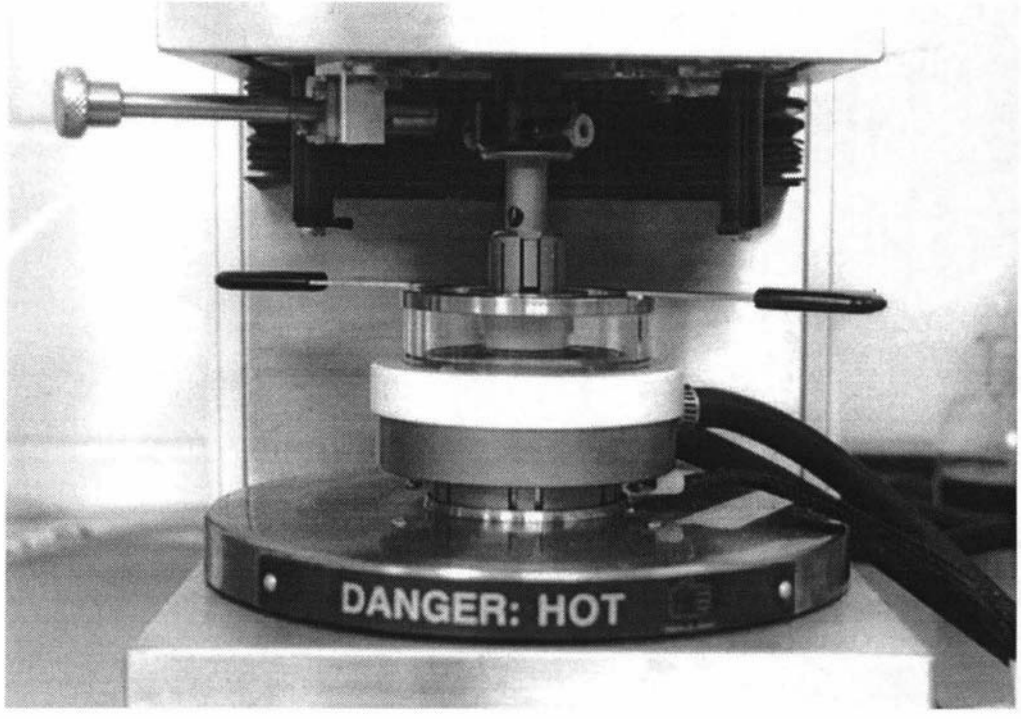

Figure 6.1:
a) A photograph of the rheometer and b) a close-up of the cell.

linear viscosity, the initial stress ranged between 1 dyn cm^{-2} to 10000 dyn cm^{-2}. Only the first seven samples were used in this experiment and the measurements were conducted immediately after the oscillatory shear experiment, assuming the first experiment did not affect the samples. The steady shear experiments were repeated again with four samples 4.99%, 10.02%, 14.00% and 17.7%, where on those occasions the samples were fresh and were used only in the steady shear flow experiment.

6.2 Results

Figure 6.2 shows a family of experimental data, $G'(\omega)$ *vs* ω, obtained in the oscillatory shear experiment and fitted to the Doi & Edwards model (eq 2.67, 2.68). The theoretical curve was written in MATLAB and is shown in appendix B. Unlike in the reptation theory fits to the mean square displacement data, where the only two parameters which were fitted were the tube diameter and the center of mass diffusion coefficient, the three parameters used to fit the storage modulus, were the plateau modulus, the tube disengagement time and the equilibrium time, and these were independently adjusted. Table 6.1 shows the fitted parameters and the calculated values of the tube diameter. a obtained from eq. 2.70:

$$G_N^{(0)} \cong \frac{c_k b^2}{a^2} k_B T \tag{6.1}$$

where $b = l c_\infty^{1/2}$[2,33], l is the average bond length for a vinyl polymer chain and $c_\infty = \lim_{n\to\infty} \langle r^2 \rangle_0 / \sum_i n_i l_i^2$ is called the characteristic ratio and serves as a measure of the effect of short-range interactions[88]. Figure 6.3 shows the scaling of τ_d, $G_N^{(0)}$ and a with the mass concentration. Simple linear regression fits to these log-log plots indicate $\tau_d \sim c^{3.17}$, $G_N^{(0)} \sim c^{2.38}$ and $a \sim c^{-0.69}$. The values of τ_d found in the oscillatory shear experiment are significantly higher than the same values obtained in the PGSE-NMR measurements as is the calculated scaling exponent for that parameter. The scaling of the plateau modulus with concentration is slightly larger than that found elsewhere[14,15] but the difference is within our measurement error. The tube diameter, which was calculated from the plateau modulus, is significantly smaller than the parameter a which was fitted in the Doi & Edwards mean square displacement *vs* time (figure 5.4). However, the scaling law resulting from the data fits the model by Colby and Rubinstein[18] in which $a \sim c^{-2/3}$.

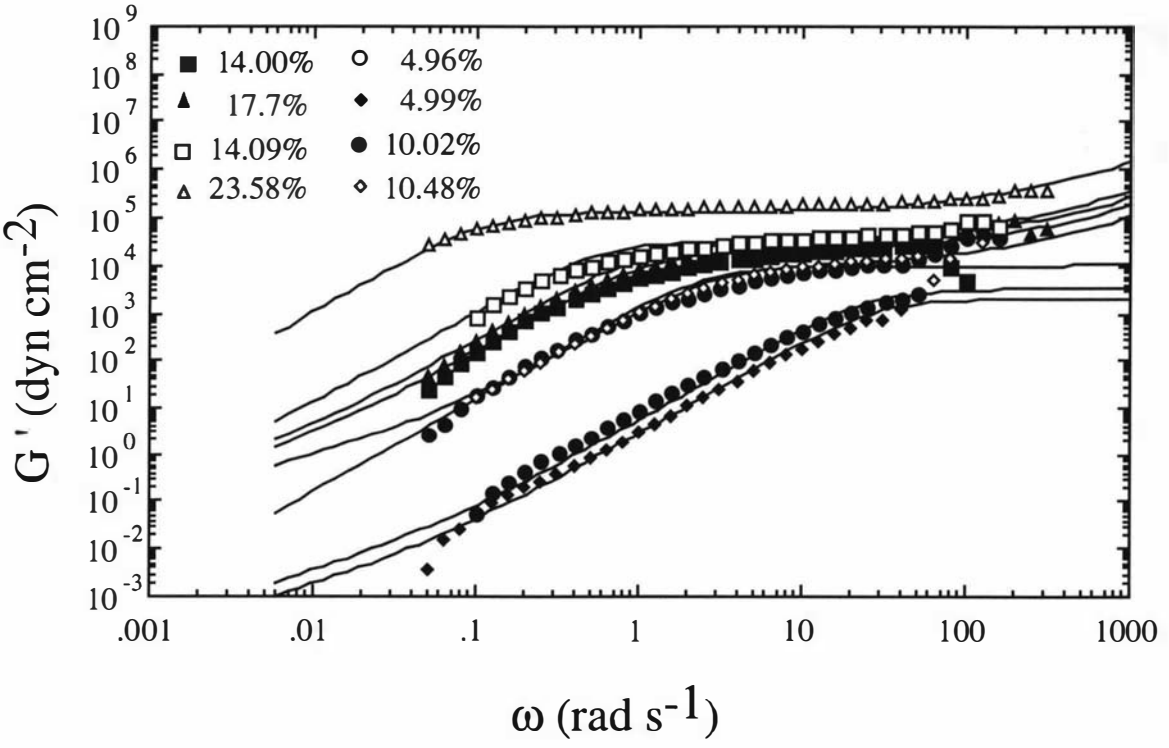

Figure 6.2:
Concentration dependence for G' *vs* ω at fixed molar mass (3.9×10^6 daltons) for polystyrene in deuterated toluene. The different concentrations are shown above.

M_p	c (w/v)	$G_N^{(0)}$ (N/m^2) (fitted)	a ($\mathring{A}$) (calculated from eq 2.66)	τ_d (s) (fitted)
$3.9x10^6$	4.96%	$3.5x10^4$	42	3.3
$3.9x10^6$	4.99%	$2.0x10^5$	55	3
$3.9x10^6$	10.02%	$1.0x10^6$	35	32
$3.9x10^6$	10.48%	$1.1x10^5$	34	25
$3.9x10^6$	14.00%	$2.0x10^6$	29	70
$3.9x10^6$	14.09%	$4.0x10^5$	20	120
$3.9x10^6$	17.7%	$2.9x10^6$	27	75
$3.9x10^6$	23.58%	$1.6x10^7$	13	700

Table 6.1:

Experimental and fitted parameters relevant to the oscillatory shear experiment.

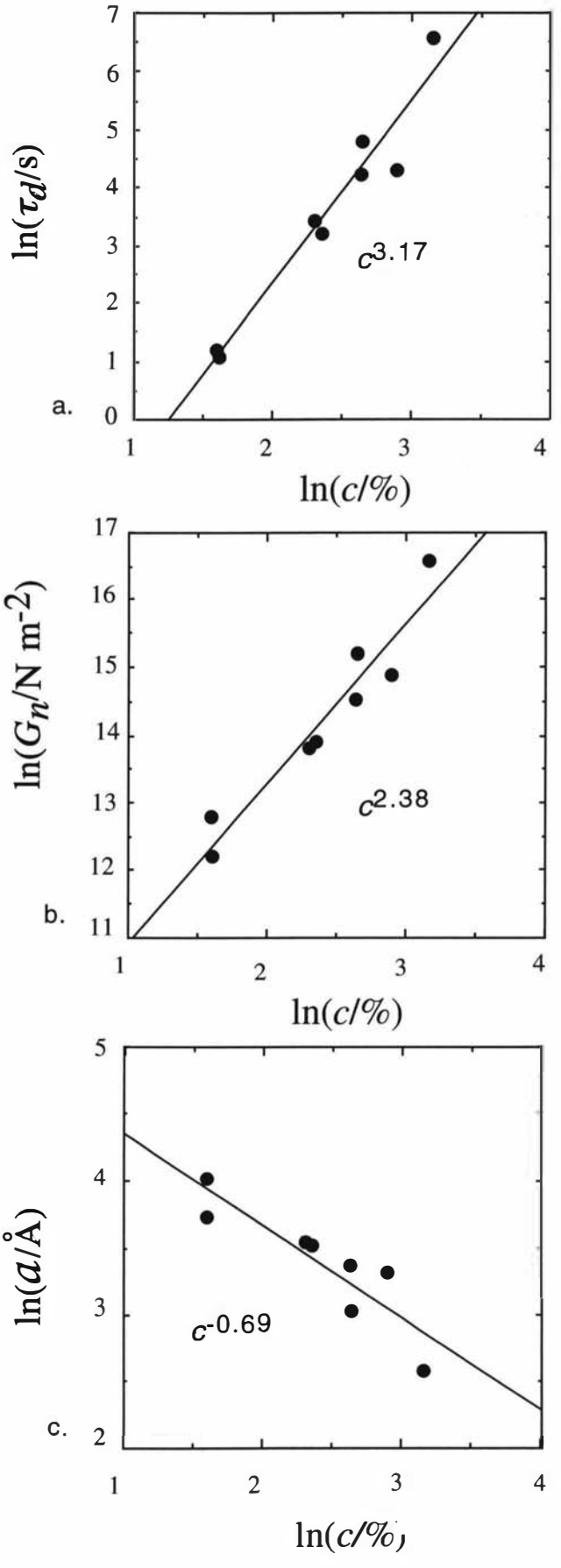

Figure 6.3:
Concentration dependence of a) the tube disengagement time, b) the plateau modulus and c) the tube diameter as obtained from fitts using the Doi-Edwards theory to linear viscosity measurements of $G'(\omega)$.

Figure 6.4 shows the flow curves obtained in the steady shear experiments. Table 6.2 shows the experimental parameters relevant to the estimation of τ_d and the calculated value. τ_d was calculated from eq. 2.75. The tube disengagement times in this part of the experiment, while not consistent with those obtained in the oscillatory shear measurements are broadly similar to the values obtained by PGSE-NMR. However, the steady shear experiments scaling law, $\tau_d \sim c^{3.65}$ (figure 6.5), is rather close to that obtained in the oscillatory shear experiment, although it must be acknowledged that the data are very scattered.

6.3 Discussion

The difficulty in obtaining consistent flow curve data for very high molecular weight polymers in semidilute solutions is well known[89]. Variations are believed to arise due to slip effects and to problems in maintaining a well-filled gap in the face of steady elastic normal forces. While our data is strongly scattered, we are however able to observe some important trends and to gain insight regarding the apparent disengagement time. The oscillatory shear experiments in the linear regime were more consistent; however, the disengagement times obtained were anomalous. We now discuss the comparative values of the parameters which were measured in both the NMR and rheological experiments.

The concentration scaling of τ_d and a resulting from all the experiments reported in this thesis up to this point, are broadly in agreement with the reptation theory and its standard modifications. In the case of the tube diameter an estimate can be made by calculating the tube diameter according to the principles which were reviewed in section 2.4 by assuming the $a \sim \xi_c$, the inter entanglement distance.

$$c_k = \frac{g}{a^3} \tag{6.2}$$

$$a = bg^{\upsilon} \tag{6.3}$$

where c_k is the Kuhn segments concentration and g is the number of Kuhn segments per correlation length a. The combination of eq. 6.2 and 6.3 gives

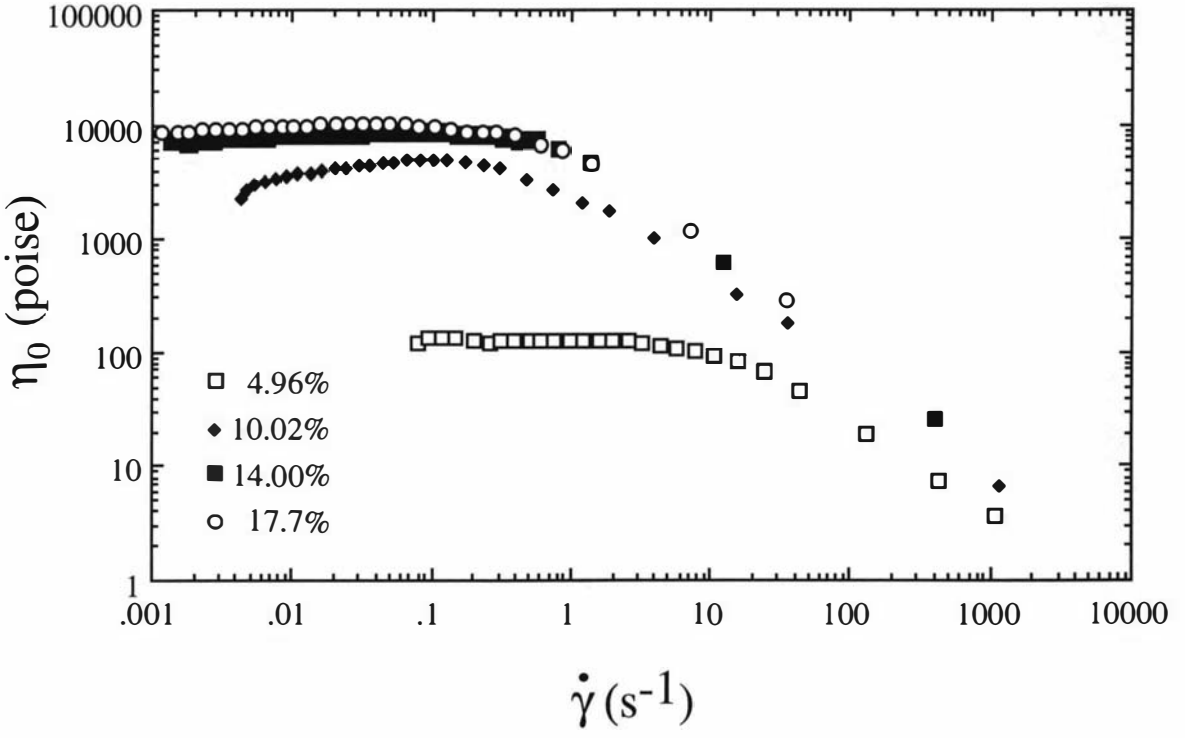

Figure 6.4:
A sample of four flow curves obtained in the steady shear experiments. The different concentrations are shown above.

c (w/v)	$\dot{\gamma}$ (s^{-1}) (at which $\eta = \frac{1}{10}\eta_0$)	τ_d (s)
4.96%	234	0.026
4.99%	317	0.019
*4.99%	481	0.012
*10.02%	30.4	0.20
10.02%	15	0.40
*14.00%	8.26	0.73
14.00%	4.2	1.4
14.09%	1.23	4.88
*17.7%	10	0.60
17.7%	1.6	3.7

* data acquired from the "fresh" samples

Table 6.2:

Experimental and fitted parameters relevant to the steady shear flow experiment.

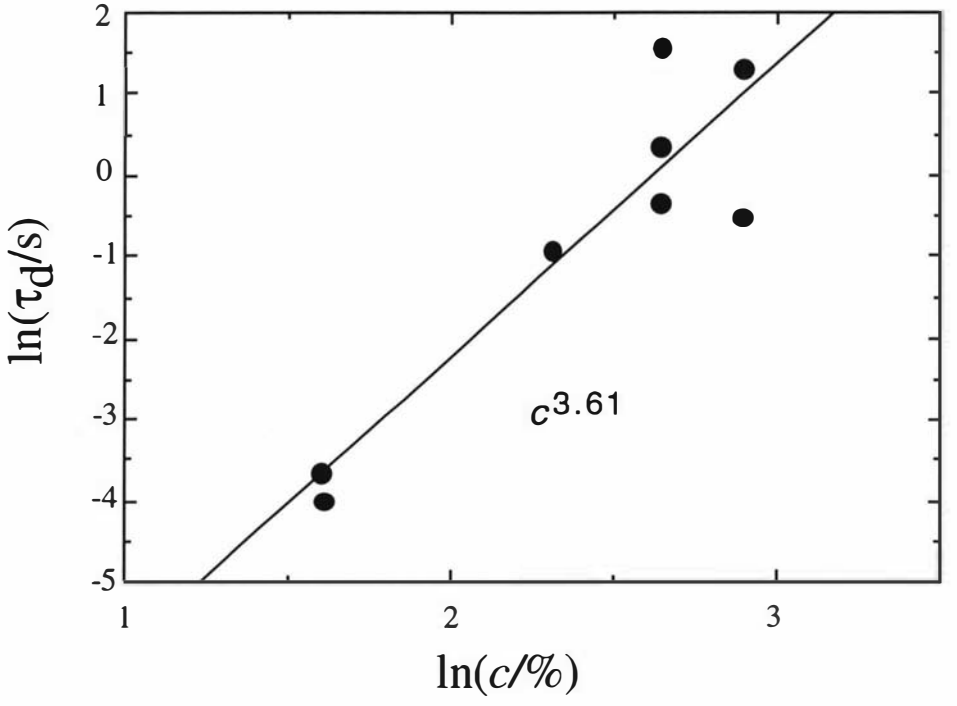

Figure 6.5:
Concentration dependence of the tube disengagement times obtained from the steady shear experiments

$$c_k = \frac{a^{1/\upsilon - 3}}{b^{1/\upsilon}} \tag{6.4}$$

Table 6.3 show the values of a calculated for $\upsilon = 0.5, 0.6$ and 0.55 along with the values which were measured via both techniques, NMR and rheology. Note, that the calculated values for a where $\upsilon = 0.55$ are the closest to the values obtained in the rheology measurements. This similarity supports our assumption, based on the scaling value found for τ_d *vs* concentration, which suggests that, at the tube diameter length scale, the polymer coil is in an intermediate state between theta and good solutions so that ν lies between 0.6 and 0.5. The NMR measurements exhibit higher values for a, but this can be explained by considering the nature of the NMR measurements. In NMR methods we measured *directly* the motion (mean square displacement) of a polymer segment in an equilibrium state. The reptation theory assumes that the entanglements form a solid tube in which only the ends of the chain can diffuse freely. This assumption is, however, simplistic. The polymeric surroundings should be considered more as a dynamic elastic network. Gaps exists between the entanglements and loops of polymer can diffuse through so that the effective tube diameter increases. Elastic fluctuations of the network mean that the walls of the tube are "soft", further assisting lateral migration. As a result of this effect lateral displacement of polymer segments within the tube could appear larger than the static entanglement distance.

Although the τ_d values obtained in the steady shear flow experiment are quite scattered, they seem to agree with the corresponding NMR values. However, the fact that the values for the tube disengagement times which were measured in both NMR and steady shear experiments are different from those obtained in oscillatory shear is very interesting. The method by which we extracted τ_d from the oscillatory shear data was by fitting the storage modulus data to the Doi & Edwards model curve. An alternative empirical approach to obtaining the polymer terminal relaxation time is to use the frequency at which the storage and loss modulus "cross over". This cross over frequency between G' and G'', the storage modulus and loss modulus, indicates a relaxation time in which $1/\omega_c$ may be taken to be of the order of magnitude of the longest relaxation time[89]. Consequently, we analyzed the oscillatory shear data, this time calculating the longest relaxation time and comparing the results with our previous data (Table 6.4). It is clear from the table that the longest relaxation time found from the cross over point nicely matches the NMR and steady shear results. The concentration scaling behavior of the longest relaxation time is very close to that of the τ_d exponent found for the oscillatory shear experiment.

c (w/v)	a ($\mathring{A}$) (NMR)	a ($\mathring{A}$) (from the plateau modulus)	a ($\mathring{A}$) (calculated $\nu = 0.5$)	a ($\mathring{A}$) (calculated $\nu = 0.6$)	a ($\mathring{A}$) (calculated $\nu = 0.55$)
4.96%	300	42	68.4	35.7	45.8
4.99%		55	68.0	35.5	45.6
10.02%		35	33.8	21.0	25.3
10.48%	200	34	32.5	20.4	24.4
14.00%		29	24.2	16.4	19.0
14.09%		20	24.4	16.5	19.2
16.64%	180				
17.7%		27	19.2	13.8	15.7
23.58%	160	13	14.5	11.1	12.3

*The molecular weight of the NMR sample was 3.04×10^6 dalton.

Table 6.3:

Summary of the tube diameter values which were both measured and calculated in this thesis.

c (w/v)	τ_d (s) (G' fitted to Doi-Edwards model)	τ_d (s) (cross point, $G' = G''$)	τ_d (s) (steady shear)	τ_d (s) (PGSE-NMR)
4.96%	3.3	0.05	0.026	0.039
4.99%	3	0.033	0.012	
10.02%	32	0.25	0.20	
10.48%	25	0.25		0.44
14.00%	70	0.76	0.73	
14.09%	120	0.88	4.88	
16.64%				0.72
17.7%	75	0.83	0.60	
23.58%	700	12.5		1.7

*The molecular weight of the NMR sample was 3.04×10^6 daltons.

Table 6.4:

Summary of the tube disengagement time values which were obtained from PGSE-NMR and steady shear measurements, from the cross over frequency and from fitting the Doi-Edwards theory to the storage modulus data in the oscillatory shear experiment..

It is interesting to note that Graessley[90] in 1980 pointed out that the relaxation time obtained from the cross over frequency is significantly smaller than that calculated by fitting the Doi & Edwards model. The reason suggested for this discrepancy was the dynamic nature of the tube, so that the various modifications for the theory, which were mentioned in section 2.5, should be embedded into any master equation of the dynamic modulus. This may be a plausible explanation although it is not a part of this thesis to enter the debate. We simply note the discrepancy and observe that these exact considerable discrepancies in reported linear and non-linear viscoelasticity parameter found in the literature pertaining to semidilute solution of polystyrene, with no clear consensus regarding their cause.

7

SPIN-DIFFUSION

An unexpected bonus of our research on reptation was the observation of spin-diffusion effects. We became interested in this phenomenon while measuring the mean square displacement of the three highest molecular weight samples. The measurement of self-diffusion coefficients over three decades of observation time requires the use of two pulse sequences, the spin echo for short observation times and the stimulated echo for long observation times. When the mean square displacement *vs* time was obtained for the high molar mass samples, a difference between the spin echo and the stimulated echo data was noticed. This chapter reviews the spin-diffusion process and the dipolar interaction (which underlies this phenomenon). We argue that the observed difference between spin echo and stimulated echo data indicates an influence from the spin-diffusion process.

7.1 The Dipolar Interaction

The dipolar interaction is the magnetic interaction between neighboring magnetic moments, and in the case of nuclear magnetic resonance experiments, the dipolar interaction acts in the presence of an external magnetic field. A spin-1/2 nucleus which precesses in an external magnetic field exists in either an "up" or "down" projection. Those projections cause a slight change in the magnetic micro-environment surrounding each nucleus. When two such spins are present the change in the local magnetic field, introduced by the one nuclear spin, will change slightly the Larmor frequency of the other and vice versa. The strength of the dipolar coupling depends on the relative orientation of the spins with the inter-nuclear vector and on the distance between them. The dipole-dipole coupling between two spins j, $\mu_j = \gamma_j \hbar \boldsymbol{I}^j$, and k, $\mu_k = \gamma_k \hbar \boldsymbol{I}^k$, can be written:

$$W_{jk} = \frac{\gamma_j \gamma_k \hbar^2}{r_{jk}^3} \left\{ \boldsymbol{I}^j \cdot \boldsymbol{I}^k - 3 \frac{\left(\boldsymbol{I}^j \cdot \boldsymbol{r}_{jk}\right)\left(\boldsymbol{I}^k \cdot \boldsymbol{r}_{jk}\right)}{r_{jk}^2} \right\}. \tag{7.1}$$

The dipole dipole interaction between identical spins in a large external magnetic field in generally substantially smaller than the Zeeman interaction thus can be treated as a perturbation. The total Hamiltonian of the system is then written:

$$\hbar H = \hbar\left(B_0 + B_1\right) \tag{7.2}$$

where B_0 is the Zeeman Hamiltonian of the system:

$$\hbar H_0 = -\gamma\hbar \mathrm{B}_0 \sum_j I_z^j \tag{7.3}$$

and the perturbed $\hbar B_1$ is the Dipolar Hamiltonian of the system:

$$\hbar B_1 = \sum_{j<k} W_{jk} = \frac{\mu_0}{4\pi}\sum_{j<k}\frac{\hbar^2\gamma^2}{r_{jk}^3}\left\{\boldsymbol{I}^j\cdot\boldsymbol{I}^k - 3\frac{\left(\boldsymbol{I}^j\cdot\boldsymbol{r}_{jk}\right)\left(\boldsymbol{I}^k\cdot\boldsymbol{r}_{jk}\right)}{r_{jk}^2}\right\}. \tag{7.4}$$

Writing the dipolar Hamiltonian for two identical spins j and k separated by distance r, in terms of the zeroth order representation in which the quantization axis, z, is along the B_0 field gives six terms:

$$W_{jk} = \frac{\gamma^2\hbar^2}{r^3}(A+B+C+D+E+F) \tag{7.5}$$

$$\left.\begin{aligned}
A &= \boldsymbol{I}_z^j\boldsymbol{I}_z^k\left(1-3\cos^2\theta\right)\\
B &= -\frac{1}{4}\left(1-3\cos^2\theta\right)\left(\boldsymbol{I}_+^j\boldsymbol{I}_-^k + \boldsymbol{I}_-^j\boldsymbol{I}_+^k\right) = \frac{1}{2}\left(1-3\cos^2\theta\right)\left(\boldsymbol{I}_z^j\boldsymbol{I}_z^k - \boldsymbol{I}^j\cdot\boldsymbol{I}^k\right)\\
C &= -\frac{3}{2}\sin\theta\cos\theta e^{-i\phi}\left(\boldsymbol{I}_z^j\boldsymbol{I}_+^k + \boldsymbol{I}_z^k\boldsymbol{I}_+^j\right)\\
D &= C^* = -\frac{3}{2}\sin\theta\cos\theta e^{i\phi}\left(\boldsymbol{I}_z^j\boldsymbol{I}_-^k + \boldsymbol{I}_z^k\boldsymbol{I}_-^j\right)\\
E &= -\frac{3}{4}\sin^2\theta e^{-2i\phi}\boldsymbol{I}_+^j\boldsymbol{I}_+^k\\
F &= E^* = -\frac{3}{4}\sin^2\theta e^{2i\phi}\boldsymbol{I}_-^j\boldsymbol{I}_-^k
\end{aligned}\right\}. \tag{7.6}$$

To first order in perturbation theory, only two terms in eq. 7.6 effect the energy levels of the Hamiltonian, namely the diagonal elements A and B[52].

Term A describes the change of the z component of the magnetic field of a nuclei spin due to the magnetic moment of the neighboring spin, i.e. it represent the classical interaction of magnetic moments in a strong magnetic field. The term B has a particular importance in our research, since it contains the "flip flop" terms

corresponding to a simultaneous change of states between the two spins. The mechanism of the flip-flop is that precession of one spin at the resonance frequency results in a resonant rotating magnetic field at the other spin, thus causing a reciprocal transition. This is an energy conserving magnetization transfer which enables the process known as spin-diffusion to occurs. The other terms in eq. 7.6 represent off-diagonal elements of the perturbation Hamiltonian and thus contribute only second-order shifts to the energy levels. The off-diagonal terms have the effect of causing energy-changing transitions between the eigenvalues of the Zeeman levels. However to produce these transitions it is necessary that the terms fluctuate in amplitude at a frequency equal to the energy difference between the states. Fluctuations occur if the molecular vector reorients due to rotational motion, i.e. if θ and ϕ are functions of time, and the frequency component of them fluctuating at 0, ω_0 and $2\omega_0$ result in transitions which are responsible for transverse (T_2) and longitudinal (T_1) relaxation (ω_0 and $2\omega_0$ only) [91].

7.2. Spin-Diffusion

Spin-diffusion is the process of magnetization migration via mutual flip-flop, caused by the flip-flop terms, $\left(I_+^j I_-^k + I_-^j I_+^k\right)$, in the dipolar Hamiltonian (term B). This phenomenon can be observed when the nuclear magnetization component along B_0, at any given time is not uniform in space. The spin evolves toward an equilibrium uniform magnetization by means of successive flip-flops between neighboring spins[92]. In other words the spin-diffusion process is responsible for eliminating spin temperature gradients[54]. Since the process of spin-diffusion affects only the component of magnetization lying along the direction of B_0, in order to observe the phenomenon the detected magnetization must be "locked" for a certain time along the z-axis.

The evolution of the magnetization density, $M(r,t)$, can be described using the classical diffusion equation:

$$\frac{dM}{dt} = D_{SD}\nabla^2 M \tag{7.7}$$

where spin-diffusion coefficient, D_{SD}, equals:

$$D_{SD} = cb^2\omega_i \tag{7.8}$$

b being the distance between the spins undergoing mutual flip-flop, c being a numeric factor on the order of unity and ω_i being the root-mean-square spin-spin interaction strength between neighboring spins which, in the classic dipolar case, is on the order of T_2^{-1}[93].

There are several ways of calculating the spin-diffusion depending on the details of the atomic or molecular structure[52,55] but in the end, each depends on the strength of the dipolar interaction and the distance between the spins squared. Previously, detecting spin-diffusion process was only indirect by measuring the T_1 relaxation time which is strongly affected by spin-diffusion[94-97]. Recent methods which utilize magnetic field gradients enable one to detect directly the spin-diffusion coefficient[49,98]. Of course magnetization can be transported not only by spin-diffusion but also by the translational diffusion of spin-bearing particles. In general, in ordered solids, where translational motion is suppressed, spin-diffusion is the dominant type of diffusion, while translational diffusion is on the order of bond fluctuations and thus negligible[99]. In less-ordered solids, defects allow long range motion and in liquid crystals, translational diffusion become significant. In the limiting case of small molecules such as liquids, the translational diffusion dominates the spin-diffusion. In such experiments the diffusion coefficient which is measured in any experiment based on magnetization transfer is the translational diffusion coefficient alone.

In polymer melts and in high molecular weight semidilute solutions, the materials dealt with in this work, the translational diffusion and the spin-diffusion may be on the same order of magnitude so that the effective diffusion coefficient obtained in "magnetization migration" experiments consists of both, Brownian translational and spin-diffusion term, i.e.

$$\langle R(t) - R(0) \rangle^2 = 6D_{trans}t + 6D_{SD}t \tag{7.9}$$

where D_{trans} and D_{SD} are the translational diffusion and spin-diffusion coefficients respectively. The theory of spin-diffusion in polymers has been extensively described by Fatkullin. One of the findings of this thesis is that there is a crucial difference in the nature of the spin-diffusion motion between polymer melts and high molecular weight semidilute polymer solutions. In polymer melts, the spin magnetization hops randomly from one polymer chain to another (figure 7.1a) and the regime in which this motion can

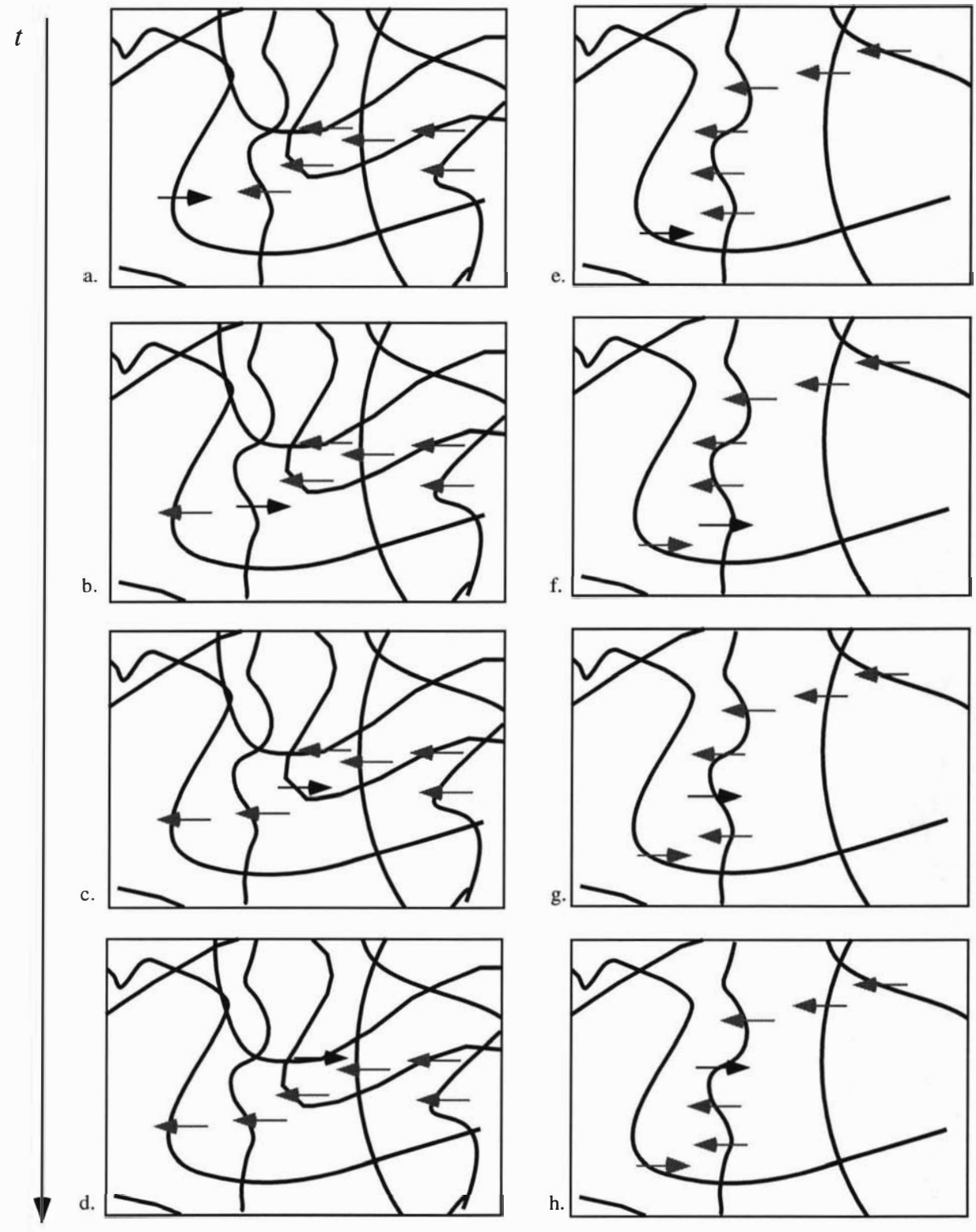

Figure 7.1:
The spin diffusion process. a-d) Polymer melt: the spins hopping randomly from one polymer chain to another, and e-h) polymer semidilute solutions: the chance of spins to undergo successive flip-flops is bigger within the polymer chain.

be detected is in the free center of mass diffusion regime when the detection time is larger than the tube disengagement time. By contrast in semidilute solutions the distance between polymer chains is bigger and the spin-diffusion tends to be confined to spins on a single chain. The resulting motion is no longer that of free three dimension Brownian motion but rather that of diffusion along a curvilinear path (figure 7.1b). As a consequence the laboratory frame mean square displacement of the motion scales as $t^{1/2}$ and indeed can be detected only in the regimes inside the tube where $t^{1/2}$ motion is dominant.

7.3 Direct measurement of Spin-Diffusion

Spin (as oppose to molecular) diffusion coefficients can be directly extracted from the Pulsed Gradient Spin Echo experiment. This possibility was first suggested by Fatkullin[99] in 1991 where he calculated the contribution of the spin-diffusion process to the effective diffusion coefficient of polymer melt resulting from the Pulsed Gradient Stimulated Echo experiment. The physical basis of this phenomenon relies on the fact that if the magnetization is locked on the z-axis for sufficient time for the spins to perform a flip-flop, this will modify the echo attenuation just as if there were an additional Brownian motion of magnetization "quasiparticles". This spin-diffusion contribution results in a bigger effective diffusion coefficient than one would obtain from the translational motion alone. Note that in order to detect the diffusive spin-flips the magnetization must be locked along the direction of the external magnetic field. The spin-diffusion effects only occur in the Stimulated Echo sequence and not in the Spin Echo where there is no phase coherence between spins precessing in the transverse plane.

The pulse sequence for the stimulated echo PGSE (PGSTE) experiment is shown in figure 3.8. This sequence consists of three 90° rf pulses and two gradient pulses of duration δ. The interval between the first and second rf pulses is τ_1 and the time interval between the second and third pulses is τ_2. The echo is acquired at time $2\tau_1 + \tau_2$ and the attenuation can be written as:

$$A(G) = \exp\left(-\frac{2\tau_1}{T_2}\right)\exp\left(-\frac{\tau_2}{T_1}\right)\frac{1}{N_s}\sum_k \left\langle \exp\left[i(\varphi_{2k} - \varphi_{1k})\right]\right\rangle \qquad (7.10)$$

where T_1 and T_2 are the spin lattice and spin-spin relaxation times, respectively, φ_{1k} and φ_{2k} are the phase shift of spin k acquired during the two gradient pulses.

$$\varphi_{1k} = \gamma \int_0^{\delta} \boldsymbol{G} \cdot \boldsymbol{r}_k(\tau) d\tau$$

$$\varphi_{2k} = \gamma \int_0^{\delta} \boldsymbol{G} \cdot \boldsymbol{r}_k(\tau_1 + \tau_2 + \tau) d\tau \tag{7.11}$$

where γ is the gyromagnetic ratio, $\boldsymbol{G}$ is the magnetic field gradient $\boldsymbol{r}_k(\tau)$ is the vector describing the position of spin k at time τ. The first two terms in equation 7.10 describe the relaxation process while the last exponential term, which contains the difference of those two phase shifts, expresses the attenuation due to spatial displacements of magnetic quasiparticles.

By repeating the experiment in the absence of the gradient pulses and dividing the two signals obtained, with and without gradient, one obtains a function independent of relaxation and dependent only on the diffusion attenuation.

$$A(G) = \frac{1}{N_s} \sum_k \left\langle \exp\left\{ i(\varphi_{2k} - \varphi_{1k}) \right\} \right\rangle. \tag{7.12}$$

In order to calculate the influence of the dipolar Hamiltonian on the final stimulated echo attenuation Fatkullin first introduces the general spin Hamiltonian.

$$H = H_0 + H_{dd} + H_{rf} + H_G \tag{7.13}$$

where

$$H_0 = \sum\nolimits_j \hbar \omega_j I_z^j \tag{7.14}$$

is the Zeeman Hamiltonian

$$H_{dd} = \sum_{j<k} \gamma^2 \hbar^2 \left(\frac{\boldsymbol{I}^j \boldsymbol{I}^k}{r_{jk}^3} - 3 \frac{\left(\boldsymbol{r}_{jk}(t) \boldsymbol{I}^j\right)\left(\boldsymbol{r}_{jk}(t) \boldsymbol{I}^k\right)}{r_{jk}^5} \right) \tag{7.15}$$

is the dipolar Hamiltonian of the system where $\boldsymbol{r}_{jk}(t)$ is the vector joining spin j and k at time t and $\boldsymbol{I}_j$ is the spin's vector operator.

$$H_{rf} = \sum_j \frac{\pi}{2} \hbar I_x^j \left[\delta(t) + \delta(t-\tau_1) + \delta(t-\tau_1-\tau_2)\right] \tag{7.16}$$

is the 90° rf pulse Hamiltonian. This Hamiltonian rotates the spin system by $\pi/2$ around the x axis. And

$$H_G = \sum_j \hbar\gamma G z_j \left(t I_z^j \left[\delta(t) + \delta(t-\tau_1-\tau_2)\right]\right) \tag{7.17}$$

is the Hamiltonian of the magnetic field gradient pulses, where $z_j(t)$ is spatial coordinate of spin j in time t.

The rf and gradient pulses are assumed to be infinitesimally small so that no relaxation or diffusion process occur during this time. Introducing the dipolar Hamiltonian to the system complicates the equations and in fact there is no exact solution to the problem. In order to overcome this problem one should take the dipolar Hamiltonian as a perturbation and take only the first non-zero term i.e. the second moment. All the other terms of the system Hamiltonian have an exact solution. Taking all the above under consideration, Fatkullin shows that the stimulated echo amplitude of the nth spin is:

$$\begin{aligned} A(G) = &\sum_j \left\langle \exp\left\{ i\left(\varphi_{2j} - \varphi_{1j}\right)\right\}\right\rangle \times \left(1 - P_{jj}(\tau_2) - 2P_{2j}^{'}(\tau_1) - P_{1j}^{'}(\tau_2)\right) \\ &+ \sum_{j\neq k} \left\langle \exp\left[i\left(\varphi_{2k} - \varphi_{1j}\right)\right]\right\rangle \left[P_{jk}(\tau_2) - 2P_{2jk}^{''}(\tau_1) - P_{1jk}^{''}(\tau_2)\right] \end{aligned} \tag{7.18}$$

Equation 7.18 is constructed from two parts. The first part describes phase shift of the spin magnetization which remains on spin j for the whole experimental time. Its weighting factor contains the probability of magnetization loss of spin j to the flip-flop process ($P_{jj}(\tau_2)$), transverse relaxation process ($2P_{2j}^{'}(\tau_1)$) and spin lattice relaxation process ($P_{1j}^{'}(\tau_2)$). The second part of the equation gives the contribution from the magnetization which was created at first on spin k, but which resides on spin j in the

end of the experiment. Its weight consists of the following terms: $P_{fjk}(\tau_2)$ is the probability of spin k to flip-flop to the j state, $2P^{\cdot\cdot}_{2jk}(\tau_1)$ is the traverse relaxation process and $P^{\cdot\cdot}_{1jk}(\tau_2)$ is the spin lattice relaxation process. Another matter Fatkullin deals with in his theory is the effect of the gradient pulse itself on the relaxation process which he incorporates into the echo amplitude calculation.

The complete amplitude of the stimulated echo experiment is written as.

$$E(G) = \frac{A(G)}{A(0)} = E_{sp}(G) + E_{df}(G) \tag{7.19}$$

where

$$\begin{aligned} E_{sp}(G) = &\sum_j \left[\left\langle \exp\left[i\left(\varphi_{2j} - \varphi_{1j}\right)\right]\right\rangle \left[1 - P_{fj}(\tau_2)\right]\right] \\ &+ \sum_k \left[\left\langle \exp\left[i\left(\varphi_{2k} - \varphi_{1j}\right)\right]\right\rangle \left[1 - P_{fjk}(\tau_2)\right]\right] \end{aligned} \tag{7.20}$$

is the contribution of the flip-flop process to the signal attenuation and

$$\begin{aligned} A_{df} = &\sum_{j\neq k} \left[\left\langle \exp\left[i\left(\varphi_{2j} - \varphi_{1j}\right)\right]\right\rangle - \left\langle \exp\left[i\left(\varphi_{2k} - \varphi_{1j}\right)\right]\right\rangle \right] \\ &\times \left[2P^{\cdot\cdot}_{2jk}(\tau_1) + P^{\cdot\cdot}_{1jk}(\tau_2)\right] \end{aligned} \tag{7.21}$$

is the contribution of the gradient pulse to the relaxation process, the defactorization term. The characteristic time for the defactorization factor is calculated to be in the order of $\tau_{df} \cong \alpha^{-1} T_1$, in typical situations $\alpha \approx 0.1 - 0.25$. In the narrow gradient pulse approximation and in experimental time on the order of single T_1 the defactorization term is negligible.

Using equation 7.11 and neglecting the defactorization term, Fatkullin writes the spin-diffusion signal resulting in the stimulated echo experiment.

$$E(G) \approx E_{sp} = \sum_j \left[\left\langle \exp\left[i\gamma\delta G\left(r_j(\tau_D) - r_j(0)\right)\right] \right\rangle \left[1 - P_{jj}(\tau_2)\right]\right] + \sum_k \left[\left\langle \exp\left[i\gamma\delta G\left(r_k(\tau_D) - r_j(0)\right)\right] \right\rangle \left[1 - P_{jk}(\tau_2)\right]\right] \quad (7.22)$$

where $\tau_D = \tau_1 + \tau_2$

At this point it is important to emphasis that the flip-flop process can be detected as a diffusion phenomenon (and not as a relaxation process only) when the magnetization is aligned with the B_0 axis, as happens between the second and third pulse of the stimulated echo experiment (figure 7.2a). This phenomenon cannot be seen in similar diffusion experiment such as Pulsed Gradient *Spin* Echo (figure 7.2b) where the magnetization precesses in the *x*-*y* plane for the whole experimental time (i.e. and is not locked along the *z* axis).

In most liquids the translational diffusion is so large that the spin-diffusion, if it exists, is negligible. The diffusion coefficient extracted from the PGSTE experiment in this case is the diffusion coefficient of the Brownian motion only [99]. In the case of solids the only motion responsible for this phase shift is magnetization migration via spin-diffusion. Cory and Zhang[98] used the same PGSE pulse sequence, modified to match the special conditions required when dealing with solid state NMR, to measure the spin-diffusion coefficient in two directions, [001] and [111], of single crystal of CaF_2. The diffusion coefficient which was found in this case was:

$$D_{\parallel}[001] = 7.14 \pm 0.52 \times 10^{-16} \text{ m}^2 \text{ s}^{-1}$$
$$D_{\parallel}[111] = 5.31 \pm 0.34 \times 10^{-16} \text{ m}^2 \text{ s}^{-1}. \quad (7.23)$$

In the case of flexible polymer chains, melts and high molecular weight semidilute solutions, the interpretation of the stimulated echo attenuation is much more complicated since one must take into consideration the nature of the motion of the polymer[74]. Unlike solids where the atoms are confined to lattice sites and the dipolar interaction fairly strong and independent of time, flexible polymer chains are mobile and as a consequence the dipolar interaction is fairly small and the local strength will vary with time. However the flip-flop processes still exist and depend on the probability that remote spins will approach within a distance of a few Angstroms, for just enough time for the flip-flop process to be effective. The polymer segment then continues its Brownian motion after the flip-flop process with a new magnetization and so the quasiparticle migrates. As can be seen one is dealing here with two random motions,

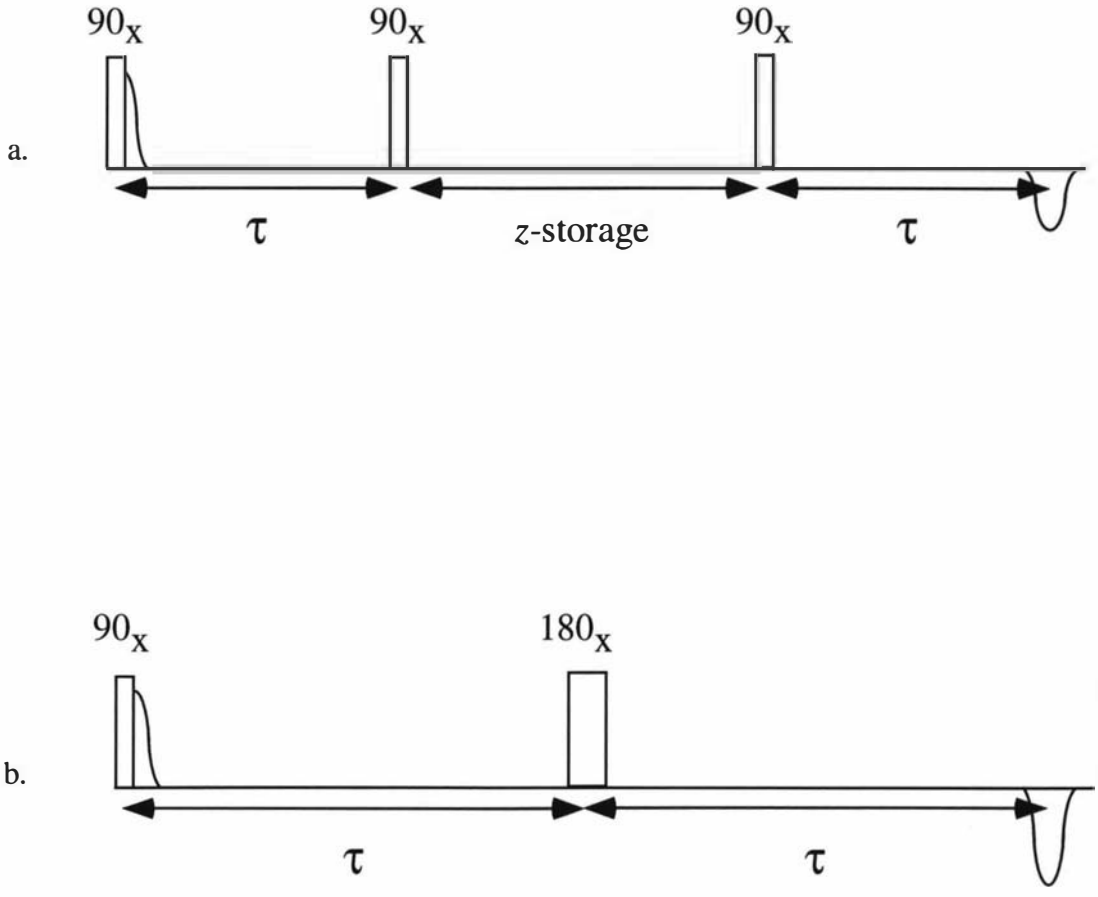

Figure7.2:
a) Stimulated echo experiment. Between the second and third pulse the magnetization is locked at the *z* direction hence the spins can flip-flop. b) Spin echo experiment. At all times the spins are dephase and rephase in the *x-y* plane and thus the spin diffusion process is eliminated.

namely the spin-diffusion and the Brownian motion the first riding above the other. Thus the diffusion coefficient obtained in the PGSTE experiment in case of polymer melts and semidilute solutions can be written:

$$D_{sp} = \frac{1}{6t}\left(\left\langle r^2(t) + a_0^2 \right\rangle\right) \tag{7.24}$$

where $r^2(t)$ is the translational rms displacement of the polymer segments and a_0 is the rms displacement of the magnetization.

The reason we believe that only remote spin flips contribute to the spin-diffusion signal obtained in the experiment is because the spin-diffusion process occurring between neighboring spins is too slow to be noticed. For example calculating the spin-diffusion coefficient of neighboring spins in high molecular weight Polystyrene solution, taking T_2 as 35 ms and distance between neighboring spins as 2 Angstroms, one obtains:

$$D \sim Wb^2 = \frac{1}{T_2} b^2 = \frac{1}{35 \text{ ms}} \cdot \left(2\,\mathring{A}\right)^2 = 1.14 \times 10^{-18} \text{ m}^2 \text{ s}. \tag{7.25}$$

This is an exceptionally low value, some 2 or 3 orders of magnitude below that detectable by PGSE NMR. Although, in soft condensed matter, the flip-flop process which can be detected is between remote spins, there is a difference between the two cases of melts and semidilute solutions. In the polymer melts samples the flip-flop process occurs *between* the polymer chains, so the anisotropic motion of the polymer segment as described in chapter 2 can no longer be detected (figure 7.3) [74]. In the case of the semidilute solutions the tube diameter is bigger and chains are more mobile. Collision between segments within a chain are more likely than collisions between segments on different chains. Thus the flip-flop process is dominated by exchange process involving spins on the same chain.

7.4 Results

Figure 7.4 shows a complete set of $\langle Z^2 \rangle$ vs t for three molecular weight of polystyrene: 3.0×10^6, 15.4×10^6 and 20.0×10^6 daltons, in which the spin echo data are shown as open symbols while the stimulated echo data are shown as filled symbols. A good agreement between data sets acquired using different echo schemes (i.e. the

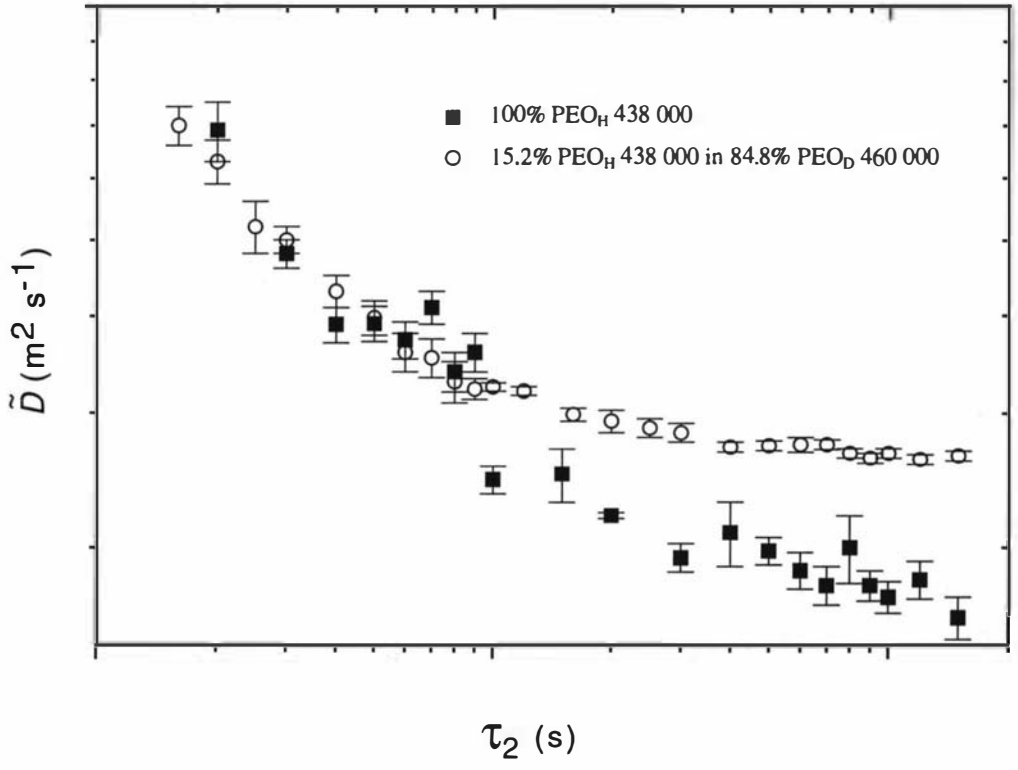

Figure 7.3[74]**:**
Effective spin diffusivities of (undeuterated)PEO_H 438 000 in bulk and dispersed in a matrix of 84.8% (deuterated) PEO_D 460 000 at 80° C and 200 MHz proton resonance frequency. The field gradient was 60 T m^{-1}. Note that the deuterated matrix inhibits the inter-chain spin diffusion.

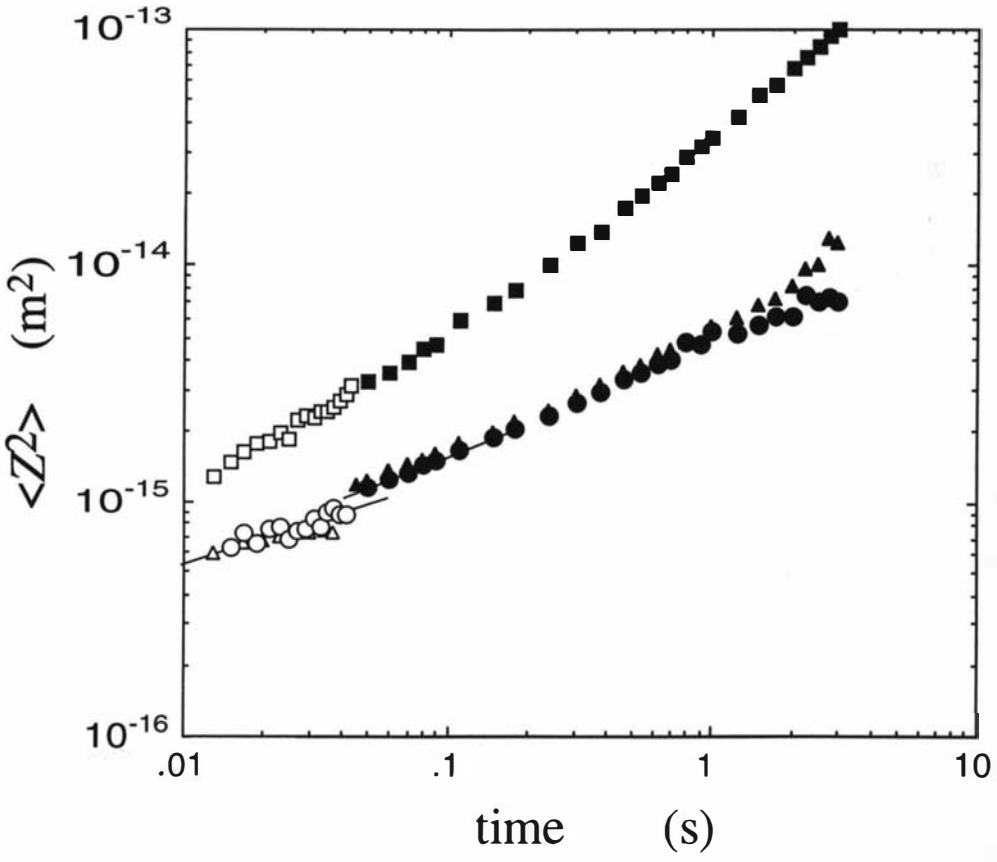

Figure 7.4[19]:
log(<Z^2>) *vs* log(*t*) for 3.04x10^6 daltons (squares), 15.4x10^6 daltons (triangles), and 20.0x10^6 dalton (circles) polystyrene at 4.96% (w/v) in deuterated toluene. Spin echo data are shown as open symbols and the stimulated echo data are shown as filled symbols.

3.0×10^6 daltons sample in figure 7.4), indicates that spin-diffusion does not play a role. On careful inspection, of the graphs obtained by the 15.4×10^6 and 20.0×10^6 daltons sample, it can be seen that in the vicinity of the spin echo/stimulated crossover (around 40 ms), the values of $\langle Z^2\rangle$, of the spin echo experiment, are now noticeably smaller in the case of these larger molar mass polymers and that the weak spin-diffusion process is now visible as a discrepancy between the two data sets. The spin-diffusion process was apparent also in the 10.2×10^6, 8.42×10^6, 6.5×10^6 daltons 4.96% and 3.04×10^6 daltons 10.58% samples.

In order to elucidate this effect, we have carried out a series of stimulated echo experiments for the 15.4×10^6 daltons 4.96% w/v sample at a fixed value of $\Delta = 45$ ms in which the time between the second pair of 90° rf pulses (the *z*-storage time) is varied thus gradually transforming the stimulated echo into a spin echo (figure 7.5). The resulting plot of mean-squared displacement *vs* storage time is shown in figure 7.6. It is clear from this data that the additional mean-squared displacement resulting from *z*-storage, which we attribute to the effect of spin-diffusion, is not linear in time, as one might expect in a three dimensional Gaussian random walk. Indeed, these data suggest that this spin-diffusion displacements may vary as $t^{1/2}$, a proposition which we test in figure 7.7. The agreement is very good.

In order to support the finding of the previous experiment we needed an experiment which suppresses all the inter-chain flip-flops and allows only intra-chain interaction. 2.92% protonated 3.04×10^6 daltons polymer chain and 12.85% deuterated polystyrene $M_w = 3.13\times10^6$ manufactured in Polymer Laboratories, Shropshire, UK, were dissolved in deuterated toluene. This results in isolated "NMR-visible" protonated polymer chains inside a deuterated polymer matrix in which all inter-chain flip-flops are suppressed. Figure 7.8 shows the $\langle Z^2\rangle$ *vs* t for this sample with the Doi & Edwards reptation curve. One can see that even though these inter-chain flip-flops are suppressed the spin-diffusion process can still be observed, which clearly indicates that intra-chain flip-flops are dominant.

7.5 Discussion

In the experiments of Fischer *et al* [74] carried out in a polymer melts, the extra displacements due to spin-diffusion were most apparent at the longest times, when the

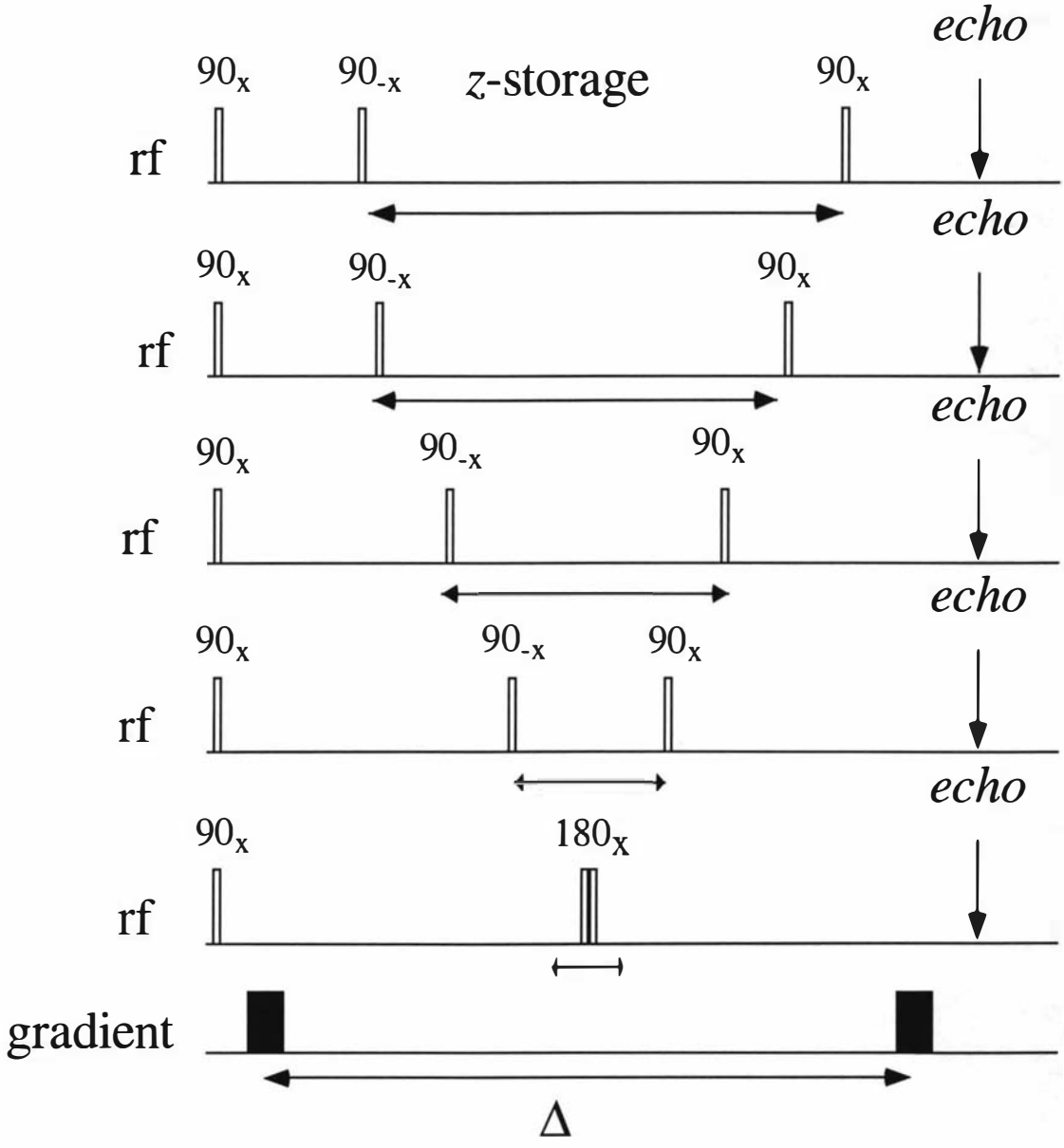

Figure 7.5:
By gradually reducing the *z*-storage, less time is available for the spins to flip-flop, thus gradually the spin diffusion process is inhibited. When the *z*-storage becomes zero the stimulated echo experiment turns into a spin echo experiment.

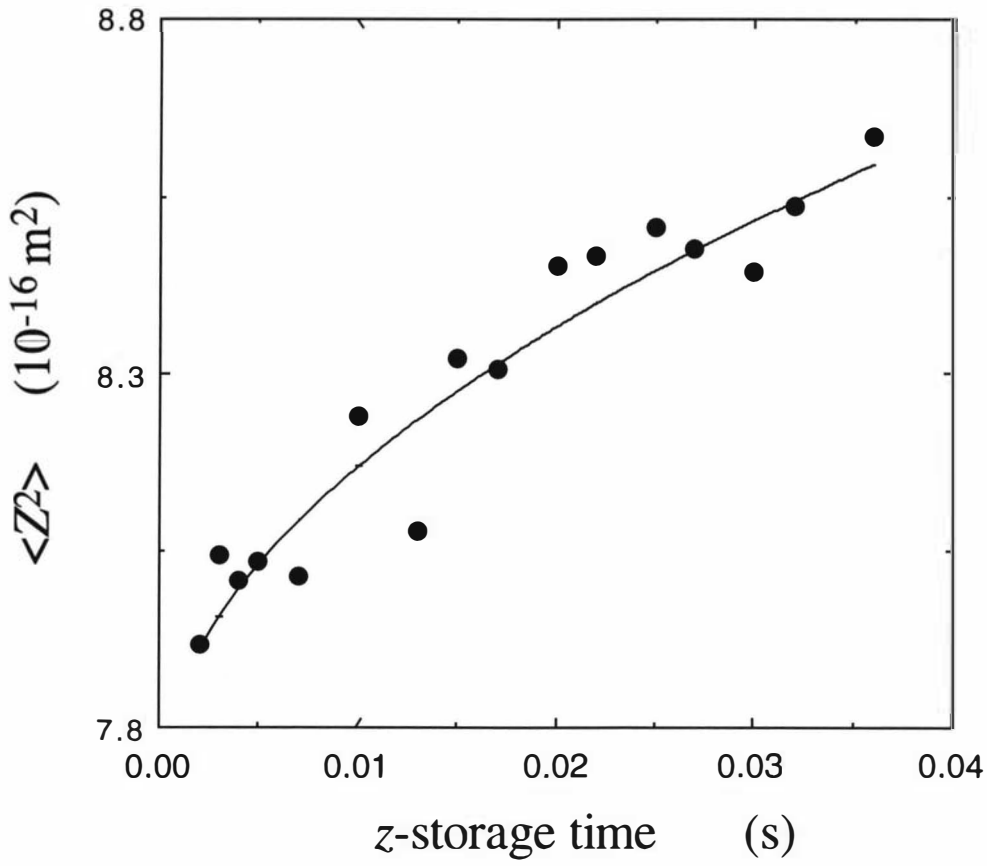

Figure 7.6[19]**:**
Mean square displacement *vs* storage time for 4.96% (w/v) 15.4×10^6 daltons, exhibiting $\langle Z^2_{SD} \rangle \sim t^{1/2}$ behavior.

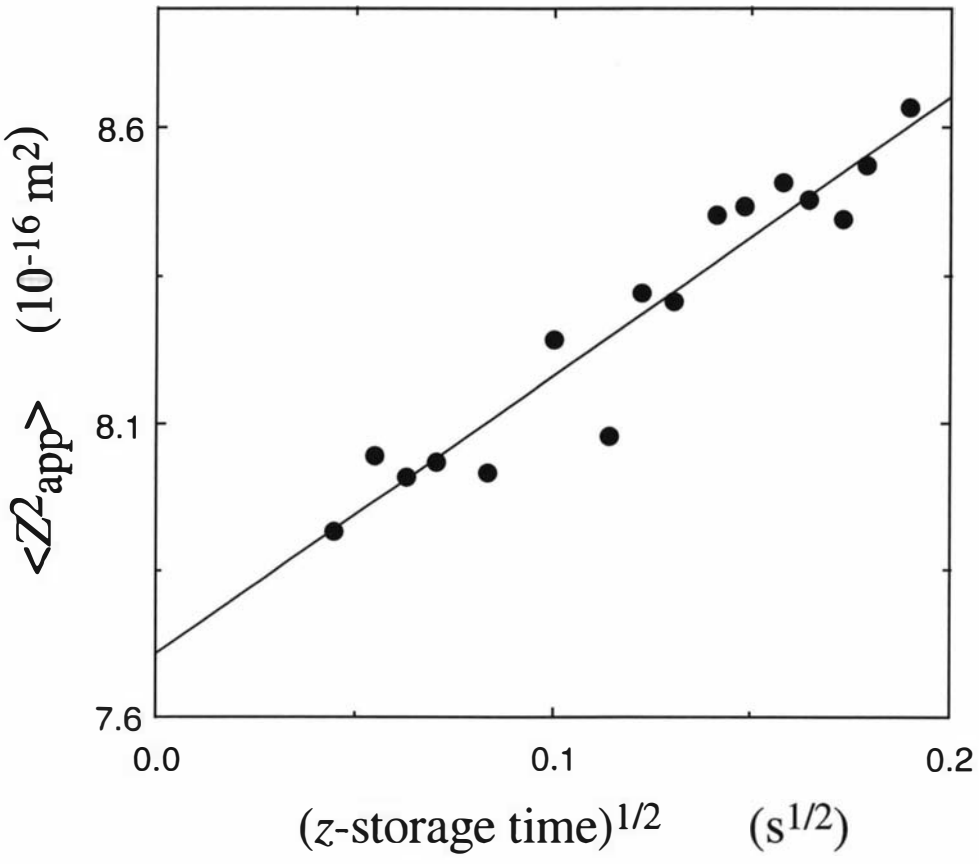

Figure 7.7[19]**:**
Data from figure 7.6 plotted as $\langle Z^2_{app} \rangle$ *vs* $(t_{z\text{-storage}})^{1/2}$. The slope yields the spin diffusion coefficient, D_{SD} via eq. 7.26, where t is $t_{z\text{-storage}}$ and $\langle Z^2 \rangle$ is constant.

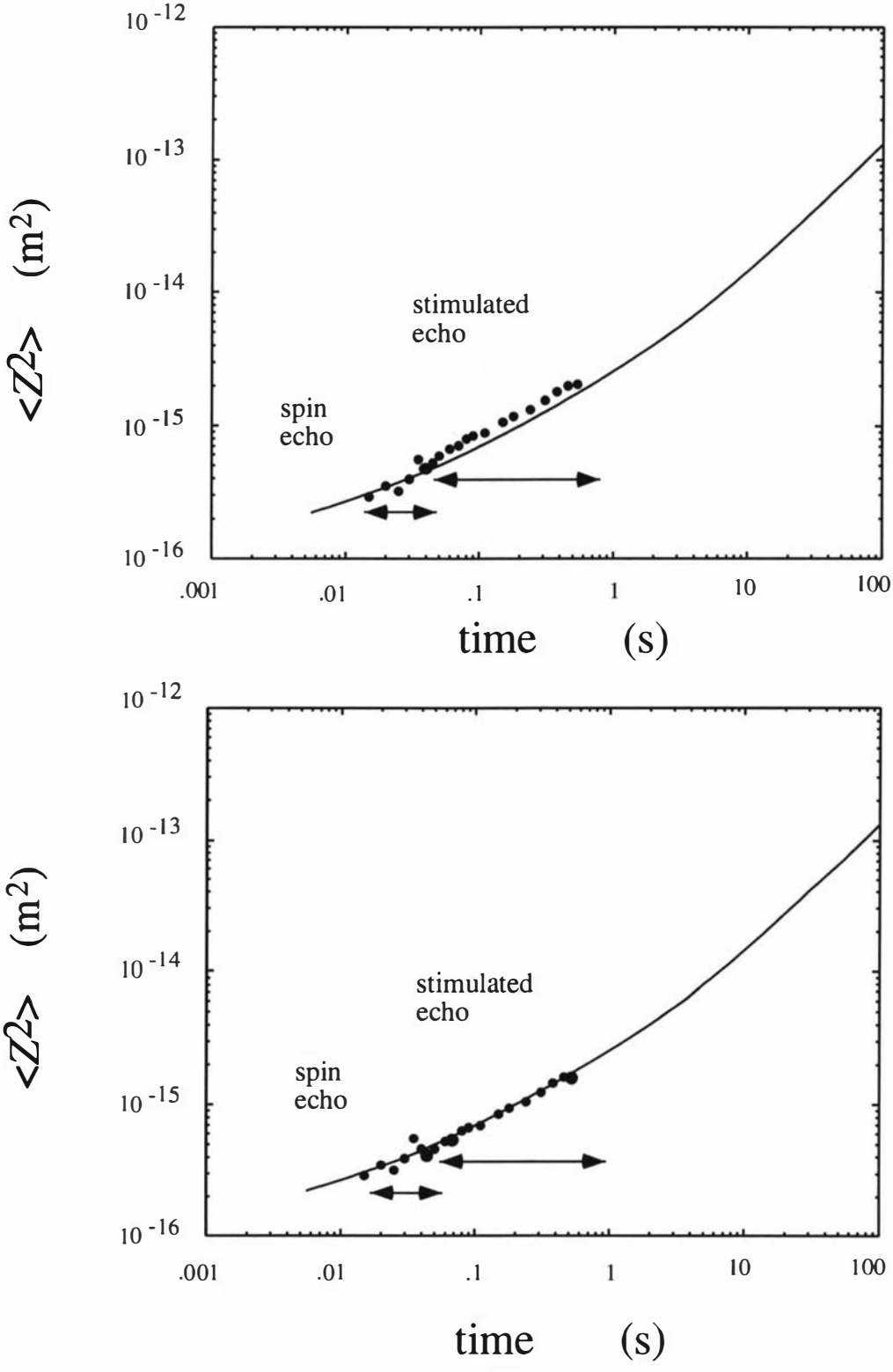

Figure 7.8:
log(<Z^2>) *vs* log(*t*) for 2.92% 3.04x10^6 daltons protonated polystyrene immersed in a 12.85% 3.13x10^6 daltons deuterated polystyrene, fit on the Doi-Edwards reptation curve. a) Before spin diffusion correction and b) after the spin diffusion correction.

apparent diffusion coefficient of the polymer has its minimum value. This is precisely the result we would expect if the spin-diffusion quasiparticles are transported as $\langle Z_{SD}^2 \rangle = 2D_{SD}t$. In our own data, obtained in semidilute solution, where we observe by contrast a scaling of the form $\langle Z_{SD}^2 \rangle \sim t^{1/2}$, the effect of spin-diffusion will be weak at the longest times where the polymer segmental displacements are expected to vary as $\langle Z_{SD}^2 \rangle \sim t$ and similarly weak at the shortest times, in regime II, where we expect $\langle Z_{SD}^2 \rangle \sim t^{1/4}$. The mechanism which we suggest for spin-diffusion, in the case of semidilute solutions, is one in which the quasiparticles are largely confined to the path of the single polymer in which they originate, possibly escaping to neighboring chains in longer times than those used for the measurements. Furthermore, the fact that we observed a spin-diffusion process on the protonated polymer chain immersed in a deuterated polymer matrix, where any inter-chain spin-diffusion was suppressed, proves that the diffusion indeed takes place along the polymer chain. Whether or not such a transition to $\langle Z_{SD}^2 \rangle \sim t$ occurs at a longer time is immaterial as far as it affects any systematic spin-diffusion correction which is to be made to the apparent segmental displacements, since this correction must, of necessity, be less than the already small effect seen in the vicinity of the spin echo/stimulated echo crossover.

A possible reason for this semi-confinement of spin-diffusion to a single chain, and hence to the primitive path, is that unlike the case of the melt, the probability of inter-segment contacts within a chain is significant higher than that probability of contact between two different chains, at length scales smaller than the blob dimension ξ_c. Supporting this assumption are the results from the concentration dependence experiment. These results show an evidence for spin-diffusion only in the 10.48% sample where the other samples, 4.96% 16.64% and 23.58%, results shows translational diffusion only. In the case of the 4.96% sample it is quite obvious that the translational diffusion is high enough to overwhelm the spin-diffusion contribution. While in the case of the 4.96% there might be spin-diffusion which we cannot observe in the 16.64% and 23.58% spin-diffusion process is suppressed. The reason for the suppression is probably the blob size which decreases when the concentration is increased, thus the probability of intra-blob contacts for the 16.64% and 23.58% concentration sample become negligible. Note, the results of the diffusion *vs* concentration dependence measurements pointed out the possibility of very small blob sizes.

As a consequence of all the above, the apparent mean squared displacement (in the case of the stimulated echo) of the actual segmental displacement $\langle Z^2 \rangle$ can written as a combination of a free segmental diffusion and a mean square displacement on a curvilinear path eq 2.21:

$$\langle Z_{app}^2 \rangle = \langle Z^2 \rangle + \frac{1}{3}(2D_{SD}t)^{1/2} a \tag{7.26}$$

where a is, as always, the tube diameter, and we allow that $\langle Z^2 \rangle = \frac{1}{3}\langle (R_n(t) - R_n(0))^2 \rangle$. D_{SD} may be estimated directly from the data shown in figure 7.7, as 3.5×10^{-15} m^2 s^{-1}. This value is quite close to that found by Fischer *et al* for polymer melts[74]. In practice absolute *a priori* estimates are hard to make. While one might expect the flip-flop time, τ_f, to be somewhat longer in the semidilute solution, the quasiparticle jump distance may well be greater owing to greater local mobility of the chain segments.

In each case where a discrepancy was found between stimulated echo and spin echo data (the five highest molar masses and 10.48% 3.0×10^6 daltons) equation 7.26 was used to correct the stimulated echo $\langle Z^2 \rangle$ data across the entire range of experimental times, adjusting D_{SD} so as to obtain the smoothest crossover to the spin echo. A comparison of the raw $\langle Z_{app}^2 \rangle$ and corrected $\langle Z^2 \rangle$ *vs* t data confirms that the correction is only significant in the region of intermediate times where the spin echo and stimulated echoes meet.

8

ANISOTROPY OF SEGMENTAL MOTION

In chapter 5, the data obtained from measurements of mean square displacements of polymer segments was shown to be consistent with predictions of the Doi-Edwards model. This model is based on the assumption of a topological tube in which lateral segmental motion is restricted but motion along the tube is permitted. Inherent in this model is the concept of local translational motion anisotropy. In other words, the polymer segments should exhibit large scale motion along the tube then transverse to the tube, provided that the chosen observation time is sufficiently short. In order to see such local anisotropy, it is therefore necessary that we carry out measurements in the $t^{1/4}$ regime.

Note that while the local motion of an individual segment may be anisotropic, the overall distribution of displacement by all polymer segments is clearly isotropic, since there is no favored axis in the sample. Thus we need to use the double-PGSE method to observe such local behavior. In this chapter I will show how we managed to observe an anisotropic segmental motion directly by using the double-PGSE method.

8.1 Double-PGSE signal attenuation for the reptation model

As mentioned in section 3.3.3 the difference in the signal attenuation between double-PGSE NMR experiments in which the two pairs of pulses are applied successively in the z-z directions and z-x directions gives one insight regarding the character of any anisotropic motion. According to the reptation model, when the mean square displacement of a polymer segment exceeds the tube diameter, the motion of the segment is no longer isotropic but confined to diffuse along its own contour path. However, since the polymer dynamics is that of a random walk, the associated correlation function decays rapidly. Thus, beyond few steps, Z, on the primitive path the local motion will become uncorrelated and will appear isotropic. Given this constraint, the two intervals in the Double-PGSE experiment must be short and close together compared with the Rouse time. In this section we attempt[100] to predict the signal attenuation, from a Double-PGSE experiment, for possible anisotropic motions of polymer segments before the motion becomes uncorrelated.

8.1.1 Local one dimensional motion

In order to present a simplified theory, we begin by assuming that the local motion is purely one dimensional, so that the polymer segments diffuse along a narrow tube. Of course in reality, the contour along the tube will change direction once we move beyond a step length, *a*, but for simplicity we will assume that provided we are in the $t^{1/4}$ regime the direction of successive steps along the contour will still be correlated and that completely random reorientation will not take place until the $t^{1/2}$ regime is reached. We call this the correlated uni-directional model.

Suppose one-dimensional displacement axis lies at an angle θ (figure 8.1) to the first gradient direction G_z. Then the effective mean-squared displacement along G_z will be $\langle Z^2 \rangle \cos^2\theta$. If a second gradient pulse pair is applied to encode for motion along G_z again then the measured displacement along will again be $\langle Z^2 \rangle \cos^2\theta$. If the second encoding is along G_x then the displacement measured in the second interval will be $\langle Z^2 \rangle \sin^2\theta\cos^2\phi$.

Suppose we use the same gradient pulse amplitude, G, to encode in each direction. In general, where the displacement during the first interval along the first gradient direction is Z_1 and the displacement during the second interval along the second gradient is Z_2, we can write the resulting echo attenuation as $\langle \exp(i2\pi q Z_1)\exp(i2\pi q Z_2)\rangle$. For diffusive motion the distributions, $P(Z_1)$ and $P(Z_2)$, will be Gaussian with uncorelated rms. width , so that we may generalize the result to:

$$E = \exp\left(-2\pi^2 q^2 \langle Z_1^2 \rangle - 2\pi^2 q^2 \langle Z_2^2 \rangle\right) \tag{8.1}$$

where $\langle \cdots \rangle$ is the ensemble average.

<u>case 1:</u> The two sets of gradients are both in the *z* direction.

$$\begin{aligned} E_{zz}(q) &= \exp\left(-2\pi^2 q^2 \langle Z^2 \rangle \cos^2\theta\right)\exp\left(-2\pi^2 q^2 \langle Z^2 \rangle \cos^2\theta\right) \\ &= \exp\left(-4\pi^2 q^2 \langle Z^2 \rangle \cos^2\theta\right) \end{aligned} \tag{8.2}$$

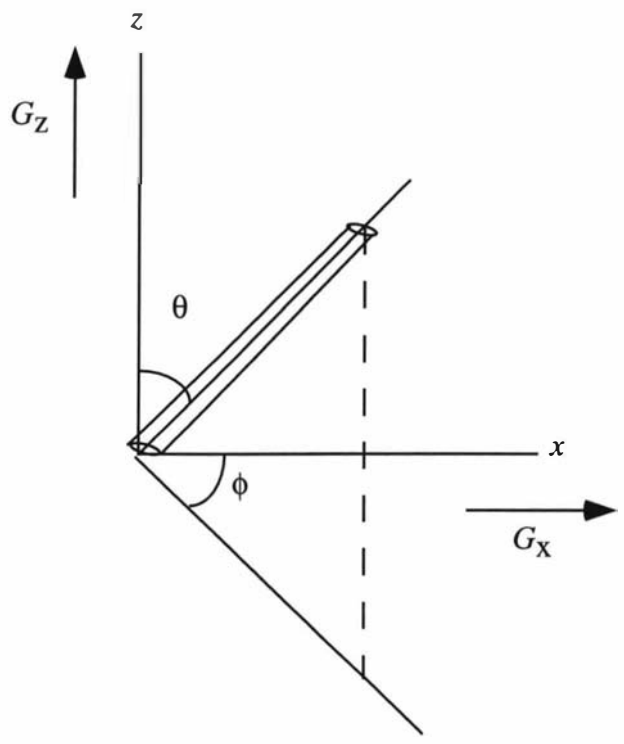

Figure 8.1:
The locally anisotropic director relevant to the NMR double-PGSE experiment. A director is shown lying with polar angle θ to the G_z direction and at azimuthal angle ϕ. to the G_x direction.

case 2: One set of gradient is in the z direction and the second set is in the x direction.

$$E_{zx}(q) = \exp\left(-2\pi^2 q^2 \langle Z^2 \rangle \cos^2\theta\right) \exp\left(-2\pi^2 q^2 \langle Z^2 \rangle (1-\cos^2\theta)\cos^2\phi\right). \tag{8.3}$$

Since in polymer melts and semidilute solutions the tubes are randomly distributed in space we must average for all possible tube directions, i.e. integrate over all θ and ϕ. As a result the echo attenuations become:

case 1: G_z, G_z

$$E_{zz}(q) = \frac{\int_0^{2\pi} d\phi \int_0^{\pi} \sin\theta d\theta \exp\left(-4\pi^2 q^2 \langle Z^2 \rangle \cos^2\theta\right)}{\int_0^{2\pi} d\phi \int_0^{\pi} \sin\theta d\theta} = (4\pi)^{-1} \int_0^{2\pi} d\phi \int_0^{\pi} \sin\theta d\theta \exp\left(\left(-4\pi^2 q^2 \langle Z^2 \rangle \cos^2\theta\right)\right) \tag{8.4}$$

case 2: G_z, G_x

$$E_{zx}(q) = (4\pi)^{-1} \int_0^{2\pi} d\phi \int_0^{\pi} \sin\theta d\theta \exp\left(-2\pi^2 q^2 \langle Z^2 \rangle \left[\cos^2\theta + \left((1-\cos^2\theta)\cos^2\phi\right)\right]\right). \tag{8.5}$$

Figure 8.2 shows a MATLAB calculation of echo attenuations for case 1 and 2. It is clear that the echo attenuations deviate to the second order (i.e. beyond the regime $q \to 0$) and that the zx experiment gives a greater degree of attenuation than the zz experiment.

8.1.2 Locally anisotropic motion model (constant anisotropy)

We now generalize the model to allow for locally anisotropic motion in which the polymer segments have diffusion coefficient $D_{\parallel}$ along the director at polar angle θ and $D_{\perp}$ in the plane normal to this director. Figure 8.3 shows the geometry relevant to this assumption. Note that for convenience we can choose two representative orthogonal axes in the plane of $D_{\perp}$ with (polar, azimuth) directors, ($\theta + \pi/2$, ϕ) and ($\pi/2$, $\phi + \pi/2$) as shown.

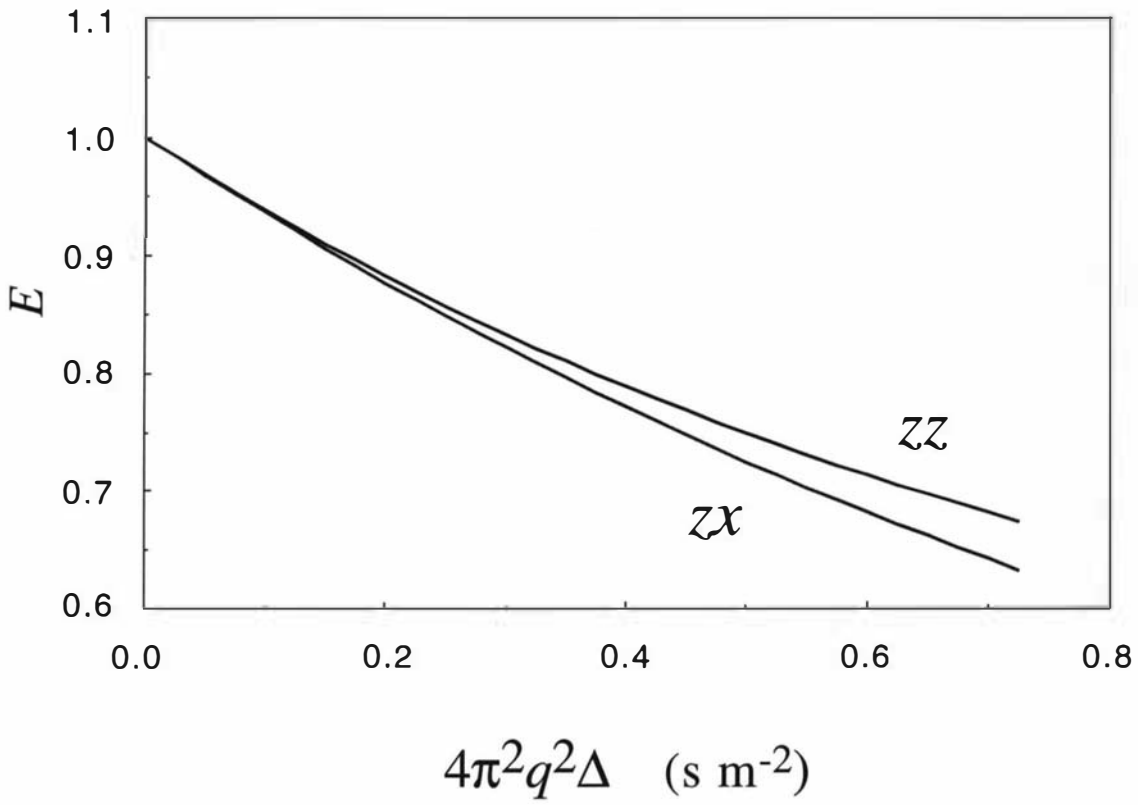

Figure 8.2:
MATLAB calculation of echo attenuation expected for the case of model 1 in which the locally anisotropic diffusion is confined to a single direction over the period of the double-PGSE sequence.

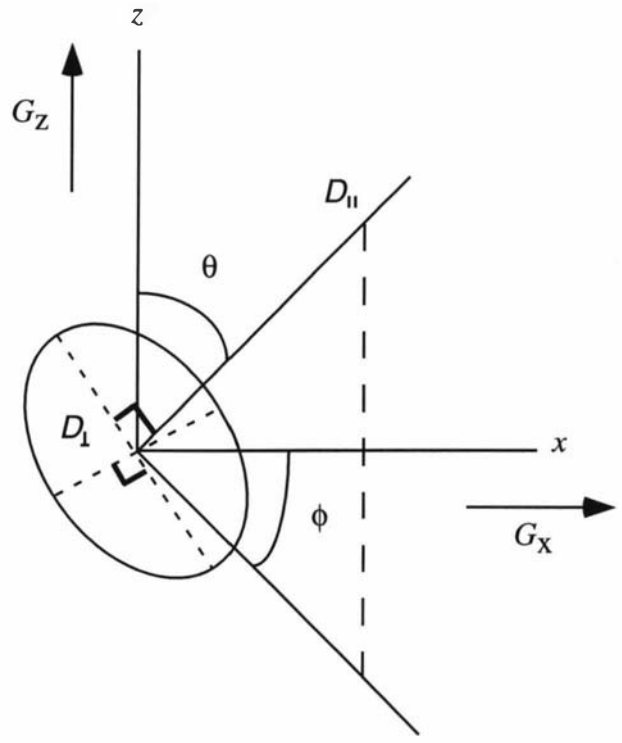

Figure 8.3:
Locally anisotropic director relevant to NMR double-PGSE experiment in which diffusion is confined to a plane.

We will allow in general that $D_{\|}$ and $D_{\perp}$ can take any values. Then it may be shown

$$E_{zz} = (4\pi)^{-1} \int_0^{2\pi} d\phi \int_0^{\pi} \sin\theta d\theta \exp(-4\pi^2 q^2 \Delta[2D_{\|} \cos^2\theta + 2D_{\perp} \sin^2\theta])$$

$$= \frac{1}{2} \int_0^{\pi} \sin\theta d\theta \exp(-4\pi^2 q^2 \Delta[2D_{\|} \cos^2\theta + 2D_{\perp} \sin^2\theta]) \tag{8.6}$$

$$E_{zx} = (4\pi)^{-1} \int_0^{2\pi} d\phi \int_0^{\pi} \sin\theta d\theta \exp(-4\pi^2 q^2 \Delta[D_{\|} \cos^2\theta + D_{\|} \sin^2\theta \cos^2\phi + D_{\perp} \sin^2\theta + D_{\perp} \cos^2\theta \cos^2\phi + D_{\perp} \sin^2\phi]) \tag{8.7}$$

It is interesting to note that for all relative values of $D_{\|}$ and $D_{\perp}$ where these two differ, we always find that the echo attenuation for E_{zx}, is greater than for E_{zz}. In other words, such an experimental result indicates local anisotropy, with the director unchanged between the first and second pulse pairs, and only the degree of the difference between E_{zz} and E_{zx} , indicates the nature of that local anisotropy.

8.1.3 Locally anisotropic motion model (changing anisotropy)

We will find, in the polymer experiments reported here, that the measured behavior is $E_{zx} > E_{zz}$, in direct contradiction with the models outlined in 8.1.1 and 8.1.2. One explanation for this observation would be if the motion was locally anisotropic but the director changed orientation between the PGSE pulse pairs. We here consider an extreme case of an orthogonal switch. Physically, this might correspond to the polymer being constrained by an entanglement during the first pulse pair, during which time it moved most easily transverse to the direction towards the obstruction, but that during this motion it met a new obstruction and then moved most easily transverse to its original motion.

To simulate this we consider motion during the first pulse pair along the two representative $D_{\perp}$ axes, $(\theta + \pi/2, \phi)$ and $(\pi/2, \phi + \pi/2)$, and then we switch motion during the second pulse pair to either of the available orthogonal axes (θ, ϕ) and $(\pi/2, \phi + \pi/2)$ in the case of the first motion being along $(\theta + \pi/2, \phi)$, or to the axes (θ, ϕ)

and $(\theta + \pi/2, \phi)$ in the case of the first motion being along $(\pi/2, \phi + \pi/2)$. In consequence four possible representative cases are allowed, each equally weighted by $\frac{1}{4}$. The resulting echo attenuations are:

$$
\begin{aligned}
E_{zz} = & \frac{1}{4}(4\pi)^{-1}\int_0^{2\pi} d\phi \int_0^{\pi} \sin\theta d\theta \exp(-4\pi^2 q^2 D_\perp \Delta[\cos^2\theta + \sin^2\theta]) \\
& + \frac{1}{4}(4\pi)^{-1}\int_0^{2\pi} d\phi \int_0^{\pi} \sin\theta d\theta \exp(-4\pi^2 q^2 D_\perp \Delta[\sin^2\theta]) \\
& + \frac{1}{4}(4\pi)^{-1}\int_0^{2\pi} d\phi \int_0^{\pi} \sin\theta d\theta \exp(-4\pi^2 q^2 D_\perp \Delta[\cos^2\theta]) \\
& + \frac{1}{4}(4\pi)^{-1}\int_0^{2\pi} d\phi \int_0^{\pi} \sin\theta d\theta \exp(-4\pi^2 q^2 D_\perp \Delta[\sin^2\theta])
\end{aligned}
\tag{8.8}
$$

$$
\begin{aligned}
E_{zx} = & \frac{1}{4}(4\pi)^{-1}\int_0^{2\pi} d\phi \int_0^{\pi} \sin\theta d\theta \exp(-4\pi^2 q^2 D_\perp \Delta[\cos^2\theta + \sin^2\theta\cos^2\phi]) \\
& + \frac{1}{4}(4\pi)^{-1}\int_0^{2\pi} d\phi \int_0^{\pi} \sin\theta d\theta \exp(-4\pi^2 q^2 D_\perp \Delta[\sin^2\theta + \sin^2\phi]) \\
& + \frac{1}{4}(4\pi)^{-1}\int_0^{2\pi} d\phi \int_0^{\pi} \sin\theta d\theta \exp(-4\pi^2 q^2 D_\perp \Delta[\sin^2\theta\cos^2\phi]) \\
& + \frac{1}{4}(4\pi)^{-1}\int_0^{2\pi} d\phi \int_0^{\pi} \sin\theta d\theta \exp(-4\pi^2 q^2 D_\perp \Delta[\cos^2\theta\cos^2\phi])
\end{aligned}
\tag{8.9}
$$

A comparison of E_{zz} and E_{zx} is shown in figure 8.4, where it is clear that for this case the result $E_{zx} > E_{zz}$ is indeed found.

8.2 Materials, methods and results

The double-PGSE NMR method is a new technique. In order to use it to detect locally anisotropic motion in polymers, its needed to be tested on isotropic system and on systems of known local anisotropy. We refer to the latter as a "reference system". Note, that the x and y directions are theoretically identical since they are both orthogonal to the B_0 direction (i.e. z). Even though our gradient coil designed to give gradient pulses in the y direction, we referred to it here as x direction to be consistent with the theory which was presented in the previous section.

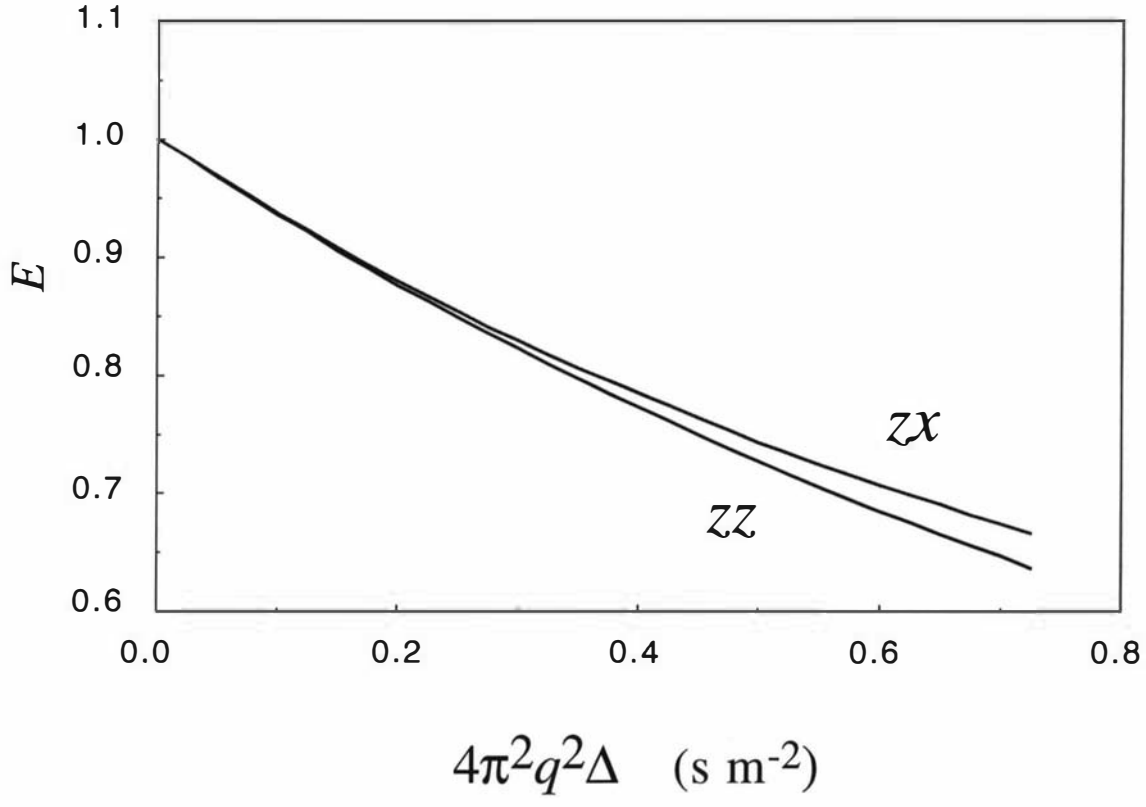

Figure 8.4:
MATLAB calculation of echo attenuation expected for the case of model 3 in which the locally anisotropic diffusion is confined to a plane over the first interval and then in orthogonal plane over the second interval of the double-PGSE sequence.

8.2.1 Instrumentation test

Before the double-PGSE experiment was performed on a reference system we had to test the experimental set-up and the pulse program on a totally isotropic system. The echo attenuation from such a system should be identical for all experiments, independent of the gradient directions. Four double-PGSE experiments, G_zG_z, G_xG_x, G_zG_x, G_xG_z and two single pulse pair PGSE experiments, G_z and G_x were performed on pure glycerol. Figure 8.5 shows the echo attenuation of PGSE and double-PGSE for pure glycerol. The experiments were performed at room temperature, $G = 14.4$ T m^{-1}, $\Delta = 4$ ms and $\delta_{min} = 0.2$ ms for the double PGSE and $\Delta = 8$ ms. It is apparent from the figure that the various attenuation curves are similar and as a consequence we had confidence in our experimental set-up and could test the theory mentioned in section 8.1 on a reference system.

8.2.2 Reference system

In order to achieve the desirable double-PGSE attenuation for pure reptation, one needs to apply the method on a reference system. This system should imitate the dynamics of an isolated material confined inside a set of tubes which are randomly oriented in space. The chosen reference system was glycerol trapped inside an Anodisc 47 filter, made by Whatman International Ltd, England. The Anodisc Membranes are filters made of aluminum oxide, with a precise non-deformable honeycomb pore structure[101]. The pore size was 0.02 μm and the average membrane thickness was 60 μm. The reason for choosing this sample as a reference system is that the distance which the glycerol, diffusion coefficient on the order of 10^{-12} m^2 s^{-1}, can move during the experimental time is around 0.1 μm. This means that the glycerol motion will be restricted in one direction and unrestricted in the other. The glycerol was forced into the membrane by filtering it under vacuum using a Buchner funnel. After filtering the Anodisc surface was carefully wiped to eliminate the free glycerol and than crushed to a fine powder to create a macroscopically isotropic environment. The powder was placed inside a 3 mm home built NMR tube.

Two single pulse pair PGSE experiments, G_z and G_x, were performed. Figure 8.6 shows the echo attenuation of PGSE for the glycerol-Anopore system, $G = 7.2$ T m^{-1}, $\Delta = 8$ ms and $\delta = 0.2$ ms. In this figure we can see that there is a difference between the two echo attenuations which means that the sample is *macroscopically* anisotropic where the glycerol motion is restricted in the x direction and unrestricted in the z direction. These results are intriguing. Given the way the sample was made there

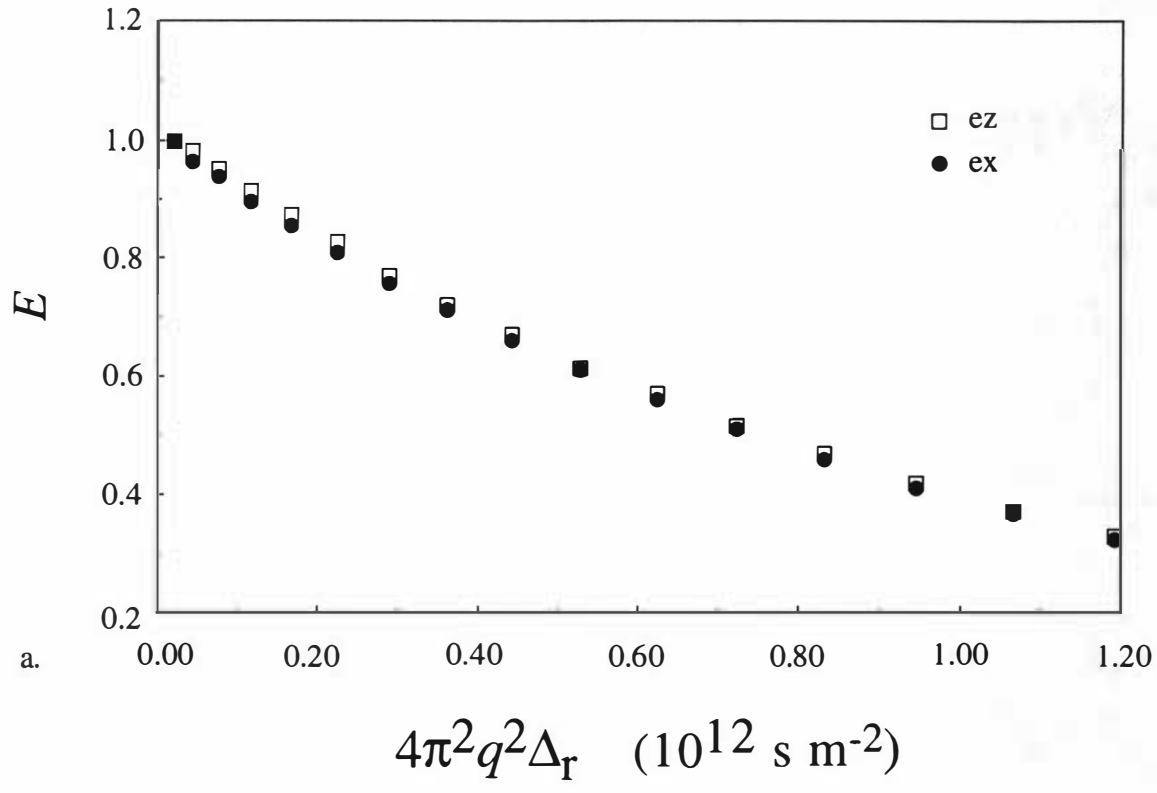

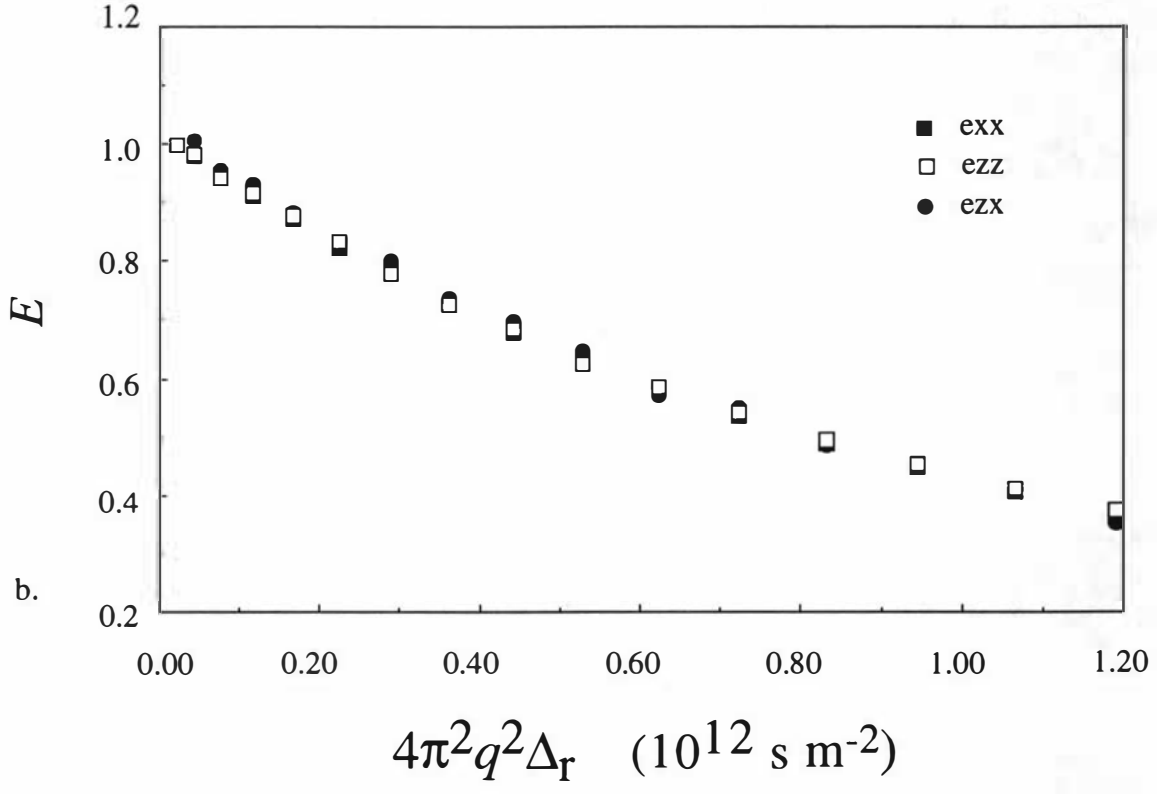

Figure 8.5:
Echo attenuations for a) PGSE and b) double-PGSE experiments for pure glycerol G=14.4. T m^{-1}, Δ=8 ms and Δ=4 ms respectively and δ=0.2 ms.

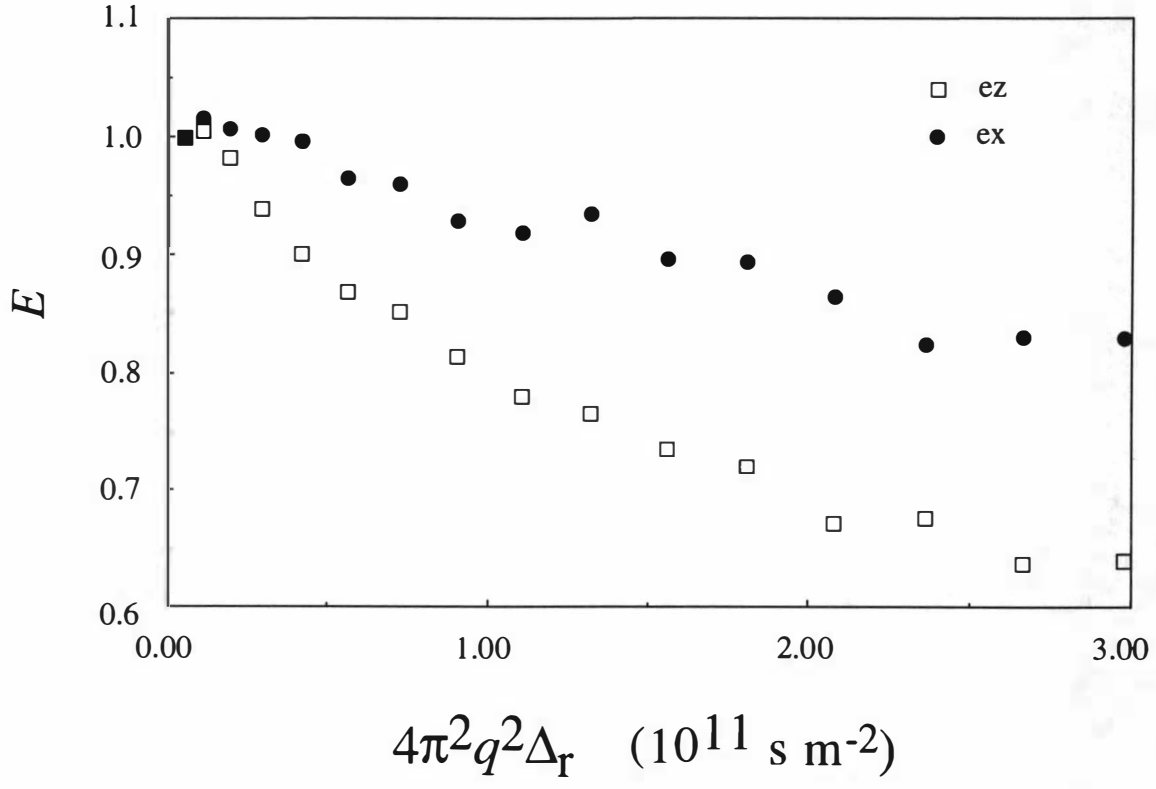

Figure 8.6:
Echo attenuations for single pulse pair PGSE experiments for glycerol trapped in "randomly oriented" Anodic 47 filter fragments. G=7.2 T m^{-1}, Δ=8 ms and δ=0.2 ms.

is no reason to believe that the system is macroscopically anisotropic. However, since the results clearly indicate this kind of anisotropy, they suggest that the Anodisc membranes must align in the presence of a strong magnetic field.

As an alternative we choose as a second reference system AOT/water[63], mixed with crushed glass. The AOT/water sample was prepared by mixing 40% of Aerosol OT (bis(2-ethylhexyl) sodium sulfosuccinate from Sigma) and 60% water and the sample left to equilibrate for 7 weeks. The AOT/water solution in this composition forms a lamella phase at room temperature in which its director tend to align with the magnetic field. However, where placed in contact with a glass surface the director aligns normal to the surface[63]. When the glass fragments are randomly oriented we should obtain a material which is macroscopically isotropic but whose water self-diffusion coefficient is microscopically anisotropic. The single pulse pair PGSE experiments in both gradient directions indicated an isotropic sample. The four double-PGSE experiments, G_zG_z, G_xG_x, G_zG_x and G_xG_z were performed and the resulting attenuations are shown in figure 8.7 ($G = 3.6$ T m^{-1}, $\Delta = 10$ ms and $\delta = 0.2$ ms). The attenuation resulting from the G_zG_z experiment is clearly higher than that resulting from the G_xG_z experiment. This behavior is consistent with the model suggested in section 8.1.2 Unfortunately the attenuation from the G_xG_x experiment and the G_zG_x experiment overlap which implies an isotropic behavior. A second set of experiments was performed on a similar sample a week later but local anisotropic behavior was not clearly detected.

8.2.3 Polymer system

Two polymer samples, $15.4\text{x}10^6$ daltons 4.96% (w/v) and $3.04\text{x}10^6$ 16.64% (w/v) polystyrene in deuterated toluene, were studied. Four sequential double-PGSE experiments, G_zG_z, G_xG_x, G_zG_x and G_xG_z, were conducted on each sample. All experiments conducted at room temperature and their parameters are as follows: $G = 25.2$ T m^{-1}, $\Delta = 10$ ms and $\delta = 0.28$ ms. Note that the choice of Δ ensures that the mean square displacement as close as possible to the $t^{1/4}$ regime. Figure 8.8 shows the double-PGSE echo attenuation for the $15.4\text{x}10^6$ daltons polymer sample. It can be clearly seen in the figure, that the attenuations which result from the G_zG_z and G_xG_x pulse sequences are greater then the attenuations which result from the G_zG_x and G_xG_z, experiment. This result is intriguing, and was something we had never expected. Certainly the simple correlated uni-directional picture for the double-PGSE attenuation for the tube model (see section 8.1.1), predicts the opposite behavior. We repeated this experiment with the same sample and experimental set up and the results were

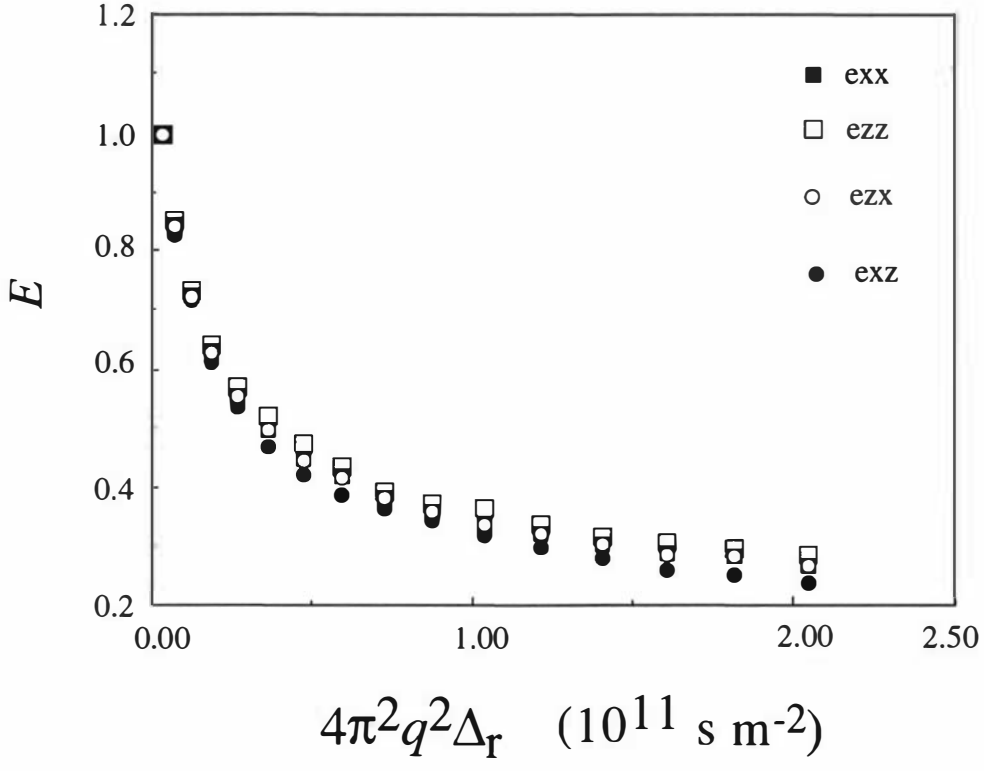

Figure 8.7:
Echo attenuations for double-PGSE experiments for 40% AOT/ 60% water lamella phase dispersed in randomly oriented crushed glass. G=3.6 T m^{-1}, Δ=10 ms and δ=0.2 ms.

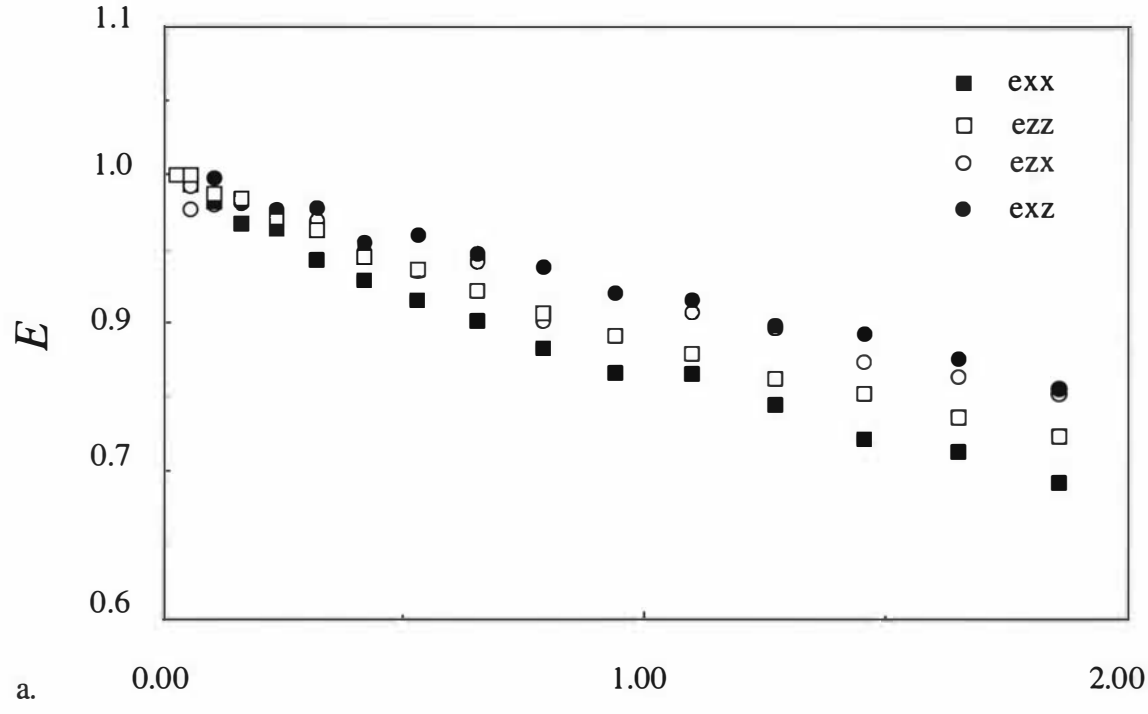

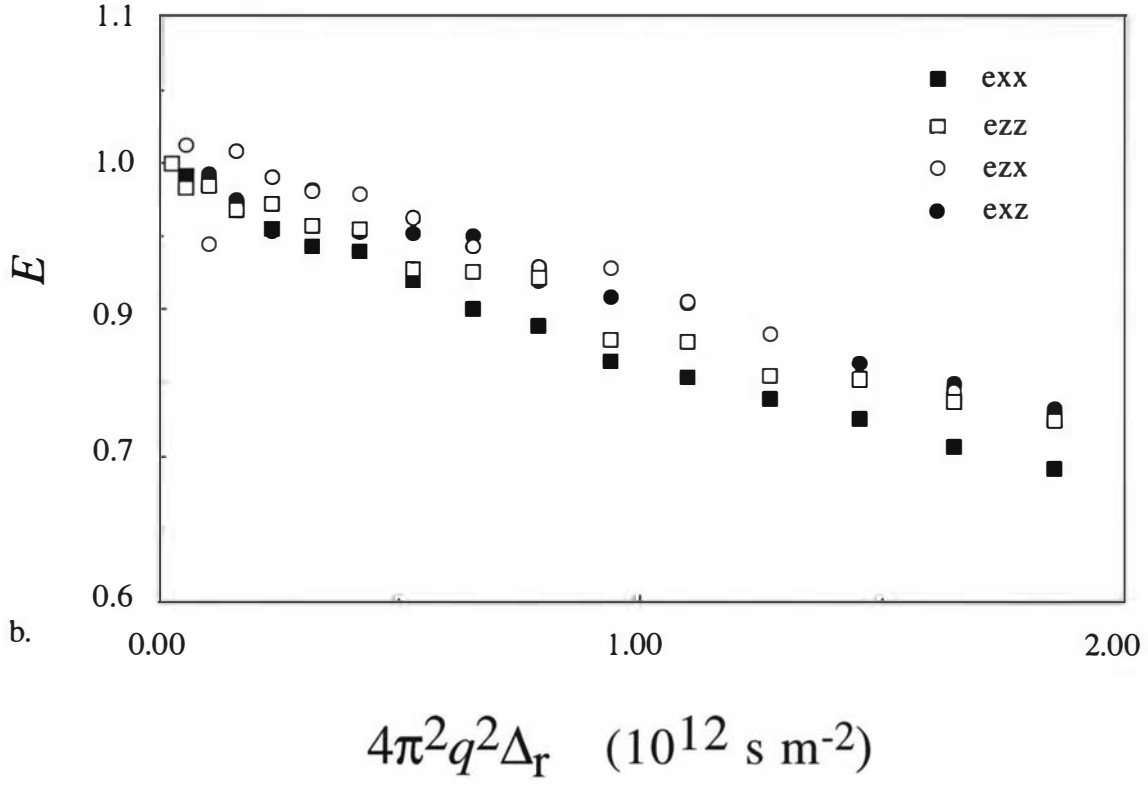

Figure 8.8:
Echo attenuations for double-PGSE experiments for 4.96% (w/v) 15.4x10^6 daltons polystyrene in deuterated toluene a) and b) are two repeated experiments on the same sample. G=25.2 T m^{-1},Δ=10 ms and δ=0.28 ms.

confirmed (figure 8.8b). As a consequence the question arises as to whether the tube model accurately represents the dynamics of polymer coil in semidilute solutions.

Figure 8.9 shows the echo attenuations which results from the double-PGSE experiment which was conducted on the 3.04×10^6 daltons sample. The local anisotropy in this sample, according to the data, is not so pronounced as the results from the 15.4×10^6 daltons sample. While the attenuation which results from the G_xG_z experiment is less than for G_zG_z and the G_xG_x, G_zG_x attenuation overlaps the G_zG_z results. Thus it may be concluded that on average we see a similar but weaker anisotropy effect as that seen in the 15.4×10^6 daltons sample. We note that the 4.96% 15×10^6 daltons data and the 16.64% 3.04x106 data sample have tube diameters and Rouses time which are very different (see Tables 5.1 and 5.2). The different degree of local anisotropy observed in the cases of the 3.04×10^6 and 15.4×10^6 daltons samples may reflect the importance of the measurement length scale in relation to the tube diameter, and the degree to which $\Delta \leq \tau_R$. In the case of 15.4×10^6 sample $\tau_R \cong 10$ ms whereas for the 3.04×10^6 daltons sample $\tau_R \cong 6$ ms. This means that the measurements for the 15.4×10^6 daltons sample is closer to the $t^{1/4}$ regime.

8.3 Discussion

The experiments which were presented in the previous sections are still in their preliminary stage. The measurement of anisotropic motion of polymer coil in semidilute solutions cannot be completed without conducting a series of successful double-PGSE experiments on a proper reference system. However, our preliminary results indicates an interesting behavior which puts in question the correlated uni-directional picture of the reptation theory. The second model which was presented in section 8.1 indicates that any type of constrained motion should result in greater attenuation for the G_xG_z and G_zG_x double-PGSE experiments. Furthermore, even when incorporating the standard modification of the reptation theory to the model, as long as one direction is microscopically favored over the other the during the experimental interval Δ, G_xG_z and G_zG_x attenuation will be greater than the G_xG_x and G_zG_z attenuation. Our findings suggests a radically different type of motion which is directed in one direction at the first interval of the double-PGSE experiment and in an orthogonal direction during the second interval of the experiment. One physical interpretation of the data could imply a motion of polymer loops in one random direction during the first interval toward an entanglement which cannot be crossed. As a result the polymer segments must change their direction. This type of behavior, however, can be observed only well

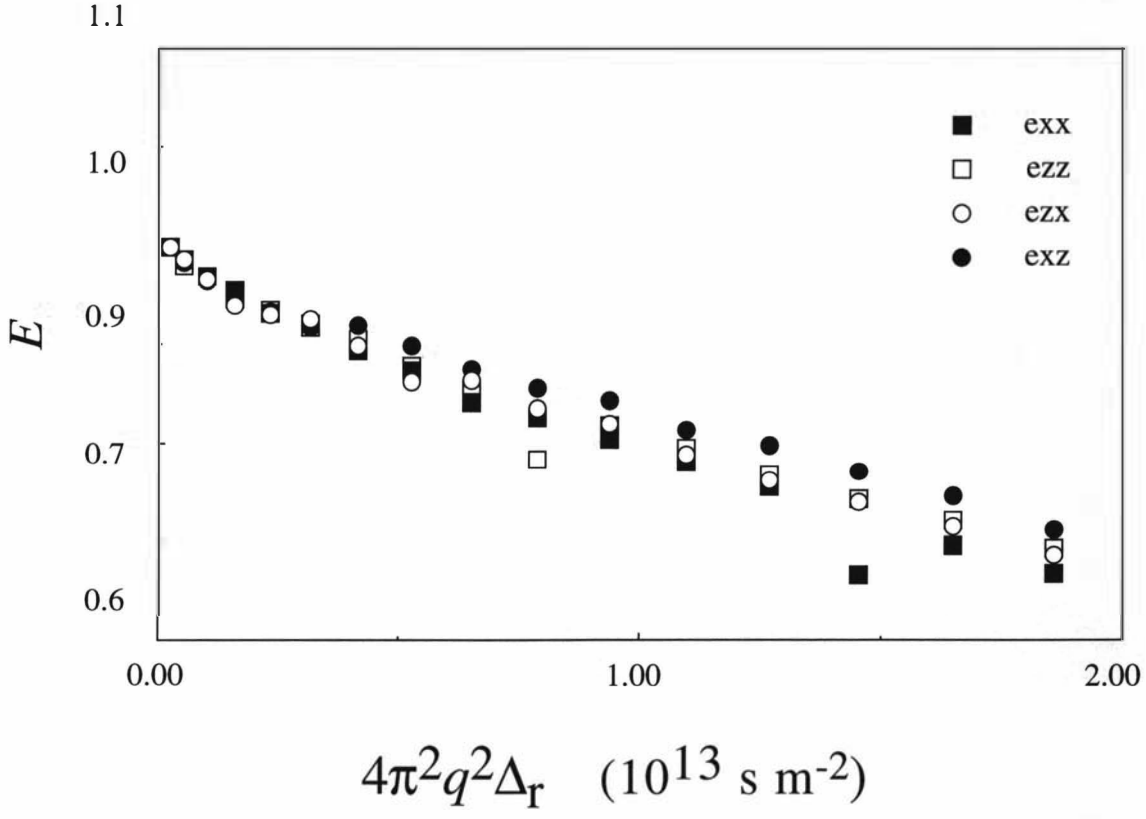

Figure 8.9:
Echo attenuations for double-PGSE experiments for 16.64% (w/v) 3.04×10^6 daltons polystyrene in deuterated toluene. G=25.2 T m^{-1}, Δ=10 ms and δ=0.28 ms.

into the $t^{1/4}$ where $\Delta \leq \tau_R$, since the observed mean square displacement must be in the order of the entanglement length. Supporting this finding is the double-PGSE experiment which was conducted on the 16.64% 3.04×10^6 daltons sample. This sample's tube diameter and Rouse time are shorter than for the 15.4×10^6 daltons 4.99% sample, hence the experimental observation time for the later sample was well into the $t^{1/4}$ while for the 16.64% sample our observation window was still in the cross over between the $t^{1/4}$ and $t^{1/2}$. The weaker anisotropic behavior of the 16.64% sample (figure 8.8) serves as an evidence for this assumption.

The mode-mode coupling theory suggests a cooperative motion in which two segments of the chain can move freely to a random direction while the rest of the chain rearranges itself accordingly. As was acknowledged in section 2.5, the mode-mode coupling theory does predict similar scaling to the mean square displacement of the polymer segments, thus it can describe the polymer dynamics. Since this theory gives no quantitative results for mean square segmental displacement, no quantitative figures for the key parameters are available. Still, our double-PGSE results may agree more with the concept of the mode-mode coupling theory. However, it is important to emphasize that since a proper experiment could not be done on a reference system, the double-PGSE analysis of a confined motion still needs to be proved.

9
SUMMARY & FUTURE WORK

9.1 Summary

This thesis set out to investigate whether the reptation theory of polymer dynamics indeed explains features of the segmental motion of a polymer coil in semidilute solutions. In order to do so we measured the mean square displacements of a range of different molar mass polystyrenes in semidilute solutions of toluene over three decades of observation time and found that the predictions of Doi-Edwards theory fitted our data very well. We compared the observed molar mass and concentration scaling for the center of mass diffusion, the tube disengagement times and tube diameters with the prediction of the reptation theory. At first sight the scaling laws which were found in this work did not agree exactly with the pure reptation theory but they did agree when standard modifications were made in order to allow for a more flexible tube.

The tube disengagement time and tube diameter parameters were compared with those obtained by fitting data from mechanical deformation experiments. While conducting the rheology measurements we found that the Doi & Edwards curves matched the oscillatory shear data but that the resulting relaxation times, (i.e. the tube disengagement times) were found to be 100 times larger than the tube disengagement times obtained in PGSE-NMR and steady shear flow experiments. A rough estimation of the tube disengagement time from the frequency of cross over between the loss and storage modulus gave much better agreement. This discrepancy leads us to believe that tube model for the oscillatory shear is deficient.

The last set of the experiments described in this work questioned a basic assumption of the reptation theory regarding local motion anisotropy and left us with few open questions regarding the polymer dynamics. In carrying out the double-PGSE experiments we expected to get echo attenuations which indicated anisotropic motion confined to a tube. However, we observed an anomalous echo attenuation relation which indicated somewhat different motion. While the motion of the polymer must be locally anisotropic, according to the data a random motion from any part of the chain in one direction for a period of time tends to be followed by a orthogonal change of direction over a subsequent period. This result calls into question the simple correlated uni-directional picture for reptation, since that theory is based on the assumption that the polymer ends are the only part of the chain which can freely move while the rest of the chain is confined inside a tube and can only diffuse along its contour length. The

rival mode-mode coupling theory suggests a cooperative motion in which any two segments of the chain can move freely while the rest of the chain rearranges itself accordingly and may be more consistent with our observations of local anisotropy. The fact that the scaling laws which we found in PGSE-NMR work agree with the predictions of the reptation theory presents another question: if this theory does not explain the local dynamics of segmental motion in semidilute solution why do its predicted scaling laws work so well? Another interesting question is whether polymer melts follow the reptation model more accurately or whether they too will give the same anomalous results as found for semidilute solutions in the double PGSE experiment?

The apparatus which had to be built in order to measure the diffusion coefficient of the polymer samples included a very high magnetic gradient coil. Working with such a high magnetic field gradient and measuring slow diffusion coefficients forced us to deal with problems that do not normally appear in standard PGSE-NMR. Among the problems we had to deal with was the Lorentz force which results in mechanical vibrations of the gradient coil with each given gradient pulse. When measuring mean square displacements of few microns those vibrations, caused by the force, are negligible, but when one tries to measure mean square displacement of few hundreds of Angstrom those vibrations interfere with the results. Apart from the mechanical vibrations the other most pronounced problem was the need to obtain good matching of the two gradient pulses. Since our experiment requirement was of pulses matched on the order of 1 ppm, it was crucial to find the right power supply and work within it limits. The power supply is currently the factor that limits our experiments.

While we were measuring the mean square displacements of very high molecular weight polystyrene we encountered the spin diffusion process. This phenomenon appeared as the difference between the mean square displacement obtained from the stimulated echo experiment and the mean square displacement obtained in the spin echo experiment. This research, which was a spin-off from our main research about the polymer dynamics, produced an interesting result which had not been observed before: the spin diffusion process in semidilute solution, unlike that in a melt, is directed along the polymer chain and does not involve magnetization quasiparticles hopping randomly from chain to chain.

9.2 Suggestions for future work

The work which might continue from this thesis can follow several directions: involving a continuing test of the predictions of the reptation theory, further investigation of spin diffusion and further improvement to the instrumentation.

In the instrumentation section it was mentioned that the current experimental limitations depend on our ability to produce well-matched high current pulses. At the moment the power supply can produce accurate pulses of few milliseconds each, only when it delivers up to 50% of the maximum current (i.e. 15 Amp) in the case of the PGSE experiment, and 35% in the case of the double PGSE. Improving the power supply will enable us to give stronger and narrower gradient pulses which will extend the measurement to times shorter than 10 ms (the $t^{1/4}$ regime) for high molecular weight polymer. Furthermore, the interesting part of the double PGSE experiment is in the lower part of the attenuation. Currently with the experimental limitation we cannot see the whole attenuation thus with a better power supply we might be able gain more information than is possible at currently available attenuation levels.

The spin diffusion section of this thesis is almost complete. The only part that might be missing is the total suppression of the spin diffusion along the polymer chain in order to absolutely confirm our interpretation. One way to totally suppress the curvilinear spin diffusion is by doing the experiments on a block co polymer which is constructed from blocks of protonated and deuterated segments. Thus two set of blocks cannot communicate via energy conserving flip-flops and will inhibit the passage of magnetization via spin diffusion.

The most interesting work which can be followed, in my opinion, is that concerning tests of the reptation theory. Even though the double-PGSE measurements we conducted are at a preliminary stage they raise too many questions to be ignored. First of all we did not manage to find a good reference system which is macroscopically isotropic but which can model locally anisotropic diffusion. The AOT/water with the crushed glass system seemed promising. The pure AOT/water system was macroscopically anisotropic while the AOT/water with crushed glass seemed to be too locally isotropic, thus an AOT/water sample with a smaller amount of larger crushed glass fragments might give us the desired results. Another possible reference system is a few short water capillaries which are attached to a bluetack in the shape of a porcupine, essentially a large scale ensemble of randomly oriented tubes. This kind of system is too big to fit the 3 mm high magnetic field gradient coil, but since the liquid inside the capillaries is water there is no need for a high magnetic field gradient and the experiment can be conducted in the commercial Bruker micro-imaging system which has a large coil volume. Nevertheless, more experiments on polymer in semidilute solutions and melts should be conducted to see whether this effect depends on concentration or whether it represents a consistent form of polymer dynamics.

BIBLIOGRAPHY

1 P. G. de Gennes, *Journal of Chemical Physics* **55,** 572 (1971).

2 M. Doi and S. F. Edwards, *The Theory of Polymer Dynamics* (Clarendon Press, Oxford, 1986).

3 P. E. Rouse, *Journal of Chemical Physics* **21,** 1272 (1953).

4 K. S. Schweizer, M. Fuchs, G. Szamel, M. Guenza, and H. Tang, *Macromolecular Theory & Simulation* **6** 1037 (1997).

5 D. Richter, K. Binder, B. Ewen, and B. Stuhn, *Journal of Chemical Physics* **88,** 6618 (1984).

6 D. Richter, B. Ewen, B. Farago, and T. Wagner, *Physical Review Letters* **62,** 2140 (1989).

7 D. Richter, L. Willner, A. Zirkel, B. Farago, L. J. Fetter, and J. S. Huang, *Macromolecules* **27,** 7437 (1994).

8 S. F. Edwards, *Proceeding of the Physical Society* **92,** 9 (1967).

9 S. F. Edwards, *Polymer* **9,** 140 (1977).

10 H. A. Barnes, J. F. Hutton, and K. Walters, *An Introduction to Rheology*, Fourth ed. (Elsevier, Amsterdam, 1996).

11 J. D. Ferry, *Viscoelastic Properties of Polymers*, Third ed. (John Wiley & Sons, New York, 1980).

12 M. Rubinstein, in *Theoretical Challenges in the Dynamics of Complex Fluids*, edited by T. C. B. McLeish (Kluwer Academic Pablishers, the Netherlands, 1997), p. 21.

13 P. J. Flory, *Principle of Polymer Chemistry* (Cornell University Press, Itaca NY, 1953).

14 Y. Takahashi, I. Noda, and M. Nagasawa, *Macromolecules* **18,** 2220 (1985).

15 M. Adam and M. Desanti, *Journal de Physique* **44,** 1185 (1983).

16 T. A. Kavassalis and J. Noolandi, *Macromolecules* **22,** 2709 (1989).

17 F. Brochard and P. G. de Gennes, *Macromolecules* **10,** 1157 (1977).

18 R. H. Colby and M. Rubinstein, *Macromolecules* **23,** 2753 (1990).

19 M. E. Komlosh and P. T. Callaghan, *Journal of Chemical Physics* **109,** 10053 (1998).

20 D. W. McCall, D. C. Douglass, and E. W. Anderson, *Journal of Chemical Physics* **30,** 771 (1957).

21 N. Nemoto, M. Kishine, T. Inoue, and K. Osaki, *Macromolecules* **24,** 1648 (1991).

22 M. Doi, *Journal of Polymer Science polymer Letters Edition* **19,** 265 (1981).

23 M. Doi, *Journal of Polymer Science: Polymer Physics Edition* **21,** 667 (1983).

24 M. Rubinstein, *Physical Review Letters* **59,** 1946 (1987).

25 J. des Cloizeaux, *Europhysics Letters* **5,** 437 (1988).

26 M. Rubinstein and R. H. Colby, *Journal of Chemical Physics* **89,** 5291 (1988).

27 J. des Cloizeaux, *Macromolecules* **23,** 4678 (1990).

28 J. des Cloizeaux, *Macromolecules* **23,** 3992 (1990).

29 J. des Cloizeaux, *Macromolecules* **25,** 835 (1992).

30 J. Klein, *Macromolecules* **11,** 852 (1978).

31 J. Klein, *Macromolecules* **19,** 105 (1986).

32 H. Watanabe and M. Tirrell, *Macromolecules* **22,** 927 (1989).

33 W. W. Graessley, *Advance in Polymer Sciences* **47,** 67 (1982).

34 P. F. Green and E. J. Kramer, *Macromolecules* **19,** 1108 (1986).

35 S. T. Milner and T. C. B. McLeish, *Physical Review Letters* **81,** 725 (1998).

36 S. T. Milner and T. C. B. McLeish, *Macromolecules* **30,** 2159 (1997).

37 J. Skolnick, R. Yaris, and A. Kolinski, *Journal of Chemical Physics* **88,** 1405 (1988).

38 J. Skolnick and R. Yaris, *Journal of Chemical Physics* **88,** 1418 (1988).

39 F. Bueche, *Journal of Chemical Physics* **20,** 1959 (1952).

40 F. Bueche, *Physical Properties of Polymers* (Interscience, New York, 1962).

41 I. Szleifer and R. F. Loring, *Journal of Chemical Physics* **95,** 2080 (1991).

42 G. Ronca, *Journal of Chemical Physics* **79,** 1031 (1983).

43 M. Fixman, *Journal of Chemical Physics* **89,** 3892 (1988).

44 M. Fixman, *Journal of Chemical Physics* **89,** 3912 (1988).

45 K. S. Schweizer and G. Szamel, *Journal of Chemical Physics* **103,** 1934 (1995).

46 K. S. Schweizer, *Journal of Chemical Physics* **91,** 5822 (1989).

47 K. S. Schweizer, *Journal of Chemical Physics* **91,** 5802 (1989).

48 R. Kimmich, N. Fatkullin, and H. W. Weber, *Journal of Non-Crystalline Solids* **172-174** 689 (1994).

49 E. Fischer, R. Kimmich, and N. Fatkullin, *Journal of Chemical Physics* **104,** 9174 (1996).

50 N. Fatkullin and R. Kimmich, *Journal of Chemical Physics* **101,** 822 (1994).

51 D. Park, *Introduction to quantum theory*, Third Edition ed. (McGraw-Hill, Inc, New York, 1992).

52 A. Abragam, *The Principles of Nuclear Magnetism* (University Press, Oxford, 1978).

53 A. E. Derome, *Modern NMR techniques for chemistry research*, Second ed. (Pergamon Press, Oxford, 1988).

54 R. R. Ernst, G. Bodenhausen, and A. Wokaun, *Principles of Nuclear Magnetic Resonance in One and Two Dimensions* (Oxford University press, Oxford, 1987).

55 C. P. Slichter, *Principles of Magnetic Resonance*, Third ed. (Springer-Verlag, Berlin, Heidelberg, 1992).

56 R. Kimmich, *NMR - Tomograpy Diffusometry Relaxometry* (Springer, Berlin, 1997).

57 P. T. Callaghan, *Principles of Nuclear Magnetic Resonance Microscopy* (Oxford University Press, Oxford, 1991).

58 E. L. Hahn, *Physical Review* **80,** 580 (1950).

59 E. O. Stejskal and J. E. Tanner, *Journal of Chemical Physics* **42,** 288 (1965).

60 H. Y. Carr and E. M. Purcell, *Physical Review* **94,** 630 (1954).

61 P. T. Callaghan, K. W. Jolley, J. Lelievre, *Biophysical Journal* **28,** 133 (1979).

62 D. G. Cory, A. N. Garroway, and J. B. Miller, *Polymer Preprints* **31,** 149 (1990).

63 P. T. Callaghan and O. Soderman, *Journal of Physical Chemistry* **87,** 1737 (1983).

64 Y. Assaf, G. Navon, and Y. Cohen, *Magnetic Resonance in Medicine* **37,** 197 (1997).

65 L. Tsoref, H. Shinar, and G. Navon, *Magnetic Resonance in Medicine* **39,** 11 (1998).

66 P. T. Callaghan, M. A. LeGros, and D. N. Pinder, *Journal of Chemical Physics* **79,** 6372 (1983).

67 P. T. Callaghan, S. L. Codd, and J. D. Seymour, *Concepts in Magnetic Resonance* **11,** 181 (1999).

68 Y. Cheng and D. G. Cory, *Journal of the American Chemical Society* **121,** 7935 (1999).

69 P. T. Callaghan, *Journal of Magnetic Resonance* **88,** 493 (1990).

70 A. Coy, Ph. D, Massey, 1995.

71 P. T. Callaghan and A. Coy, *Physical Review Letters* **68,** 3176 (1992).

72 R. Kimmich, W. Unrath, G. Schnur, and E. Rommel, *Journal of Magnetic Resonance* **91,** 136 (1991).

73 G. Fleischer and F. Fujara, *Macromolecules* **25,** 4210 (1992).

74 E. Fischer, R. Kimmich, and N. Fatkullin, *Journal of Chemical Physics* **106,** 9883 (1997).

75 J. Kaerger, H. Pfeifer, and W. Heink, *Advances in Magnetic Resonance* **12,** 1 (1989).

76 J. E. M. Snaar, P. Robyr, and R. W. Bowtell, in *4th International Meeting on Recent Advanced in MR Applications in Porus Media* (Trondheim, Norway, 1997).

77 E. Vasina, V. Skirda, V. Volkov, A. Nechaev, and B. Mchedlishvili, in *4th International Conference on Magnetic Resonance Microscopy and Macroscopy* (Albuquerque, New Mexico, 1997), pp. 122.

78 P. T. Callaghan, M. E. Komlosh, and M. Nyden, *Journal of Magnetic Resonance* **133,** 177 (1998).

79 F. Candau, C. Strazielle, and H. Benoit, *European Polymer Journal* **12,** 95 (1975).

80 J. des Cloizeaux and G. Jannink, *Polymers in Solution* (OUP, Oxford, 1990).

81 G. C. Berry, *Journal of Chemical Physics* **44,** 4550 (1966).

82 N. Nemoto, M. R. Landry, I. Noh, T. Kitano, J. A. Wesson, and H. Yu, *Macromolecules* **18,** 308 (1985).

83 C. H. Adams, L. R. Hutching, P. G. Klein, T. C. B. McLeish, and R. W. Richards, *Macromolecules* **29,** 5717 (1996).

84 H. Tao, E. v. Meerwal, and T. P. Lodge, *unpublished results* .

85 T. P. Lodge, *Bulletin of the American Physical Society* **43,** 204 (1998).

86 P. T. Callaghan and D. N. Pinder, *Macromolecules* **17,** 481 (1984).

87 G. Weill and J. des Cloizeau, *Journal de Physique* **39,** 77 (1978).

88 *Polymer Handbook*, edited by J. Brandrup and E. H. Immergut (John Wiley & Sons, New York, 1989).

89 M. J. Reimer and J. M. Dealy, *Journal of Rheology* **40,** 167 (1996).

90 W. W. Graessley, *Journal of Polymer Science: Polymer Physics Edition* **18,** 27 (1980).

91 N. Bloembergen, E. M. Purcell, and R. V. Pound, *Physical Review* **73,** 679 (1948).

92 A. Abragam and M. Goldman, *Nuclear Magnetism: Order and Disorder* (Clarendon Press, Oxford, 1982).

93 A. G. Redfield, A. N. Yu, *Physical Review* **169,** 443 (1968).

94 N. Bloembergen, *Physica* **15,** 386 (1949).

95 N. Bloembergen, S. Shapiro, P. S. Pershan, and J. O. Artman, *Physical Review* **114** 445 (1959).

96 T. T. Cheung, *Physical Review B* **23,** 1404 (1981).

97 S. Zhang, B. H. Meier, and R. R. Ernst, *Physical Review Letters* **69,** 2149 (1992).

98 W. Zhang and D. G. Cory, *Physical Review Letters* **80,** 1324 (1998).

99 N. F. Fatkullin, *Sov. Phys. JETP* **72,** 563 (1991).

100 P. Callaghan, *unpublished communication* (1999).

101 Whatman catalog, *www.Whatman.con/catalog/cache/21* .

APENDIX

Appendix A:

The MATLAB program which was used to fit the mean square displacements results to the Doi & Edwards model.

```
%DG=Centre of mass diffusion coefficient (fitted parameter)
%Z number of steps on the primitive path
%p= 1-10
%R=mean square displacement.
%taud tauR =tube disengagement time and Rouse time respectively
% C=concentration
% a= tube diameter (fitted parameter)

clear all;
C=20;
a=(160)*10^(-10);
M=3.04*10^6
DG=2.3*10^(-16);
timemin=5*10^(-3);
timemax=10^(2);
Rsq=M*6.084*10^(-21)*(C/5)^(-0.25);
Z=Rsq/(a^2)
taud=Rsq/(3*pi*pi*DG)
tauR=taud/(3*Z)
Dc=DG*3*Z;
Nmax=100;


ratio=exp((1/Nmax)*log(timemax/timemin));

for N=1:Nmax
        t=timemin*(ratio)^N;
        tm(N)=(t);
```

```
        philong2(N)=(0);
        philong1(N)=6*DG*t;
        phishort2(N)=(0);
        phishort1(N)=2*Dc*t;
        for p=1:100;
        xlong(N,p)=(4*Rsq/((p^2)*pi^2))*(1/2)*(1-exp(-(t*p^2)/taud));
                philong2(N)=philong2(N)+xlong(N,p);
                xshort(N,p)=(4*Rsq/(3*(p^2)*pi^2))*(1/2)*(1-exp(-(t*p^2)/tauR));
                phishort2(N)=phishort2(N)+xshort(N,p);
        end;
end;

tm;
E=(1/3)*(philong1+sqrt(2/pi)*a*sqrt((pi/(2*a^2))*philong2.^2+phishort2));
```

Appendix B:

The MATLAB progrem which was used to fit the oscilltory shear data of the storage modulus to the Doi & Edwards model.

```
% G(omega) - storage modulus
% Gn - plateau modulus (fitted parameter)
% omega - frequency
% taud - tube disengagement time (fitted parameter)
% taue - equilibrium time (fitted parameter)

clear all

Gn=2*10^7
taud=0.04
taue=0.000001
freqmin=5*10^(-3);
freqmax=10^(5);
Nmax=100;

ratio=exp((1/Nmax)*log(freqmax/freqmin));

for N=1:Nmax
        f=freqmin*(ratio)^N;
        omega(N)=(f);


                G(N)=(0);

                for m=1:5
                        p=2*m-1;
                        xGlong(p,N)=((pi/2)*omega(N)*taue)^1/2;

        xG(p,N)=(1/(p^2))*(((omega(N)*taud/p^2)^2)/(1+(omega(N)*taud/p^2)^2)) ;
                        G(N)= xG(p,N);
                        Gl(N)= xGlong(p,N);

                end;

end;


Go=Gn*((8/(pi^2))*G+Gl); %dyn/cm^2
```

Appendix C:

NMR pulse programs used in this work.

I. PGSE

```
; Pulse-Gradient-Spin-Echo - linear increment delay method with ramped gradients.
; vers. 7/9/95 bm

;!!! in memory acquisition !!!
        1s ze          ; zero data block and initialize
        5m thi
10      d1 o1          ; relaxation delay, set transmitter o1
11      d3             ; rf-grad delay
12      p31:ngrad      ; step gradient up, start of loop for dummy pulses
        d11
        lo to 12 times l3
        p31:ngrad      ; first q pulse
        d4             ; q duration
13      p31:ngrad      ; step gradient down
        d11
        lo to 13 times l3
        p31:ngrad      ; q gradients off
        d5             ; delay for big DELTA
        lo to 11 times l5  ; end of loop for dummy pulses
        p1 ph1         ; (90 degree) excitation  hard pulse
        d3             ; rf-grad delay
30      p31:ngrad      ; step gradient up
        d11
        lo to 30 times l3
        p31:ngrad      ; first q pulse
        d4             ; q duration
40      p31:ngrad      ; step gradient down
        d11
        lo to 40 times l3
        p31:ngrad      ; q gradients off
```

```
        d5              ; delay for big DELTA
        p2 ph2          ; 180 degree hard pulse
        d3              ; rf-grad delay
50      p31:ngrad       ; step gradient up
        d11
        lo to 50 times l3
        p31:ngrad       ; second q gradient on
        d4              ; q duration delta
60      p31:ngrad       ; step gradient down
        d11
        lo to 60 times l3
        p31:ngrad       ; q gradients off
        d8 ph3      ; delay for echo
        aq adc          ; acquisition
        rcyc=10 ph0     ; ns=1
        d1 st           ; increment echo pointer
        5m id4          ; increment delay
        5m dd5                  ; decrement delay
        5m dd8
        lo to 10 times nbl ; nbl=number of projections
        5m rd4          ; reset delay
        5m rd5          ; reset delay
        5m rd8
        5m ip0          ; phase cycle
        5m ip0          ; phase cycle
        5m ip1          ; phase cycle
        5m ip1          ; phase cycle
        3u
        lo to 10 times l1 ; # of averages
        d1 wr #0        ; write data to disc
        exit
ph0 = 0
ph1 = 0
ph2 = 1
ph3 = 0
```

```
; pw=rd=0
;!!! in memory acquisition !!!
```

II. PGSTE

```
; Pulse-Gradient-Stimulated-Echo -linear increment delay method with ramped gradients
; vers. 8/3/96 bm mn

;!!! in memory acquisition !!!

1       5m ze          ; zero data block and initialize
        5m thi
10      d1 o1          ; relaxation delay, set transmitter o1
        d1
        p1 ph1         ; (90 degree) excitation  hard pulse
        d3               ; rf-grad delay
30      p31:ngrad      ; step gradient up
        d11
        lo to 30 times l3
        p31:ngrad      ; first q pulse
        d4           ; q duration
40      p31:ngrad      ; step gradient down
        d11
        lo to 40 times l3
        p31:ngrad      ; q gradients off
        d5             ; delay for big DELTA
        p1 ph2         ; 90 degree hard pulse
        d3
        p31:ngrad      ; crusher on
        d7
        p31:ngrad      ; crusher off
        d6             ; z storage time
        p1 ph2         ; 90 degree hard pulse
        d3             ; rf-grad delay
50      p31:ngrad      ; step gradient up
```

```
        d11
        lo to 50 times l3
        p31:ngrad       ; second q gradient on
        d4              ; q duration delta
60      p31:ngrad       ; step gradient down
        d11
        lo to 60 times l3
        p31:ngrad       ; q gradients off
        d8 o1
        go=10 ph31      ; acquisition
        5m st           ; increment echo pointer
        5m id4          ; increment delay
        5m dd5                  ; decrement delay
        5m dd8          ; decrement delay
        lo to 1 times nbl ; nbl=number of projections
        d1 wr #0        ; write data to disc
        exit

ph1 = 0 0 1 1 2 2 3 3
ph2 = 1 3 2 0 3 1 0 2
ph31 = 0 0 1 1 2 2 3 3
```

III. Double-PGSE

```
; Two echoes in the Pulse-Gradient-Spin-Echo - one after each PGSE
;sequence.
;linear incr delay method with ramped gradients
; vers. 11/11/97 mk

;!!! in memory acquisition !!!

        1s ze           ; zero data block and initialize
        5m thi
10    d1 o1             ; relaxation delay, set transmitter o1
```

```
        setf2^2          ;background grad.
        setf2l3      ; set Robin box to first channel by ttl on.
        100u             ; switching delay
        setf2^4          ; shut second channel in Robin box by ttl off
11      d3               ; rf-grad delay
12      p31:ngrad        ; step gradient up, start of loop for dummy pulses
        d11
        lo to 12 times l3
        p31:ngrad     ; first q pulse
        d4          ; q duration
13      p31:ngrad        ; step gradient down
        d11
        lo to 13 times l3
        p31:ngrad        ; q gradients off
        d5               ; Tau
        d15          ; d5+d15=delay for big DELTA
        lo to 11 times l5  ; end of loop for dummy pulses
        p1 ph1         ; (90 degree) excitation  hard pulse
        d3               ; rf-grad delay
30      p31:ngrad        ; step gradient up
        d11
        lo to 30 times l3
        p31:ngrad     ; first q pulse
        d4          ; q duration
40      p31:ngrad        ; step gradient down
        d11
        lo to 40 times l3
        p31:ngrad        ; q gradients off
        d5               ; Tau
        p2 ph2           ; 180 degree hard pulse
        d15          ;d5+d15=delay for big DELTA.
        d3               ; rf-grad delay
50      p31:ngrad        ; step gradient up
        d11
        lo to 50 times l3
        p31:ngrad        ; second q gradient on
```

```
        d4                ; q duration delta
60      p31:ngrad         ; step gradient down
        d11
        lo to 60 times l3
        p31:ngrad         ; q gradients off
        d8
        setf2|4           ;turn on second channel on Robin box
        100u              ;switching delay
        setf2^3           ;turn off first channel on  Robin box
        d18
70      p31:ngrad         ;step gradient up
        d11
        lo to 70 times l3
        p31:ngrad         ; q gradient on
        d4              ;q duration delta
80      p31:ngrad         ; step gradient down
        d11
        lo to 80 times l3
        p31:ngrad         ;q gradients off
        d5              ; Tau
        p2 ph2            ;180 degree hard pulse
        d15             ;d5+d51=delay for big DELTA.
        d3              ; rf grad delay
90      p31:ngrad         ; step gradient up
        d11
        lo to 90 times l3
        p31:ngrad         ; 4th q gradient on
        d4              ; q duration delta
100     p31:ngrad         ;step gradient down
        d11
        lo to 100 times l3
        p31:ngrad         ;q gradient off
        d9 ph3 o1
        aq  adc           ; acquisition
        setf2|2           ;turn off background grad.
        rcyc=10 ph0       ; ns=1
```

```
        d1 st           ; increment echo pointer
        5m id4          ; increment delay
        5m dd5                  ; decrement delay
        5m dd8
        5m dd9
        lo to 10 times nbl ; nbl=number of projections
        5m rd4          ; reset delay
        5m rd5          ; reset delay
        5m rd8
        5m rd9
        5m ip0          ; phase cycle
        5m ip0          ; phase cycle
        5m ip1          ; phase cycle
        5m ip1          ; phase cycle
        3u
        lo to 10 times l1 ; # of averages
        d1 wr #0        ; write data to disc
        exit

ph0 = 0
ph1 = 0
ph2 = 1
ph3 = 0

; pw=rd=0

;!!! in memory acquisition !!!
```